



XVI Reunião da Sociedade Brasileira de  
Cristalografia

# Resumos



# XVI Reunião da Sociedade Brasileira de Cristalografia

16 a 19 de Março de 2003.  
Instituto de Física de São Carlos – USP  
São Carlos – SP

## COMISSÃO ORGANIZADORA:

Coordenadora: Yvonne P Mascarenhas, presidente da SBCr, Instituto de Física de São Carlos/USP

Nivaldo Spezialli – Dep. de Física, ICEX/UFMG

Rosangela Itri – Instituto de Física/USP

Íris Torriani – Membro do Conselho da SBCr, IFGW/UNICamp

César Cusatis – Instituto de Física/UFPr

Valmor Mastelaro – Secretária da SBCr, IFSC/USP

Carlito Lariucci – Membro do Conselho da SBCr, Inst. De Física/UFG

Fernando Rizzo – Lab. De Materiais, PUC-Rio

## APOIO FINANCEIRO:

FAPESP – Fundação de Amparo à Pesquisa do Estado de São Paulo.

CNPq – Conselho Nacional de Desenvolvimento Científico e Tecnológico.

CAPES – Coordenação de Aperfeiçoamento de Pessoal de Nível Superior.

DAIRIX Equipamentos Analíticos Ltda.

Bruker-AKS Inc.

Editores do livro de resumos

Hamilton B. Napolitano

Yvonne P. Mascarenhas



*Sociedade  
Brasileira de  
Cristalografia*

*Fundada em 1971*

### **Diretoria**

Presidente: Yvonne Primerano Mascarenhas

Vice-presidente: Aldo Felix Craievich

Secretário Geral: Valmor Mastelaro

Secretário: Rosangela Itri

Tesoureiro: Marcia de Abreu Fantini

Secretário para Assuntos de Ensino: Carlos de Oliveira Paiva Santos

### **Conselho**

#### **Membros Titulares**

Iris Torriani

Cesar Cusatis

Maria Teresa do Prado Gambardella

Glaucius Oliva

Carlos Alberto de Simone

Carlito Lariucci

#### **Membros Suplentes**

Nivaldo Spezialli

Ivo Vencato

Daniel Atencio

# Apresentação

A Cristalografia visa essencialmente ao conhecimento da estrutura da matéria condensada a nível atômico, tanto sob o ponto de vista da estrutura cristalográfica e molecular como de seus defeitos, e ao relacionamento dessa estrutura com as respectivas propriedades físicas, químicas, bioquímicas e biológicas. Disto resulta o seu forte caráter interdisciplinar que obriga a estruturação de um programa educacional muito específico para a formação de um cristalógrafo verdadeiramente capaz de usar de forma objetiva e crítica tanto o arsenal de recursos fornecidos pelo desenvolvimento de poderosos recursos computacionais disponíveis como dos sistemas de obtenção e purificação de amostras, preparação de cristais e coleta de dados usando diversas fontes de radiação e de sistemas de detecção. O grande e rápido desenvolvimento de novas metodologias é uma característica de todas as áreas da ciência e, em particular da Cristalografia. Na etapa atual de desenvolvimento isto exige uma formação continuada dos cristalógrafos a fim de se manterem atualizados e a realização de reuniões científicas deve ser um recurso para promover tal atualização.

A situação atual da Cristalografia no Brasil pode ser considerada muito promissora, tanto sob o ponto de vista da formação de especialistas em nível de pós-graduação como de integração com as demais áreas científicas que buscam, cada vez mais, a participação de cristalógrafos, tanto na área biológica como na de materiais com potenciais aplicações tecnológicas.

O desempenho das atividades em Cristalografia no Brasil pôde atingir resultados compatíveis com o nível internacional graças, tanto à presença de modernos equipamentos em vários laboratórios de grupos de pesquisa acadêmicos, como o acesso à radiação sincrotron. Assim, um fator importante para a realização de muitos trabalhos reside na existência do Laboratório Nacional de Luz Síncrotron (LNLS) onde se estabeleceram condições excepcionais de pesquisa que podem ser usufruídas pela comunidade através da apresentação de propostas. Uma característica importante desse Laboratório tem sido o continuado empenho no aperfeiçoamento das condições já existentes e criação de novas linhas. Pode-se destacar nos últimos dois anos a conclusão e entrada em operação do anel de reforço ao anel de armazenamento (booster), o aperfeiçoamento da estação para difração de pó já existente e a estruturação de uma nova linha, o aperfeiçoamento da estação de SAXS com a capacidade de realizar medidas simultâneas de SAXS e WAXS, a próxima inserção de um wiggler para a estação de proteínas e a inserção de um ondulador (undulator) na linha de ultravioleta.

Deve-se ainda salientar que uma profícua cooperação tem sido freqüentemente estabelecida com cristalógrafos latino-americanos tanto através do uso de equipamentos nos laboratórios acadêmicos como no LNLS. Assim, os recursos aplicados nessas instituições têm contribuído para o estabelecimento de fortes vínculos de pesquisa com a comunidade científica regional.

Temos a esperança de que todos esses fatores poderão incentivar a comunidade científica brasileira em Cristalografia a perseverar na realização de ideais de desenvolvimento científico, cultural e tecnológico tanto de nosso país como dos demais países de nossa região.

# Índice

As siglas PC, O e P indicam respectivamente Palestra Convidada, Apresentação Oral e Painel.

## Palestras Convidadas (PC)

PC1BIO. Ion Gating and Selectivity in Gramicidin A.

*W.L. Duax, V. Pletnev, B.M. Burkhardt, and M. Glowka* ..... 1

PC2SAS. Potencialidades do SAXS para o Estudo de Materiais Híbridos de Interesse Tecnológico

*K. Dahmouche, C.V. Santilli and A.F. Craievich* ..... 3

PC3BIO. The Crystal Structure and Catalytic Mechanism of Cellobiohydrolase CelS, the Major Enzymatic Component of the Clostridium Thermocellum Cellulosome

*Beatriz Gomes Guimarães* ..... 4

PC4PQM. Experimental Charge Density Study of Cu(II)-L-alanyl-L-valine by Synchrotron Radiation at 17 K

*José R. Sabino and Eduardo E. Castellano* ..... 5

PC5BIO. Desenho Racional de Inibidores Contra DHODH (Diidroorotato Desidrogenase). Aplicações no Tratamento da Doença de Chagas e da Praga do Amarelinho

*Maria Cristina Nonato* ..... 6

PC6INS. Study of Phase Transformations Using a Novel X-Ray Imaging Technique

*Fernando Rizzo* ..... 7

PC7MPO. The Analysis of the Measurements on a Ceria Size-Strain Round-Robin Sample

*D. Balzar* ..... 8

PC8PQM. Phase Transitions and Modulated Phases in AA'BX4 Compounds

*Nivaldo Lúcio Speziali* ..... 9

PC9BIO. Dynamics and Structure of Macromolecules Involved in Human Diseases

*Jerson L. Silva* ..... 10

PC10INS. Single-Wavelength Anomalous Phasing - Importance of Data Accuracy

*Zbigniew Dauter* ..... 11

## **Biomoléculas (BIO)**

OBIO01. Antisense Genes, Codon Bias and the Evolution of the Genetic Code <i>W.L. Duax, A. Addlagatta, V. Pletnev, R. Huether and P. Yu</i> .....	<b>12</b>
OBIO02. Structural Biology and Drug Design in Tropical Diseases <i>Oliva G., Garratt R.C., Thiemann O.H., Castilho M.S., Silva M., Trapani S., Pereira H.M., Navarro M.A.V.S., Silva C.T.P. da, Silva M.T. da, Vieira P.C., Silva M.F.F., Fernandes J.B., Corrêa A.G.</i> .....	<b>14</b>
PBIO03. Cloning, Purification and Initial Crystallographic Data of Human Adenine Phosphoribosyltransferase (APRT): Analyses and Molecular Replacement Solution <i>Iulek, J., Silva, M., Thiemann, O.H., Oliva, G.</i> .....	<b>15</b>
PBIO04. Small Angle X-Ray Studies of Protein-Polymer Interactions <i>Oliveira C. L. P., Torriani I. L., Almeida, N. L., Loh, W.</i> .....	<b>16</b>
PBIO05. Is It Possible to Determine the Solvent Content of Protein Crystals from Diffraction Intensity Analysis? <i>Napolitano, H. B., Trapani, S., Fischer, H., Craievich, A. F. and Oliva, G.</i> .....	<b>17</b>
PBIO06. Estudo da Interação Entre Azul de Metíleno e AOT por Espalhamento de Raios X a Baixos Ângulos <i>Duarte, E. L; Severino, D.; Baptista, M. S.; Itri, R.</i> .....	<b>18</b>
PBIO07. Crescimento e Controle de Tamanho de Nanopartículas Magnéticas no Interior de Micelas Reversas <i>Duarte, E. L.; Itri, R.; Baptista, M. S. e Leite, C.A.P.</i> .....	<b>19</b>
PBIO08. Estudo do Efeito de Íons da Série de Hofmeister em Sistemas Micelares <i>V. P. Barros, R. Itri, F. Casallanova, S. Schreier</i> .....	<b>20</b>
OBIO09. The Active Site Loop in the Rabbit Muscle TIM Structure: a Closed Conformation is Observed in the Absence of Ligands <i>Aparicio, R., Ferreira, S. T. e Polikarpov, I.</i> .....	<b>21</b>
PBIO10. Influence of Bovine Serum Albumin (BSA) on the Size of Aerosol-OT/n-hexane/water Reversed Micelles Investigated by Small Angle X-ray Scattering <i>Caetano W., Duarte, E. L., and Itri, R.</i> .....	<b>22</b>

PBIO11. Interaction of the Iron–TetramethylpiridylPorphyrin (FeTMPyP) with DNA as Studied by X-ray Absorption Spectroscopy (XANES and EXAFS)

*Caetano W., Duarte E.L., Scopel W.W., Itri R., Gandini S.C.M., Almeida L.E., Tabak M.* ... **23**

PBIO12. Sulfur Phasing Using Cu-K $\alpha$  Radiation from Rotating Anode

*Ambrosio, A. L. B., Nagem, R. A. P., Rojas, A. L., Navarro, M. V. A. S., Golubev, A. M., Garratt, R. C. & Polikarpov, I.* ..... **24**

PBIO13. Molecular Characterization and Preliminary Structural Studies of Leishmania major Purine Salvage Enzyme Adenylosuccinate Lyase - ADSL

*Mantovani, M.; Pedrosa, A.L.; Cruz, A.K.; Aguilar, C.F. & Thiemann, O.H.* ..... **25**

### **Filmes Finos (FFN)**

OFFN01. Local Structure in Strained Manganite Thin Films

*Souza-Neto N. M., Ramos A. Y., Tolentino H. C. N., Ranno L.* ..... **26**

OFFN02. Electrochromism in Au-NiO Films

*Ferreira, F.F.; Haddad, P.S.; Fantini, M.C.A.; Brito, G.E.S.* ..... **27**

PFFN03. In-Situ X-Ray Diffraction of Niox Films Deposited on Be Substrate

*Sánchez M. A. E., Fantini M.C.A.* ..... **28**

PFFN04. Preparação e Caracterização de uma Vitrocerâmica Obtida a Partir do Sistema Ternário Bao-B2O3-Tio2, Contendo a Fase B-BBO

*Feitosa, C. A. C., Zanatta, A. R., Mastelaro, V. R.* ..... **29**

PFFN05. Síntese e Caracterização de Filmes da Fase  $\beta$ -BaB2O4 a Partir da Composição 48BaO-48B2O3-4TiO2 Depositados Por Evaporação por Feixe de Elétrons

*Maia, L.J.Q.; De Vicente, F.S.; Zanatta, A.R.; Mastelaro, V.R.; Siu Li, M.* ..... **30**

### **Pequenas Moléculas (PQM)**

OPQM01. Supramolecular Associations via Intermolecular Secondary Interactions in Dimethyl – Thallium Complexes

*Sauli Santos-Jr, Eduardo E. Castellano, Javier Ellena, Mónica Toma, José S. Casas, María S. García-Tasende, Agustín Sánchez and José Sordo* ..... **31**

OPQM02. Use of the Cambridge Structural Database in Study of Single and Partial Double C-X (X=C,N, O) Bonds in Organic Molecules in Crystalline State

<i>Kiralj R. and Ferreira M. M. C.</i> .....	<b>32</b>
PPQM03. Crystallographic Structure of the 7 $\beta$ -hydroxy-6 $\alpha$ -oxovouacapan-17 $\beta$ -amide <i>Rodrigues, L.P.; Resende, J.A.L.C.; Guilardi, S.; Ellena, J.; Santos-Jr, S.; Branco, P.A.C.; Piló-Veloso, D.; Rubinger, M.M.M.</i> .....	<b>33</b>
PPQM04. The X-ray Structure of the N-ciclohexyl-7 $\beta$ -hydroxy-6 $\alpha$ -oxovouacapan-17 $\beta$ -amide <i>Resende, J.A.L.C.; Oliveira, G.B.; Guilardi, S.; Ellena, J.; Santos-Jr, S.; Branco, P.A.C.; Piló-Veloso, D.; Rubinger, M.M.M.</i> .....	<b>34</b>
PPQM05. Crystal Structure of Nitrooxyquinones <i>Pereira, M.A.; De Simone,C.A.; Malta,V.R.S.; Goulart, M.O.F.; Abreu F.C.; Lopes A. C. de O.</i> .....	<b>35</b>
PPQM06. Crystal Structure of ent-16a, 17b-methoxy-17-hydroxy-19-kauran Acid – ACF-158b <i>Pereira, M.A.; Malta, V.R.S.; De Simone,C.A.; Santos, G.L; Nascimento, M.C.B.S., Morais, A.A., Filho, R.B., Vieira, I.J.C.</i> .....	<b>36</b>
PPQM07. Crystal Structure of (3-Oxo-isochroman-4-yl)-acetic acid ethyl ester <i>Pereira, M.A.; De Simone, C.A.; Malta, V.R.S.; Goulart, M.O.; Cavalcanti J.C.M.</i> <b>37</b>	
PPQM08. Crystal Structure of 3 $\beta$ -(5 phenyl-2E,4E - pentadienoyloxy)-olean-12-ene <i>Pereira, M.A.; Malta,V.R.S.; De Simone, C.A.; Silva, V.R.M.; Humberto, M.M.S.; Sant'ana, A.E.G.</i> .....	<b>38</b>
PPQM09. Structural Studies of the 4-Tioxopirimidine C <sub>14</sub> H <sub>14</sub> N <sub>2</sub> O <sub>2</sub> S with potential biological activities <i>Lariucci, C., Lima, K.A.P., Vencato, I., Napolitano, H. B. and Cunha, S.</i> .....	<b>39</b>
PPQM10. Crystal Structure of the 3-benzoxazol-2-yl-7-hydroxy-chromen-2-one <i>Franca, E.F., Souza, K.C.; Machado, A.E.H.; Guilardi, S.; Santos-Jr., S.; Ellena, J.</i> .....	<b>40</b>
PPQM11. Estrutura Cristalina e Molecular do C <sub>22</sub> H <sub>26</sub> N <sub>2</sub> O <sub>4</sub> <i>Mafud, A. C., Gambardella, M.T.P.</i> .....	<b>41</b>
PPQM12. Short Hydrogen Bonds in Salts of Pyromellitic Acid [C <sub>6</sub> H <sub>2</sub> (COOH) <sub>4</sub> ] <i>Diniz, R., Ellena, J., Sansiviero, M. T. C. and Fernandes, N. G.</i> .....	<b>42</b>
PPQM13. Estudo Estrutural do Composto Orgânico C <sub>7</sub> H <sub>11</sub> ClNO <sub>3</sub> <i>Napolitano, H. C. A. S.; Santos, R. H. A.; Santos, L. da Silva; Freitas, O.</i> .....	<b>43</b>

PPQM14. Crystal Structure of a Chromite <i>Santos, J.S., Doriguetto, A.C., Fernandes, N. G.</i>	<b>44</b>
PPQM15. Charge Density of Zn[H <sub>2</sub> O] <sub>6</sub> [C <sub>10</sub> H <sub>4</sub> O <sub>8</sub> ] <i>Diniz, R., Rodrigues, B. L., Ellena, J., Gustafsson, T. and Fernandes, N. G.</i>	<b>45</b>
OPQM16. Novel Crystal Structure of a Sodium and Potassium Nitrate Obtained from the Leg of a Orthoptero of the Tridactylidae Family <i>Ellena, J.A., Castellano, E.E. and Ferreira, A.</i>	<b>46</b>
PPQM17. Molecular and Crystal Structure of the Complex [Cu <sub>2</sub> μ-(O <sub>2</sub> CC <sub>4</sub> H <sub>3</sub> O) <sub>4</sub> (H <sub>2</sub> O) <sub>2</sub> ].2H <sub>2</sub> O <i>Maia, D. F. S.; Teles, W. M.; Machado, F. C. and Speziali, N. L.</i>	<b>47</b>
PPQM18. Determinação da Estrutura Cristalina e Molecular do Polímero [Cd(Cl) <sub>2</sub> (HPz) <sub>2</sub> ] <sub>n</sub> e Estudo das Interações Entre seus Monômeros <i>Ferreira, J.G., Santos, R.H.A., Netto, A.V.G., Silva, A.M.</i>	<b>48</b>
PPQM19. A crystallographic Study of (2-acetylpyridine-κN 4-phenylthyosemicarbazone-κ <sup>2</sup> N <sup>1</sup> ,S) methyl-trans-dichlorotin(IV) <i>Gambardella M.T.P.; Francisco R.H.P., Sousa, G.F.</i>	<b>49</b>
PPQM20. Crystallography of Natural Perovskite from the Uberaba Formation Sandstones, Minas Gerais, Brazil <i>Gravina, É. G., Brod, J. A., Doriguetto, A. C., Diniz-Pinto, H.S.</i>	<b>50</b>
<b>Teoria, Instrumentação e Aplicação de SAX (SAS)</b>	
OSAS01. Viability Study For the Installation of a SANS Beam-Line at IPEN/CNEN-SP <i>José Mestnik Filho e José Teixeira</i>	<b>51</b>
PSAS02. Structure of Charged Phospholipid Vesicles by SAXS <i>Fernandez, R.M., Riske, K.A., Lamy-Freund, M.T. and Amaral, L.Q.</i>	<b>52</b>
PSAS03. Gelation and Drying of Weakly Bonded Silica-PPO Nanocomposites <i>Chaker J.A., Dahmouche K., Santilli C.V., Pulcinelli S.H. and Craievich A.</i>	<b>53</b>
PSAS04. SAXS and NMR Study of Siloxane-PMMA Hybrids Prepared by Sol-gel Process posites <i>Sarmento, V.H.V., Dahmouche, K., Santilli, C.V., Pulcinelli, S.H., Craievich, A.F.</i>	<b>54</b>

OSAS05. Isothermal Aggregation of Bi Atoms Embedded in a Soda-Borate Glass:  
Coarsening of Liquid Nanodroplets and Atomic Diffusion

*Craievich A. F. and Kellermann G.* ..... 55

PSAS06. SAXS Study of The Mechanisms of Aggregation in Sulphate Zirconia sols+

*Craievich, A., Riello, P. Minesso, A. and Benedetti, A.* ..... 56

**Método do Pó (MPO)**

PMPO01. O Efeito da Adição de Boro na Anisotropia da Expansão Térmica das Fases  
 $Nb_5Si_3$ ,  $Ta_5Si_3$  e  $Mo_5Si_3$

*Rodrigues G., Nunes C. A., Suzuki P. A., Coelho G. C.* ..... 57

PMPO02. High Resolution X-ray Diffraction Studies in Sm(Co,Cu)<sub>5</sub>

*Serrano, R. L, Madrigal, A. P., Rams, E. E.* ..... 58

PMPO03. X Ray Powder Diffraction Analysis of Phase Changes in Sintered  
Hydroxyapatite by the Rietveld Method

*Fancio, E. and Lima, N. B.* ..... 59

PMPO04. Propriedades Estruturais de Eletrocatalisadores de Pt e Ligas Bimetálicas Pt-Co  
Suportado em Carbono de Alta Área Superficial

*Salgado, J.R.C., Lopes, L.P., Mascarenhas, Y.P. e Gonzalez, E.R.* ..... 60

PMPO05. Rietveld method structural study of the Gallium doped zinc oxide

*Antonio, S.G., Paiva-Santos, C.O., Gonçalves, A.S., Davolos, M.R.* ..... 61

PMPO06. Negative Thermal Expansion Coefficient in the Triclinic Kaolinite

*Batista, W.O., Baran, Z., Keller, W.A.* ..... 62

PMPO07. Effect of Stress on 3YTZ-Al<sub>2</sub>O<sub>3</sub> Composites

*Mir M., M'Peko J.C., De Souza M.F. and Mascarenhas Y.P.* ..... 63

PMPO08. Preparation and Characterization of Y<sub>1</sub>Ba<sub>2</sub>Cu<sub>3-x</sub>Ru<sub>x</sub>O<sub>7-δ</sub> Polycrystalline Samples

*Siqueira, E. C., Macedo, A. G, Brinatti A. M., Pereira, L. A. A., Jurelo, A. R.* ..... 64

PMPO09. Rietveld Study of Ferroelectric Ceramics with Tungsten-Bronze Structure

*Lopes, L. P.; Doriguetto, A. C; Mascarenhas, Y. P.; Coimbrão, N. F.; Garcia D.; Eiras, J. A.* ..... 65

OMPO10. Crystal Structure Refinement of a Th-rich Weeksite Group Mineral

*Carvalho, F. M. S., Atencio, D. and Andrade, M. B.* ..... 66

PMPO11. Quantitative Phase Analysis of Sr <sub>2</sub> CeO <sub>4</sub> using Rietveld Refinement <i>Góes, M.S.; Ferrari, J.L.; Pires, A.M.; Paiva-Santos, C.O.; Davolos, M. R.</i>	<b>67</b>
PMPO12. Estrutura e microestrutura de Co <sub>7-x</sub> Ni <sub>x</sub> Sb <sub>2</sub> O <sub>12</sub> , (0 ≤ x ≤ 4) <i>Paiva-Santos, C. O.; Antonio, S. G.; Brito, M. S. L.; Lucena, J. B.; Gama, L.; Longo E.</i>	<b>68</b>
PMPO13. Hydrated and Anhydrous Forms of the Room Temperature Phase of K <sub>4</sub> (Mo <sub>0.5</sub> W <sub>0.5</sub> )O <sub>4</sub> <i>Moreira, A.M.; Archanjo, B.S.; Guarnieri, A.A.; Pinheiro C. B.; Speziali, N. L.</i>	<b>69</b>
PMPO14. “Structural Analysis of SnO <sub>2</sub> Doped Semiconductors by the Rietveld Method” <i>Carrió J. A. G., Piccoli S., Borgia R. A., Gutierrez S., Arana J. A. V., Paiva Santos C. O.</i>	<b>70</b>
PMPO15. Synthesis and Structural Characterization of the Y <sub>1-x</sub> Cd <sub>x</sub> MnO <sub>3</sub> System <i>Agiiero O. E. and Torriani I. L.</i>	<b>71</b>
PMPO16. The New IPEN-CNEN/SP Neutron Powder Diffractometer <i>Parente, C.B.R., Mazzocchi, V.L., Mascarenhas, Y.P.</i>	<b>72</b>
 <b>Ensino de Cristalografia (ECR)</b>	
OECR01. Protein Folder: molecular models for building 3D cartoons of protein structures <i>Garratt, R.C., Abel, L.D.S., &amp; Carvalho, J.C.Q.</i>	<b>73</b>
OECR02. Development and Study of Oxide Crystals with Programmed Lattice Parameters Gradients <i>Reyes Ardila, D., Barbosa, L. B., Kakuno, E. M., Camparin, H., Cusatis, C., Andreeata, J. P.</i>	<b>74</b>
 <b>Instrumentação e Aplicação da Radiação Sincrotron (INS)</b>	
OINS01. Evidence of Point-Defect Annihilation During Structural Relaxation of Amorphous III-V Semiconductors <i>Azevedo, G. de M.; Ridgway, M. C.; Glover, C. J.; Yu, K. M. and Foran, G. J.</i>	<b>75</b>
OINS02. Advances in High Throughput Crystallography for the Home Lab: Bright Sources, Fast Detectors, Robotics, and Cr Radiation Phasing <i>Ferrara, J.D.</i>	<b>76</b>

PINS03. Structural Modifications at the NiO<sub>6</sub> Octahedra in Nd<sub>n</sub>NiO<sub>3</sub> Across the Metal-Insulator Transition Measured by EXAFS

*Piamonteze, C., Tolentino, H. C. N., Ramos, A. Y., Massa, N. E., Alonso, J. A., Martinez-Lope, M. J., Casais, M. T.* ..... 77

**Espalhamento Múltiplo (EMU)**

PEMU01. Caracterização Estrutural de Cerâmicas Ferroelétricas (Pb,La)TiO<sub>3</sub> e Através da Técnica de Espectroscopia de Absorção de Raios-X (XAS) e da técnica de Espectroscopia de Fotoelétrons Excitados por Raios-X (XPS)

*Neves, P. P., Mastelaro, V. R., Eiras J. A., Michalowicz, A.* ..... 78

## PC1BIO. Ion Gating and Selectivity in Gramicidin A.

W.L. Duax<sup>1</sup>, V. Pletnev<sup>2</sup>, B.M. Burkhardt<sup>3</sup>. and M. Glowka<sup>4</sup>

<sup>1</sup>Hauptman-Woodward Inst., Inc. Buffalo, NY 14203 USA, <sup>2</sup>Shemyakin-Ovchinnikov Inst. of Bioorganic Chem., Russian Acad. of Sciences, Moscow 117997 RUSSIA,  
<sup>3</sup>Milliken Chem. Co., Spartanburg, SC 29304, <sup>4</sup>University of Lodz, Lodz, Poland

Seven crystal structures of ion complexes of gramicidin provide information concerning the distribution of ions and water in a single file channel. The structure (a right-hand antiparallel double strand  $\beta$ -ribbon) agree with that based on NMR measurements in organic solvents and lipid bilayers. The ion and solvent filled gramicidin A channel is a nanotube that is 25 $\text{\AA}$  long and 4 $\text{\AA}$  across.

***Ion Distribution.*** There are between 1 and 2 cations per channel distributed in partial occupancy over subsets of the same seven sites in 14 crystallographically independent channels. The partial occupancy ranges from a 15%  $\text{Cs}^+$  occupancy to a 90%  $\text{K}^+$  occupancy. The central site is consistently occupied by the larger cations ( $\text{Rb}^+$ ,  $\text{Cs}^+$ , and  $\text{Tl}^+$ ) and never occupied by  $\text{K}^+$  ions.

***Cation Coordination.*** In most cases ions in the six sites of highest occupancy make three or four contacts to the  $\pi$  clouds of the carbonyl or peptide groups of the channel walls. The  $M^+...O$  or  $N$  distances range from 2.56 to 3.80 $\text{\AA}$ . The torsion angles defining the relationship of the ions and the  $sp^2$  plane of the carbonyl groups ( $\mu_2, M^+...O=C_1N_1$ ) range from 54° to 104° (average 81°) demonstrating that ion association is to the  $\pi$  cloud over the carbonyl and peptide groups. The peptide bond  $\omega$  angles of residues involved in ion coordination exhibit significant non-planarity as a result of the withdrawal of electrons from the  $\pi$  clouds by the cations in the channel.  $^{13}\text{C}$  NMR chemical shift measurements attributed to  $\text{Na}^+$  ion interactions with leucine residues in gramicidin channels in dimyristoyl phosphatidylcholine (DMPC) bilayers correlate with these observations. The structure of gramicidin responsible for ion transport in bilayers appears to be similar to the structure in the crystals.

***Asymmetry in Water Cation Coordination.*** There are 6 to 7 water molecules in each channel distributed along its 25 $\text{\AA}$  length. The waters occupy the same seven sites where the cations are found. Electrophysiological measurements also indicate that seven water molecules are transported per cation. When there is a water molecule on either side of an ion, one water is at an average distance of 2.4  $\text{\AA}$  and the other 3.2  $\text{\AA}$  from the ion. The asymmetry of distances between the cations and the closest waters suggests that the closest contacts (2.2  $\text{\AA}$ -2.9  $\text{\AA}$ ) represent ion liganding via the backbonding orbitals of the oxygen atom of the water and the longer distances (3.0 $\text{\AA}$  – 3.6  $\text{\AA}$ ) arise when the water is oriented with its hydrogen atoms directed toward the cation.

***Channel Dipole.*** The dipoles of seventy-five percent of the waters of solvation within the channels are uniformly aligned. Cation concentration differences in the polar region on either side of a lipid bilayer could induce asymmetry in gramicidin channels embedded in the membrane producing a comparable dipole that would provide a driving force for ion transport.

*Ethanolamine Gating.* The ethanolamine at the C terminus of gramicidin A appears to play a critical role in ion entry and exit. Ethanolamine may function as a flexible hook that can associate with ions in the polar lipid interface and guide them into the channel or usher ions out of the channel by a reversal of this action. The crystal structures of gramicidin complexes provide atomic scale examples of stages of the dynamic process of ion transport in single file and the asymmetric forms captured in the crystals may have much in common with the asymmetric forms of gramicidin that must exist in order to account for ion transport across membranes and lipid bilayers.

## PC2SAS. Potencialidades do SAXS para o Estudo de Materiais Híbridos de Interesse Tecnológico

K. Dahmouche<sup>1</sup>, C.V Santilli<sup>1</sup> and A.F Craievich<sup>2</sup>

<sup>1</sup> Instituto de Química-UNESP (Araraquara-SP), <sup>2</sup> Instituto de Física-USP

(São Paulo-SP)

A estrutura de materiais híbridos Siloxano-Polieters preparados pelo processo Sol-Gel e de interesse tecnológico foi estudada por espalhamento de raios X a baixo ângulo (SAXS). Duas famílias de híbridos foram investigadas. A primeira (classe I) apresenta somente ligações “físicas” entre as fases orgânicas (polímero) e inorgânicas (siloxano) enquanto nos híbridos de classe II as interações entre as duas fases são covalentes. Os resultados de SAXS mostraram que os híbridos de classe I apresentam uma estrutura fractal constituída por agregados de siloxano (entre 30 e 80 Å de diâmetro) dispersos na fase polimérica e formados por nanopartículas de siloxano de diâmetro aproximado de 8 Å. A dimensão fractal e o tamanho dos agregados são fortemente dependente das condições de preparação (peso molecular do polímero, teor de polímero no material, pH do sol inicial). A determinação desses parâmetros revelou os mecanismos que levam à formação do gel e que são do tipo agregação monomer-cluster controlada pela difusão (DLMCA) ou cluster-cluster controlada pela reação (RLCCA). A estrutura dos híbridos de classe II é muito diferente e consiste de nanopartículas de siloxano (diâmetro  $\geq$  10 Å) localizadas nas pontas das cadeias poliméricas e formando crosslinks entre as cadeias. Essas partículas apresentam uma forte correlação espacial entre elas sendo que a distância entre partículas aumenta com o peso molecular do polímero. Essa correlação espacial aparece somente durante a secagem do gel úmido, que possui estrutura fractal. Esta estrutura fractal já existe no sol inicial e evolui durante a gelatinização do material. Quando dopados com íons alcalinos (lítio, sódio ou potassio), lantanídios (Europio, neodimio) ou de ferro, esses nanocompósitos apresentam boas propriedades de condução iônica, de luminescência ou magnéticas, respectivamente. A estrutura determinada por SAXS é fortemente dependente da concentração do dopante. No caso dos híbridos de classe I, o aumento da concentração de íons aumenta a dimensão fractal e o tamanho dos agregados inorgânicos, resultando em modificações das propriedades elétricas e óticas dos compósitos. No caso dos híbridos de classe II, e para altos teores de alcalinos, ocorre a formação de ligações cruzadas entre os cátions e os oxigênios do tipo éter das cadeias de polímero, resultando em um enrijecimento das cadeias, e consequentemente na diminuição da condutividade elétrica do material. Nas amostras dopadas com europio, os sítios de interação dos cátions e portanto os tempos de vida dos íons europio e as propriedades de luminescência dos híbridos dependem do peso molecular do polímero. A dopagem com íons lantanídios ou de ferro induz a formação de uma estrutura hierárquica nos híbridos de classe II. Essa estrutura é constituída por domínios de diâmetro  $\gg$  100 Å dispersos na matriz de polímero e interconectados por cadeias poliméricas esticadas, enquanto as nanopartículas de siloxano localizadas dentro de cada domínio estão interconectadas por cadeias enoveladas. As propriedades magnéticas dos híbridos dopados com ferro estão consistentes com o estudo estrutural efetuado por SAXS: enquanto as amostras dopadas com Fe(II) são paramagnéticas devido a dispersão dos íons ferro na matriz polimérica, os híbridos dopados com Fe(III) apresentam uma irreversibilidade magnética e térmica, devido a formação de nanodomínios de ferro nos compósitos.

# PC3BIO. The Crystal Structure and Catalytic Mechanism of Cellulbiohydrolase CelS, the Major Enzymatic Component of the Clostridium Thermocellum Cellulosome

Beatriz Gomes Guimarães  
Centro de Biologia Molecular Estrutural  
Laboratório Nacional de Luz Síncrotron

Cellulbiohydrolase CelS plays an important role in the cellulosome, an active cellulase system produced by the thermophilic anaerobe *Clostridium thermocellum*. The structures of the catalytic domain of CelS in complex with substrate (cellohexaose) and product (cellobiose) were determined at 2.5 and 2.4 Å, respectively. The protein folds into an  $(\alpha/\alpha)_6$  barrel with a tunnel-shaped substrate-binding region. The conformation of the loops defining the tunnel is intrinsically stable in the absence of substrate, suggesting a model to account for the processive mode of action of family 48 cellulbiohydrolases. Structural comparisons with other  $(\alpha/\alpha)_6$  barrel glycosidases indicate that CelS and endoglucanase CelA, a sequence-unrelated family 8 glycosidase with a groove shaped substrate-binding region, use the same catalytic machinery to hydrolyze the glycosidic linkage, despite a low sequence similarity and a different endo/exo mode of action. The nearly identical arrangement of substrate and functionally important residues in the two active sites strongly suggests an evolutionary relationship between the cellulbiohydrolase and endoglucanase families, which can therefore be classified into a new clan of glycoside hydrolases.

# PC4PQM. Experimental Charge Density Study of Cu(II)-L-alanyl-L-valine by Synchrotron Radiation at 17 K

**José R. Sabino and Eduardo E. Castellano**

Institute of Physics of Sao Carlos, University of Sao Paulo, Sao Carlos, SP – Brazil.

The bonding properties of transition metals complexes with coordination compounds (a small peptide in this project), is of great importance in the inorganic and bio-inorganic chemistry of the transition metal atoms<sup>[1]</sup>. The experimental high resolution charge density study is a direct way to determine their bond properties. Charge density analyses using the Hansen-Coppens multipole model<sup>[2]</sup> allow both, the topological study of electron density  $\rho(\mathbf{r})$  and the orbital population's analysis of the transition metals.

We report here an electron density analysis of the complex Cu(II)-L-alanyl-L-valine. Short synchrotron wavelength (0.394 Å) and liquid helium were used for the collection of three dimensional data sets with  $\sin\theta/\lambda$  up to 1.666 Å<sup>-1</sup>. The Cu<sup>2+</sup> site is a distorted square pyramid with two N and two O in the equatorial plane and one O in the apical position. 3d orbital populations have been determined. The half population obtained for the  $dx^2-y^2$  orbital is shown in the static deformation and negative Laplacian maps as an electron 4-fold depletion region in the dipeptide plane. Cu-N and Cu-O bonds showed partial closed shell and covalent characters. The values of both, the charge density  $\rho(\mathbf{r})$  (ranging from 0.3 to 0.8 e Å<sup>-3</sup>) and its curvature in the critical points located between the metal and other atoms (ranging from 8.3 to 12.6 eÅ<sup>-5</sup>) are of great chemistry interest because they show the non-ionic character of these interactions.

Also, atomic charge integration was carried out applying topological atoms partitioning (*basins*). Differences between the fitted monopole value and the *basin* charge, integrated inside the zero flux surfaces,  $\hat{n} \cdot \vec{\nabla} \rho(\vec{r}) = 0$ , are visible for most of the atoms, the largest being the charge associated to the oxygen atom.

The authors are grateful to FAPESP for a fellowship under the process number 99/07508-0 and financial support and to Guang Wu for the data collection at NSLS, Brookhaven National Laboratory.

1. Fancchin, G, Torre, M.H., Kremer, E., Piro, O.E., Castellano, E.E., Baran, E. (2000). *Zeitschrift fur Naturforschung* 55B, 1157-1162
2. Coppens, P. (1997). X-ray Charge Density and Chemical Bond.

# PC5BIO. Desenho Racional de Inibidores Contra DHODH (Diidroorotato Desidrogenase). Aplicações no Tratamento da Doença de Chagas e da Praga do Amarelinho

*Maria Cristina Nonato*

**Departamento de Física e Química,  
Faculdade de Ciências Farmacêuticas de Ribeirão Preto (FCFRP)  
Universidade de São Paulo**

A enzima diidroorotato desidrogenase (DHODH) pertence a via de síntese *de novo* de nucleotídeo de pirimidinas, fundamental na síntese de DNA e RNA, glicólise e biossíntese de lipídios de membrana [1]. DHODH atua no quarto passo desta via metabólica e é responsável pela conversão de diidrorotato em orotato. DHODH utiliza o mononucleotídeo flavina (FMN, C<sub>17</sub>H<sub>21</sub>N<sub>4</sub>O<sub>9</sub>P<sub>1</sub>) como cofator, para promover a oxidação de diidroorotato, enquanto FMN é reduzido. A enzima DHODH foi identificada como sendo o alvo farmacológico de uma série de compostos químicos e naturais, tais como isoxazol, triazina, ácido cinchonicínico e derivados de quinona. Estes compostos interferem em reações descontroladas do sistema imune, auxiliam no combate de infecções parasitárias como malária e em terapias antivirais através da diminuição da concentração intracelular de nucleotídeos de pirimidinas [2].

No presente momento, existe um grande interesse em investigar inibidores de DHODH como agentes terapêuticos no tratamento de doenças que envolvem grande proliferação celular e/ou parasitárias. Dentro deste contexto, o presente trabalho propõe a modelagem racional de inibidores baseado na estrutura cristalográfica de dois novos membros das DHODHs: Diidroorotato desidrogenase do parasita *Trypanosoma cruzi* (TcDHODH), parasita causador da doença de Chagas, e da bactéria *Xylella fastidiosa* (XfDHODH), uma bactéria fitopatogênica responsável pela “Praga do amarelinho”. A presença da via de biossíntese *de novo* de pirimidinas em ambos os organismos foi recentemente identificada e a inibição da mesma pode ser uma importante arma no combate à proliferação desses organismos patogênicos [3,4].

## Referências

- [1] Stryer, L. (1995) *Biochemistry*, 4<sup>th</sup> Edition WH Freeman and Company, NY.
- [2] Knecht,W., Henseling, J., Loffler,M. (2000) *Chemico-Biological Int.* 124, 61-76.
- [3] Simpson, et al.(2000) *Nature* 406, 151-157
- [4] Gao, G., N. T., Nakajima-Shimada J. & Aoki T. (1999) *J. Mol. Biol.* , 285, 149-161.

# PC6INS. Study of Phase Transformations Using a Novel X-Ray Imaging Technique

Fernando Rizzo

Department of Materials Science and Metallurgy  
PUC-Rio

The study of phase transformations is central to the understanding of processes that may be employed to develop specific properties of materials. In this presentation, the observation of some solid-state reactions using a novel X-Ray Imaging technique available at the Hasylab will be presented. The MAXIM technique is based on the utilization of a position sensitive detector that allows the spatial identification of the X-ray diffracted beam, thus permitting the observation "in situ" of a phase transformation. Examples of studies of reaction in a Fe-Zn system will be shown, together with the image processing developed to analize the results. Additional examples of reactions in ceramic systems will also be presented.

# PC7MPO. The Analysis of the Measurements on a Ceria Size-Strain Round-Robin Sample

D. Balzar

University of Denver and NIST, Boulder, Colorado, U.S.A.

To assess the accuracy of the determination of domain size and lattice strain, a round robin was organized under the auspices of the Commission on Powder Diffraction. The round-robin sample (ceria powder) was synthesized at the University of Rennes. To obtain measurements under different experimental conditions in order to accurately assess the physical part of line broadening irrespective of the instrument, the sample was distributed to several laboratories: (i) University of Le Mans: a “common” x-ray laboratory setup; (ii) University of Birmingham: a high-resolution x-ray laboratory setup with an incident-beam monochromator; (iii) X3B1 beamline at NSLS: 2<sup>nd</sup>-generation synchrotron, flat-plate geometry; (iv) BM16 beamline at ESRF: 3<sup>rd</sup>-generation synchrotron, capillary geometry; (v) BT1 instrument at NCNR and D1A instrument at ILL: constant-wavelength neutron sources; (vi) HRPD instrument at ISIS: Time-of-flight neutron source. Before these measurements were made available to the round-robin participants, we analyzed them to assure the self-consistency by three methods: the model assuming a lognormal size distribution of spherical crystallites, Warren-Averbach analysis, and Rietveld refinement. The last two methods have detected a relatively small strain in the sample, as opposed to the first method. Assuming a strain-free sample, the results from all three methods agree well. The scatter of results given by different instruments is relatively small, although significantly larger than estimated standard uncertainties. The round-robin participants conducted line-broadening analysis through different routes, including integral-breadth, Fourier-deconvolution, and Rietveld-refinement methods. The round-robin results showed: (i) The ceria powder shows predominantly domain-size related isotropic line broadening; (ii) Size-broadened profile is not pure Lorentzian but has a strong Gaussian contribution; (iii) The results obtained with different methods do not vary considerably, which is probably a consequence of a strain-free specimen.

# PC8PQM. Phase Transitions and Modulated Phases in AA'BX<sub>4</sub> Compounds

Nivaldo Lúcio Speziali

Laboratório de Cristalografia - Departamento de Física - UFMG

Crystals with a common composition of the type AA'BX<sub>4</sub> have been largely studied due to the extremely rich sequence of observed phase transitions with different types of symmetry and structures. The K<sub>2</sub>SO<sub>4</sub> is one of the first studied compounds and is usually used as a reference in the discussion of transitions and structures. An important characteristic of most of the members in such a family is the presence of modulated phases and/or disordered phases and/or twinned phases. The modulation is evidenced by the presence of satellite reflections in a diffraction experiment. When the relative position of the satellites varies with temperature the modulation is incommensurate. Whereas some compounds show clear and unambiguous satellites, in some cases the existence of modulation is not so evident. The compound LiKSO<sub>4</sub> is of particular interest and has been the object of intense investigation in the last decades since it exhibits numerous phase transitions and a large variety of structural phases. Above room temperature, LiKSO<sub>4</sub> undergoes two structural phase transitions at 708 K and 943 K. The higher temperature phase (phase I), between the melting point (~1005 K) and 943 K, is isomorphic to the  $\alpha$ -K<sub>2</sub>SO<sub>4</sub> phase, symmetry P6<sub>3</sub>/mmc ( $a^I = 5.295 \text{ \AA}$ ,  $c^I = 8.706 \text{ \AA}$ ,  $Z=2$ ). The room temperature phase (phase III), stable up to 708 K, has also a hexagonal symmetry but the symmetry is P6<sub>3</sub> ( $a^{III} = 5.145 \text{ \AA}$ ,  $c^{III} = 8.634 \text{ \AA}$ ;  $Z=2$ ). Some works published by different groups using different experimental techniques reveal contradictory results in the description of the intermediate phase, i.e. for T between 708 K and 943 K (phase II). Incommensurate, commensurate and twinned models have been used to explain the observed diffraction pattern, electrical conductivity, Raman and infrared spectroscopy measurements of this crystal phase.

In an X-ray diffraction investigation of LiKSO<sub>4</sub> crystals under uniaxial pressure Ventura *et al.* [1] unambiguously confirmed the existence of three kinds of orthorhombic ferroelastic domains in intermediate phase II, oriented at 120° one to another. Careful single crystal X-ray diffraction studies at different temperatures have been recently reported by Pinheiro *et al.* [2]. In this work, several models containing structural disorder and including harmonic and anharmonic atomic displacements were tested. The proposed structure is based on the existence of three domains each one with an average orthorhombic symmetry with statically disordered SO<sub>4</sub> groups. Recently, three-dimensional maps of the diffraction peaks were obtained by scanning the neighborhood of (*h*, *k*, *l*) reflections which can be characterized as the main ones - present in phase I and III - and a new set of secondary ones. It was observed that the main reflections are split in three different peaks, each one associated with one ferroelastic domain. The secondary reflections are composed by two peaks whose separation  $\Delta$  depends on temperature. The structure of phase II is interpreted in terms of three incommensurate domains, described by the wavevector  $\mathbf{q} = (0.5 - \Delta/2) \mathbf{a}^*$ , with average orthorhombic symmetry [3].

An overview of the most important results for LiKSO<sub>4</sub> will be presented and will be used to illustrate different incommensurate, commensurate and twinned models for crystal structures.

## References:

- [1] Ventura, D. R., Speziali, N. L. & Pimenta, M. A. (1996). *Phys Rev B*, **54**, 11869-11872.
- [2] Pinheiro C.B., Pimenta M.A., Chapuis G. and Speziali N.L. *Acta Cryst.* **B56** (2000), 607-617
- [3] Ventura, D. R., Pimenta, M. A. & Speziali, N. L. (2002). *Phys Rev B* (to appear)

# PC9BIO. Dynamics and Structure of Macromolecules Involved in Human Diseases

Jerson L. Silva

Departamento de Bioquímica Médica, Instituto de Ciências Biomédicas and Centro Nacional de Ressonância Magnética Nuclear de Macromoléculas (CNRMN), Universidade Federal do Rio de Janeiro, Rio de Janeiro RJ 21941-590, Brazil

Proteins and macromolecular assemblages are held together by noncovalent interactions. In addition to the free energy of interactions, the packing among the different components plays a major role. We have used several spectroscopic techniques and structural tools (such as NMR) combined with physical and chemical perturbation to dissect the role of packing and cavities in protein folding and protein-nucleic acid interactions. With this goal in mind, we have approached several problems related to metastability of biological and medical relevance, including the conversion of proteins from native to amyloidogenic forms, the lowering in stability of the tumor suppressor p53 by mutations responsible for 50% of human cancers and the fusion of viruses with cells. High pressure has the unique property of stabilizing partially folded states or molten-globule states of a protein, which main characteristic is a higher degree of hydration (Silva et al., 2001, *Trends Biochem. Sci.* 26: 612-618). The competition between correct folding and misfolding, which in many proteins leads to formation of insoluble aggregates, is an important problem in the biotechnology industry and in human diseases such as amyloidosis, Parkinson's, Alzheimer's, prion and tumor diseases. These diseases have been grouped under the name of protein conformational disorders. The population of an amyloidogenic intermediate without proceeding to aggregation is a unique property of pressure, which opens the prospect to characterize the structure of the amyloidogenic form. Overall, the pressure results on the amyloidogenic protein transthyretin, and more recently on tumor suppressor p53 protein, alpha-synuclein (related to Parkinson's Disease) and prions suggest that stable intermediates can be achieved by carefully tuning high pressure and temperature. The isolation of these intermediates provides targets for the development of antagonists capable of blocking protein misfolding and aggregation, potential drugs against protein conformation diseases (Supported by CNPQ, PRONEX and FAPERJ).

## PC10INS. Single-Wavelength Anomalous Phasing - Importance of Data Accuracy.

Zbigniew Dauter

Synchrotron Radiation Research Section, NCI, Brookhaven Nat. Lab., USA

The currently most popular method of phasing novel macromolecular structures is the multiwavelength anomalous diffraction (MAD) approach. Recently, the interest in the single wavelength (SAD) method increases due to its simplicity and many examples suggest that the power of the SAD phasing is quite high. However, the anomalous scattering signal of atoms introduced to protein crystals or inherently present in proteins is usually small. The successful use of this signal for phasing requires the accurate measurement of the diffraction data. The recent progress in the crystallographic techniques, improved hardware and powerful software for data acquisition and phasing, makes the process of structure solution easier, faster and more automatic, but the crucial factor remains the anomalous signal to noise ratio within the collected intensities. The strategies for obtaining the diffraction data of high accuracy will be discussed and illustrated by examples of single wavelength anomalous diffraction phasing based on the signal of weak anomalous scatterers such as sulfur.

# OBIO01. Antisense Genes, Codon Bias and the Evolution of the Genetic Code

W.L. Duax<sup>1,3</sup>, A. Addlagatta<sup>1</sup>, V. Pletnev<sup>2</sup>, R. Huether and P. Yu<sup>1</sup>

<sup>1</sup>Hauptman-Woodward Institute, Buffalo, NY 14203, <sup>2</sup>Shemyakin Institute, Moscow, Russia, <sup>3</sup>SUNY at Buffalo, Buffalo, NY

The short chain oxidoreductase (SCOR) family of enzymes includes over 5000 members, extending from bacteria and Archaea to humans, for which 36 have known crystal structures and 4500 have unknown function. The superfamily has at most one fully conserved residue. The signatures of subgroups of the superfamily are composed of 30-40 residues conserved at approximately 80% identity distributed throughout the 250 aa proteins. Nucleic acid sequence analysis reveals that 21% of the SCOR genes (342/1612) have an antisense open reading frame (ORF) overlapping the entire sense gene. Furthermore 5% have a third frame shift ORF. In all cases a double ORF consists of a pair of in-frame sense/antisense totally overlapping ORF's (SASORFs). The three ORF's of a triple ORF (TORF) are always composed of the two SASORFs and a third ORF in the "sense" frame related by a double frame shift. SCOR open reading frames are never found in the frame in which the wobble base of the sense codon is in the center of the nucleic acid triple. Analysis of 260 SCOR genes having double open reading frames (DORFs) and 82 having TORFs reveals that over 85% of the 250 amino acids in the proteins encoded by these genes are coded for by the GC-rich codons. When nucleic acid triple frequency is analyzed in the two alternate frames the same codon bias is observed. [In the 260,600 nucleic acid triples in the SCOR family genes having DORFs and TORFs the frequency of appearance of GC-only triples is at least ten times that of the AT-only triples.] Examination of the population of the 32 complementary pairs of nucleic acid triples rather than 64 individual triples results in the most pronounced separation of the four classes of codons (GC-only, GC-rich, AT-rich and AT-only). In addition to the complete separation of the GC-rich and AT-rich halves of the 64 codons, there is a pattern of clustering of sets of permuted nucleic acid triples. Analysis of triple frequencies in a random collection of genes reveals no comparable bias or pattern.

The recent discovery of a 22nd amino acid (Srinivasan, G., *et al.*, *Science* **296**, 1459-1461, 2002) draws renewed attention to the fact that at least fourteen codons have different definitions in different species (Maeshiro, T. *et al.*, *PNAS* **95**, 5088-5093, 1998). The majority of the codons having variable definition are AT-only or AT-rich and have as many as four known definitions. Half of the reported variations are in the mitochondria of Eukaryotes and the other half are in bacteria and Archaea. Since we only know the genetic codes of a small percentage of all species it is highly probable that additional variations exist. The patterns thus far observed predict that further codon variation will involve primarily AT-only and AT-rich codons. Thus far none of the GC-only codons have been found to have variable definitions. Blast searches for proteins having sequence homology with the hypothetical protein product of "nonsense" SCOR ORFs reveal no fragments of more than a dozen residues with 50% conserved identity.

In 1994 LeJohn described the isolation and characterization of two proteins that were products of the sense and antisense strand of the same gene, a 1063 amino acid eukaryotic glutamine dehydrogenase and a 600 amino acid heat shock protein (*J. Biol. Chem.* **269**, 4513-4531, 1994). Co-isolation of the two proteins using a monoclonal antibody suggested that the two protein products of the same gene formed a complex that was recognized by the antibody. Seventeen codons were entirely unused in the sense/antisense overlapping open reading frames (SAS ORFs) and half of the 64 codons

are responsible for the coding of 89% of the 1282 amino acids in the protein products of the overlapping strands. Our subsequent analysis of the frequency of occurrence of SASORFs in the HSP70 family revealed the presence of DORF's in 10% (36/365) of the HSP-70 genes. Two thirds of these DORFs have the same triple bias found in the SCOR SASORFs. Over 80% of the nucleic acid triples in the genes are GC-rich. However the HSP-70 codon-use pattern differs from that of the SCORs in several important ways. Members of the HSP-70 protein family share 70-80% sequence identities. No TORFs were found in the 365 HSP-70 genes examined. A BLAST search for characterized proteins having sequence homology with the hypothetical proteins in the antisense frames consistently detected homologies with fragments of glutamine dehydrogenases, calcium binding proteins, and calcium receptors. The HSP-70 DORFs that do not exhibit the GC-rich codon bias of the SCOR family have an alternate bias best characterized as the GC-rich bias with an AT-drift. This AT-drift pattern occurs in HSP-70 proteins of AT-rich species and illustrates the role of the wobble base in the evolution of genes for specific proteins from a GC-rich to an AT-rich species. Together with Carter (Cell 10, 705-808, 2002) we have suggested that (a) the existence of SASORFs in the SCOR and HSP-70 families of proteins, (b) the *bonafide* example of a eukaryotic gene that encodes an HSP-70 and a Rossmann fold containing enzyme reported by LeJohn, and (c) the structural similarities between tRNA synthetases I and II and the Rossmann fold dehydrogenase and HSP-70s respectively, support the postulate of Rodin and Ohno (Orig. Life Evo. Biosph 25, 569-589, 1995) that tRNA synthetase I and II may have evolved from SASORFs of the same primordial gene.

One possible explanation for the conservation of 260 DORFS and 82 TORFS in the family of Rossmann folds is that the primordial member of this family was encoded so early in evolution that most productive mutational development had occurred without introduction of any codons having two or more adenine or threonine residues. It has been repeatedly demonstrated that AT-rich DNA melts at a lower temperature than GC-rich DNA. This is consistent with computational data concerning the relative stability of AT- and GC-rich DNA. It would be reasonable to assume that when the genetic code was evolving the more stable GC-only and GC-rich codons would gain and retain consistent definitions and code specific amino acids more consistently and efficiently than less stable AT-only and AT-rich codons. The fact that the majority of the codons that are least used in coding in the 82 SCOR TORFs and 260 SCOR DORFs are AT-rich and include those that have multiple definitions in different species, is consistent with such a hypothesis. The fact that the partitioning of nucleic acid of triples into subgroups that are GC-only, GC-rich, AT-rich and AT-only is much more pronounced when examined as a function of complementary pairs of triples rather than codons suggests that patterns of relative population are directly related to the relative energies of complementary pairs of triples. The patterns of relative energies of triples are less pronounced in the coding frame because the coding frame is influenced by biological factors. These and other data suggest that the SCOR families of enzymes diverged from a common ancestor that evolved before the AT-rich half of the genetic code was defined. This work is supported in part by NIH Grant No DK26546

## OBIO02. Structural Biology and Drug Design in Tropical Diseases

Oliva G.<sup>1</sup>, Garratt R.C.<sup>2</sup>, Thiemann O.H.<sup>3</sup>, Castilho M.S.<sup>4</sup>, Silva M.<sup>5</sup>,  
Trapani S.<sup>6</sup>, Pereira H.M.<sup>7</sup>, Navarro M.A.V.S.<sup>8</sup>, Silva C.T.P. da<sup>9</sup>, Silva  
M.T. da<sup>10</sup>, Vieira P.C.<sup>11</sup>, Silva M.F.F.<sup>12</sup>, Fernandes J.B.<sup>13</sup>, Corrêa A.G.<sup>14</sup>

1, 2, 3, 4, 5, 6, 7, 8, 9, 10 Instituto de Física de São Carlos oliva@if.sc.usp.br, garratt@if.sc.usp.br,  
thiemann@if.sc.usp.br, castilho@if.sc.usp.br, marcios@if.sc.usp.br, stefano@if.sc.usp.br,  
hmuniz@if.sc.usp.br, navarro@if.sc.usp.br, tomich@if.sc.usp.br, teresa@if.sc.usp.br

11, 12, 13, 14 Universidade Federal de São Carlos paulo@dq.ufscar.br, dmfs@power.ufscar.br,  
djb@power.ufscar.br, agcorrea@dq.ufscar.br

Tropical infectious and parasitic diseases represent a major burden on the health of the population in under-developed or developing countries. In several cases, there is no treatment or vaccine available, and in other diseases there is strong concern related to the occurrence of resistance. The research focus of our lab are the structural studies of parasitic enzymes, potential targets for structure based drug design, and the subsequent application of the structural information in the discovery of new specific inhibitors. The integrated experimental approach includes cloning and overexpression of the parasitic enzymes, their crystallization and X-ray crystallography studies, rational drug design, synthesis and extensive screening and testing of both synthetic and natural products compounds obtained from the Brazilian biodiversity. In this conference we will present an overview of the recent advances in the area of structure based drug design and the successes that this technique has brought into the pharmaceutical development. We will also report on our recent developments obtained with the crystal structure of the target enzyme Glyceraldehyde-3-phosphate dehydrogenase from *T.cruzi* in complex with a natural product and the subsequent design and synthesis of modifications that led to novel inhibitors. Furthermore we will present the results related to the crystallization and structure determination of other parasitic enzymes in our research group: adenine phosphorybosyl transferase (APRT) and hypoxanthine-guanine phosphorybosyl transferase (HGPRT) from *Leishmania tarentolae*, phosphoenol-pyruvate carboxykinase (PEPCK) and Fe-superoxide dismutase from *Trypanosoma cruzi*, Cu,Zn-superoxide dismutase and purine nucleoside phosphorilase from *Schistosoma mansoni* and Fe-superoxide dismutase from *Plasmodium falciparum*.

Acknowledgements: WHO (TDR grant940854), FAPESP-CEPID, The Howard Hughes Medical Institute and PRONEX-CNPq.

PBIO03. Cloning, Purification and Initial Crystallographic Data of Human Adenine Phosphoribosyltransferase (APRT): Analyses and Molecular Replacement Solution

**Iulek, J.<sup>1</sup>, Silva, M.<sup>2</sup>, Thiemann, O.H.<sup>2</sup>, Oliva, G.<sup>2</sup>**

<sup>1</sup> Chemistry Department, Universidade Estadual de Ponta Grossa, Ponta Grossa-PR, Brazil.  
"iulek@uepg.br"

<sup>2</sup> Protein Crystallography and Structural Biology Group, IFF/IFSC/USP, São Carlos-SP, Brazil.

The need for new drug chemotypes for the treatment of kinetoplastid infections comes from a lack of safe drugs and widespread resistance to some of those in current use. Their purine nucleotide salvage pathway is being used by several laboratories as a potential target for the rational drug design approach due to the parasite dependence on that biosynthetic pathway. In this way, various Phosphoribosyltransferases (PRTases) from kinetoplastid protozoa have been cloned, aiming at producing the protein for structure determination and drug candidate screening. Nevertheless, to guide the efforts towards more specific drugs against only the parasites, i.e., with less side effects for the human host, the knowledge of the corresponding homologue structure is mandatory. Therefore, we also cloned, purified and crystallized one of the human proteins, Adenine Phosphoribosyltransferase (APRT). The corresponding open reading frame was inserted in the pET29a vector (Novagen). Protein production at satisfactory amounts was achieved. Purification was accomplished by affinity purification on an AMP-Agarose column followed by size exclusion chromatography on a Superose 12 H/R column. Crystallization conditions, using the hanging drop vapor diffusion method, were assayed. Conditions number 22, 35, 45, 48 and 49 (Hampton Crystal Screen Cryo) led to the formation of crystals. Nevertheless, only condition 22 (25.5% PEG 4000, 0.085 M Tris HCl pH 8.5, 0.17 M Sodium Acetate, 15% Glycerol) provided a crystal suitable for x-ray diffraction.

Data were collected at the Protein Crystallography (CPR) station at the Laboratório Nacional de Luz Síncrotron (LNLS). The crystal diffracted up to 2.06 Å resolution. Images were processed with mosflm/scala programs. A total of 95875 reflections were merged into 11527 unique reflections, with an overall R<sub>merge</sub> = 4.0 % (11.2 % in the last shell) and 99.3 % overall completeness (97.0 % in the last shell), space group P4<sub>3</sub>2<sub>1</sub>2. Molecular Replacement models were prepared from *Leishmania tarentolae* and *Saccharomyces cerevisiae* APRT's; both led to satisfactory solutions that are currently being refined.

This work receives support from FAPESP, PRONEX and WHO/TDR grants.

## PBIO04. Small Angle X-Ray Studies of Protein-Polymer Interactions

Oliveira C. L. P.<sup>ab</sup>, Torriani I. L.<sup>ab</sup>, Almeida, N. L.<sup>c</sup>, Loh, W.<sup>c</sup>

<sup>a</sup>IFGW - Unicamp, Brazil; <sup>b</sup>LNLS, Brazil; <sup>c</sup>IQ - Unicamp

*crislpo@ifi.unicamp.br*

The interaction between biological macromolecules and non-adsorbing polymers is considered of utmost importance in the study of protein crystallization processes and in the study of a large number of protein-polymer systems or artificial surfaces used in medical procedures, in which polymeric materials are in contact with blood proteins. The structural information furnished by small angle X-ray scattering (SAXS) experiments can be used to describe protein-polymer interaction in solution mixtures considering the dispersion as a two-component system. In this work, a well known protein, lysozyme, was studied in the presence of Poly(ethylene oxide) (PEO), various EO/PO copolymers of varied composition and Poly(ethylene glycol) (PEG). Thermal stability of lysozyme was studied in the presence of these polymers. X-ray scattering experiments were performed at the SAXS beamline of the Laboratório Nacional de Luz Síncrotron, Campinas, SP, using the facility available for liquid dispersions under controlled temperature. Room temperature measurements were aimed at detecting possible polymer-protein interactions. Thermal denaturation processes were studied in some of these systems in order to check the stabilizing effect of some of the polymers used, at fixed temperatures of 25, 50, 60 and 70°C. At 80°C, using a real time data acquisition system, structural changes could be followed as a function of time in a sequence of frames that show denaturation and aggregation of the protein. Real space analysis of the intensity functions was performed using a mathematical expression derived for the form factor of a system of particles of different shapes. The pair distance distribution functions of each component of the system could be calculated separately. The possibility of complex formation in the case of the proteins studied is not supported by our results. The presence of polymers may affect the protein-protein interaction and their aggregation processes.

This work was supported by Fundação de Amparo à Pesquisa do Estado de São Paulo (FAPESP Proj. #00/15087-4), Laboratório Nacional de Luz Síncrotron (LNLS) and Conselho Nacional de Desenvolvimento Científico e Tecnológico (CNPq)

- Hirai M., Arai S., Iwase H., Takizawa T. (1997), Small-angle X-ray Scattering and calorimetric studies of thermal conformational change of lysozyme depending on pH, *J. Phys. Chem. B.* **102**, 1308-1313;
- Nolan, S. L., Ronald, J. P., Cotts, P. M., Dungan, S. R. (1997), "Light Scattering Study on the Effect of Polymer Composition on the Structural Properties of PEO-PPO-PEO Micelles"; *J. Coll. Interf. Sci.*, **191**, 291-302;
- Botelho, M. G., Gralle, M., Oliveira, C. L. P., Ferreira, S. T., "Folding and stability of the extracellular domain of the human amyloid precursor protein", work in progress;

# PBIO05. Is It Possible to Determine the Solvent Content of Protein Crystals from Diffraction Intensity Analysis?

*Napolitano, H. B.<sup>1</sup>, Trapani, S.<sup>2</sup>, Oliva, G.<sup>3</sup>*

Instituto de Física de São Carlos, USP. <sup>1</sup>hamilton@if.sc.usp.br, <sup>2</sup>stefano@if.sc.usp.br,

<sup>3</sup>oliva@if.sc.usp.br.

*Fischer, H.<sup>4</sup> Craievich, A. F.<sup>5</sup>*

Instituto de Física, USP. <sup>4</sup>hannes@if.usp.br, <sup>5</sup>craievich@if.usp.br.

An important step in protein crystal structure determination is the estimation of the crystal solvent content. It is often needed, for example, to set up a molecular replacement strategy or during solvent flattening procedures. The calculation of the crystal solvent content is commonly based on the estimation of the Matthews volume ( $V_M$ ) and its comparison with the experimental  $V_M$  statistical distribution obtained by Matthews in his classical work [1]. The estimation of  $V_M$  requires that the protein molecular weight and the unit cell volume be known, and also requires a guess of the number of protein molecules in the unit cell. This approach does not always lead to a unique choice for the number of protein molecules, particularly when this number is high.

In this work we establish a simple theoretical background — based on the Parseval theorem on Fourier transforms and the Wilson intensity statistics [2] — whereby a relationship between the sum of all experimental diffraction intensities and the number of ordered atoms in the unit cell is found. Based on these results, we propose the development of a method in order to estimate the solvent content from the analysis of the diffraction intensities. As a test of the viability of this approach, a preliminary analysis over a small sample of data taken from the Protein Data Bank is presented.

Financial support: FAPESP.

## References

- [1] Matthews, B. W. (1968). J. Mol. Biol. **33**, 491-497.
- [2] Wilson, A. J. C. (1950). Acta Crystallogr. **3**, 397-398.

## PBIO06. Estudo da Interação Entre Azul de Metileno e AOT por Espalhamento de Raios X a Baixos Ângulos

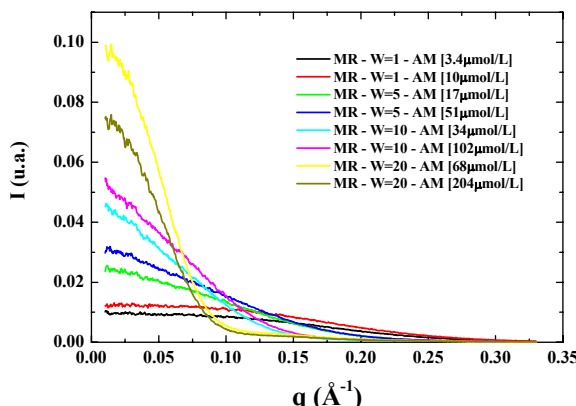
Duarte, E. L<sup>1</sup>; Severino, D.<sup>2</sup>; Baptista, M. S.<sup>2</sup>; Itri, R<sup>1</sup>

<sup>1</sup>. IF - USP – itri@if.usp.br – elduarte@if.usp.br

<sup>2</sup>. IQ - USP – baptista@quim.iq.usp.br – diseverino@yahoo.com.br

Processos de sensibilização são extremamente importantes em várias áreas incluindo a biologia, química e medicina<sup>[1]</sup>. Nesta última, tem sido muito importante especialmente em um método que vem sendo desenvolvido para o tratamento de câncer, conhecido como Terapia Fotodinâmica (PDT – *Photodynamic Therapy*)<sup>[2]</sup>. Azul de Metileno (AM) é um sensibilizador que tem sido usado *in vitro* para uma variedade de aplicações incluindo PDT. Com o intuito de investigarmos seu comportamento quando interage com sistemas biológicamente relevantes, em particular com membranas, estudamos através de medidas de Espalhamento de Raios X a Baixos Ângulos (SAXS) variações de tamanho e forma quando o AM é colocado no interior de micelas reversas (MR). Consideradas membranas modelo, MR são microemulsões de água em óleo, onde a fase aquosa é dispersa como nanogotas esféricas. Uma monocamada de moléculas surfactantes garante a estabilidade da solução através de forças de repulsão de caráter estérico. O volume interno da MR pode ser controlado pela razão das concentrações de água e surfactante na solução:  $w=[H_2O]/[AOT]$ , onde [AOT] é a concentração do *surfactante bis(2-etylhexil sulfosuccinato de sódio*.

Trabalhamos com [AOT]=0,2mol/L diluído em Iso Octano (*2,2,4 - trimetilpentano*). Fizemos soluções micelares com AM em várias concentrações e variamos o tamanho das MR de acordo com a razão  $w = 1, 5, 10$  e  $20$ . Para cada  $w$  fizemos duas concentrações de AM como mostra a curva de SAXS da figura abaixo.



Note que a intensidade para ângulos baixos aumenta com  $w$  e com a concentração de AM. A análise das curvas mostrou que as características da micela (tamanho e forma) não se alteram sob a influência da droga fotoativa, embora dados espectroscópicos<sup>3</sup> indicam variações no processo de agregação da droga na interface micelar. O aumento de intensidade em função da concentração da droga é associado a um aumento no contraste de densidade eletrônica entre a micela reversa e o solvente orgânico, revelando que o AM se localiza no meio polar aquoso.

### Referências:

- [<sup>1</sup>] V. Balzani and F. Scandola, in *Energy Resources Through Photochemistry and Catalysis*, Academic Press, New Youk, (1983).
- [<sup>2</sup>] B. W. Henderson and T. J. Dougherty, *Photochem. Photobiol.*, **55**, 145 (1992).
- [<sup>3</sup>] H.C.Junqueira et al., *Phys. Chem. Chem. Phys.*, **4**, 2320 (2002).

Pesquisa com apoio de: CNPq , FAPESP

## PBIO07. Crescimento e Controle de Tamanho de Nanopartículas Magnéticas no Interior de Micelas Reversas

Duarte, E. L.<sup>1</sup>; Itri, R<sup>1</sup>, Baptista, M. S.<sup>2</sup> e Leite, C.A.P.<sup>3</sup>

<sup>1</sup>Universidade de São Paulo, Instituto de Física – elduarte@if.usp.br – itri@if.usp.br

<sup>2</sup>Universidade de São Paulo, Instituto de Química – baptista@quim.iq.usp.br

<sup>3</sup>Unicamp, Instituto de Física – capleite@ifi.unicamp.br

Neste trabalho investigamos nanopartículas magnéticas crescidas no interior de microemulsões de água em óleo, onde a fase aquosa é dispersa como nanogotas esféricas. Na superfície destas existe uma monocamada de moléculas surfactantes que garante a estabilidade da solução através de forças de repulsão de caráter estérico. Microemulsões como estas são conhecidas como micelas reversas (MR) e estão sendo utilizadas neste trabalho como reatores na síntese de nanopartículas. O volume interno da MR pode ser controlado pela razão das concentrações de água e surfactante na solução:  $w=[H_2O]/[AOT]$  onde [AOT] é a concentração do surfactante *bis(2-etilhexil sulfosuccinato de sódio*.

Trabalhamos com uma concentração de [AOT]=0,4mol/L diluído em Iso Octano (2,2,4 - trimetilpentano). Foram sintetizadas soluções micelares com e sem nanopartículas. Chamamos de sem nanopartículas as MR formadas simplesmente com água destilada e deionizada com  $w = 5, 10, 15, 20$  e 30. As soluções com nanopartículas foram feitas adicionando FeCl<sub>2</sub> (diluído em água na concentração de 0,05mol/L) na solução de AOT variando o tamanho das MR de acordo com a razão  $w = 5, 10, 15, 20$  e 30. Com o objetivo de formar nanopartículas magnéticas compostas de magnetita (Fe<sub>3</sub>O<sub>4</sub>) no interior das MR, adicionamos a estas soluções micelares outras contendo NaOH (também diluído em água 0,2mol/L) com os respectivos  $w_s$  mencionados. O tamanho das MR com e sem nanopartículas magnéticas foi obtido através da técnica de Espalhamento de Raios X a Baixos Ângulos (SAXS) no Laboratório de Cristalografia do IFUSP. Observamos que a dimensão máxima ( $D_{max}$ ) das micelas aumenta linearmente com o  $w$  até  $w=20$ . Entre os  $w_s$  20 e 30 o aumento não é expressivo. Este comportamento já é conhecido na literatura<sup>[1-3]</sup>. Na seqüência deste trabalho realizamos a extração das nanopartículas magnéticas do interior da MR com o intuito de caracterizá-las quanto ao tamanho e composição. Todo o processo de extração<sup>[4]</sup> consistiu nas seguintes etapas:

- a solução micelar com nanopartículas passou por um processo de redução de volume com a evaporação do solvente (Iso Octano). No final deste processo obteve-se um gel muito viscoso e escuro;
- o gel concentrado foi diluído em álcool etílico e centrifugado. Este processo foi repetido por três vezes para remover o surfactante. Finalmente, o pó resultante foi misturado com acetona para agilizar a secagem feita em uma câmara de vácuo com sílica gel.

As técnicas utilizadas para a caracterização foram a Difração de Raios X (DRX) e Microscopia Eletrônica de Transmissão (TEM). Mais detalhes sobre os resultados e técnicas serão apresentados durante o encontro.

### Referências:

[<sup>1</sup>] J. Yano, H. Furedi-Milhofer *et al.*, Langmuir, 16, 9996 (2000).

[<sup>2</sup>] M.P. Pilani; J. Phys. Chem., 93, 6961 (1993).

[<sup>3</sup>] M.P. Pilani, L. Motte and F. Billoudet; J. Phys. Chem., 99, 16425 (1995).

[<sup>4</sup>] C. Liu, B. Zou *et al.*; J. Phys. Chem. B, 104, 6, 1141 (2000).

Pesquisa com apoio de:

CNPq

## PBIO08. Estudo do Efeito de Íons da Série de Hofmeister em Sistemas Micelares.

V. P. Barros\*, R. Itri\*, F. Casallanovo\*\*, S. Schreier

\* Instituto de Física da USP

\*\*Instituto de Química da USP

Neste trabalho investigamos a influência que alguns íons da série de Hofmeister tem sobre as características estruturais de micelas zwiteriônicas de 3-(N-Hexadecil-N,N-dimetilamônio) propanosulfonato (HPS) e aniónicas de dodecil sulfato de sódio (SDS), ambas formadas em sistemas aquosos com concentração de 100 mM de surfactante. As técnicas utilizadas foram espalhamento de Raios – X a baixos ângulos (SAXS) e espalhamento dinâmico de luz (DLS). Os ânions estudados são classificados como caotrópicos (mais fracamente hidratados): cloreto ( $\text{Cl}^-$ ), tiocianato ( $\text{SCN}^-$ ), fosfato ( $\text{H}_2\text{PO}_4^-$ ) e perclorato ( $\text{ClO}_4^-$ ); e cosmotrópico (mais fortemente hidratado): sulfato ( $\text{SO}_4^{2-}$ ), tendo sido adicionados à solução na forma de seus respectivos sais de sódio.

Micelas de HPS na ausência de eletrólito podem ser representadas por pequenos elipsóides prolatos de revolução (anisometria  $v \approx 1,5$ ), com a menor dimensão do interior hidrofóbico ( $R_{\text{par}} \approx 21 \text{ \AA}$ ) compatível com o tamanho da cadeia estendida de hidrocarbonetos (contração de cerca de 10 %) e espessura da camada dipolar  $\sigma \approx 8 \text{ \AA}$ , de acordo com os resultados de SAXS. A presença dos ânions caotrópicos (até 2 M) na solução aquosa não altera de maneira significativa as características intramicelares ( $R_{\text{par}}$  e  $\sigma$ ), mas induz um certo crescimento micelar:  $v \approx 1,8$  com a adição de  $\text{Cl}^-$  e  $\text{SCN}^-$  e  $v \approx 2,0$  no caso do  $\text{ClO}_4^-$ , independente da concentração de sal. No caso do íon  $\text{H}_2\text{PO}_4^-$ , a micela de HPS cresce ( $v \approx 2,0$ ) a 0,5 M de eletrólito e sofre uma transformação de forma esferoidal – cilíndrica na presença de 1 M de sal. Valores de diâmetros hidrodinâmicos obtidos com DLS concordam com as dimensões observadas por SAXS, com exceção do sistema micelar na presença de  $\text{ClO}_4^-$  aonde foi notado, através de medidas de reologia, um comportamento não-newtoniano das soluções micelares. Os resultados de SAXS indicam também uma partição seletiva dos ânions na camada dipolar zwiteriônica na sequência  $\text{H}_2\text{PO}_4^- > \text{SCN}^- > \text{Cl}^-$ . Tal afinidade com a camada dipolar deve ser mediada por forças de solvatação e formação de par iônico entre os ânions e os grupos  $\text{NH}_3^+$  que residem próximos à interface polar/apolar da micela zwiteriônica.

A adição de 0,5 M de  $\text{Na}_2\text{SO}_4$  na amostra de HPS favorece a formação de agregados maiores ( $v \approx 2,4$ ) em geometria cilíndrica, provavelmente originada pela adsorção de íons  $\text{Na}^+$  na superfície externa da micela, uma vez que o ânion  $\text{SO}_4^{2-}$  por ser cosmotrópico prefere residir no meio aquoso do que na camada dipolar micelar.

No caso de micelas de SDS, os resultados de SAXS evidenciam que estas também podem ser representadas por pequenos elipsóides prolatos ( $v \approx 1,6$ ), com  $R_{\text{par}} = 16,7 \text{ \AA}$  compatível com o tamanho da cadeia estendida e  $\sigma \approx 7 \text{ \AA}$ . A adição de  $\text{NaCl}$ ,  $\text{NaSCN}$ ,  $\text{NaH}_2\text{PO}_4$  e  $\text{NaClO}_4^-$  (até 0,50 M) não altera as características intramicelares, com um pequeno aumento na anisometria micelar e expansão da camada polar. Esta deve ser consequência do fenômeno de condensação de cátions  $\text{Na}^+$  na superfície das micelas aniónicas. Não foi observada nenhuma tendência à ligação de ânions nestas micelas. Os resultados de DLS confirmaram estas conclusões. A presença de 0,50 M de sulfato de sódio em micelas de SDS induz, possivelmente, uma transição de forma micelar esferoidal – cilíndrica.

## OBIO09. The Active Site Loop in the Rabbit Muscle TIM Structure: a Closed Conformation is Observed in the Absence of Ligands.

*Aparicio, R. (a), Ferreira, S. T. (b) e Polikarpov, I. (c)*

*(a) Universidade Estadual de Campinas - UNICAMP, aparicio@if.sc.usp.br*

*(b) Lab. Nacional de Luz Síncrotron - LNLS, Campinas/SP e UFRJ/RJ, ferreira@lnls.br*

*(c) Universidade de São Paulo - USP/IFSC - São Carlos/SP, ipolikarpov@if.sc.usp.br*

Triose phosphate isomerase (TIM) catalyzes the interconversion of GAP and DHAP in the glycolitic pathway. A dimer of identical subunits is the physiologically active species. The active site loop of triose phosphate isomerase exhibits a hinged-lid motion, alternating between the two well defined open and closed conformations. Until now, the closed conformation had been observed only in complexes with substrate analogues.

Three crystallographic structures of rabbit muscle TIM have been determined in two crystal forms. The highest resolution structure, refined to 1.5 Å, is the first native TIM structure in which one of the active site loops is in the closed conformation. Additives used during crystallization (DMSO and TRIS molecules and Mg atoms) were modeled in the electron density maps, however no specific binding of these molecules is observed in the regions at or close to the active site and the lid loop. Structural comparisons show that this unusual closed conformation can not be explained by the crystal contacts. To rationalize why the active site loop is closed in the absence of ligand, extensive comparison with the existing TIM structures was carried out, supported by the bulk of available experimental information about enzymatic kinetics and reaction mechanism. The simultaneously observed open and closed conformation of the chemically homogeneous TIM population might be directly related to a conformational heterogeneity of TIM in solution.

PBIO10. Influence of Bovine Serum Albumin (BSA) on the Size of Aerosol-OT/n-hexane/water Reversed Micelles Investigated by Small Angle X-ray Scattering.

*Caetano W., Duarte, E. L., and Itri, R.*  
Instituto de Física - USP, São Paulo

wilker@if.usp.br, elduarte@if.usp.br and itri@if.usp.br

In this work, the structural features of Aerosol-OT/hexane/ reversed micelles (RM) in three stages of micellar hydration at  $W=10$ ,  $20$  and  $30$  (= [phosphate buffer, pH 7.15]/[AOT]), and in the presence of the model-protein BSA (from  $7$  up to  $80\text{mg/ml}$  stock) were monitored by small angle x-ray scattering (SAXS). The studies in these protein-amphiphilic systems concern new developing in biocatalysis, bioseparations and to mimetize the interface water-biomembrane providing specific protein-membrane interaction information. In this case, the RM of the anionic AOT (sodium bis-2-ethylhexyl sulfosuccinate) constitute a suitable system to the study of the physico-chemical behaviour of biological macromolecules kept over controlled water environment. The analysis of the results [1-3] has revealed that the RM posses spherical shape with size-polidispersity of  $20$  -  $25\%$ , and the influence of the protein on RM properties was just sensed at high BSA concentrations and for large values of  $W$ . In this context, the RM radius of gyration  $R_g$  decreases from c.a.  $42$  to  $33\text{\AA}$  at  $W=30$  and from  $33$  to  $29\text{\AA}$  at  $W=20$ , respectively, whereas the  $R_g$  increases slightly at  $W=10$  ( $20$  to  $23\text{\AA}$ ) upon BSA incorporation ( $60$ - $80\text{mg/ml}$  stock) within the uncertainties. The RM SAXS and  $p(r)$  curves amplitude in the presence of BSA has presented a decrease of the intensity attributed mainly to a change in the electronic contrast density due the presence of the protein attached to the RM interface. Furthermore the presence of higher BSA levels induces the appearance of attractive intermicellar forces in the system, evidenced by the significant increasing in the RM averaged hydrodynamic radius in the presence of BSA, evaluated from dynamical light scattering (DLS) measurements. The secondary and tertiary structure of the protein have been monitored by circular dichroism and fluorescence spectroscopy and will be discussed complementing the SAXS results.

Support and acknowledgments: Brazilian agencies FAPESP (through contracts N°. 98/02757-0 and 01/02147-1), CNPq, IF-USP (Crystallography research Group) and IQ-USP.

References:

1. A.Guinier, G.Fournet, Small Angle Scattering of X-Rays; John Wiley and Sons: New York, 1955; Chapter 6.
2. O.Glatter. Data treatment. In Small Angle X-ray Scattering. O. Glatter and O. Kratky, editors. Academic Press, London. 119 -196 (1982).
3. R. Itri, C.L.C. Amaral and M.J. Politi. Journal of Chemical Physics v.111, n.16, 7668-7674 (1999).

**PBIO11. Interaction of the Iron–TetramethylpiridylPorphyrin (FeTMPyP) with DNA as Studied by X-ray Absorption Spectroscopy (XANES and EXAFS).**

*Caetano W.<sup>1</sup>, Duarte E.L.<sup>1</sup>, Scopel W.W.<sup>1</sup>, Itri R<sup>1</sup>, Gandini S.C.M<sup>2</sup>, Almeida L.E.<sup>2</sup>, Tabak M.<sup>2</sup>*

<sup>1</sup> Instituto de Física - USP, São Paulo

<sup>2</sup> Instituto de Química de São Carlos - USP, São Carlos,SP.

wilker@if.usp.br, elduarte@if.usp.br, wscopel@if.usp.br, itri@if.usp.br and  
mtabak@sc.usp.br.

The biological efficacy of porphyrin and their derivatives (PPh) depends significantly on their physico-chemical properties, which are in turn strongly affected by the phenomenon of aggregation [1-3]. For example, the porphyrin aggregate formation may lead to changes in their photochemical properties affecting the production of singlet oxygen, an essential step for the use of porphyrins in PDT (Photodynamic Therapy) of cancer. The interaction of PPh with DNA has a considerable interest due to its potential biomedical application in PDT, and since in the organism DNA constitutes an important target [1,2]. This work was undertaken in order to get a better understanding of the characteristics of the binding of FeTMPyP to DNA, specially in the aggregate state, by using XAS (XANES and EXAFS). XAS measurements were carried out at XAS beam line of the LNLS light source (Campinas, Brazil), at room temperature, using a Si(111) double-crystal monochromator. Samples were prepared from aqueous phosphate 5mM buffer solution of the porphyrin at 5 and 10 mM, pH 6.8, followed by addition of DNA (5 and 10 mM) to make a ratio of DNA/PPh of 1:1 or 3:1. XANES spectra has showed a typical spectrum for Fe(III) for pure solid FeTMPyP, and addition of imidazole to the pure porphyrin and to the Fe(III) porphyrin-DNA complexes provided very reticent changes in the XANES peaks, when compared to the pure FeTMPyP and FePO<sub>4</sub> patterns. Fourier transform of the EXAFS spectra has showed mainly an increase in the amplitude of FeTMPyP-Imidazole of a factor 6/4 according to the appearing of additional two next nitrogen neighbors related to the pure FeTMPyP porphyrin. In the case of the FeTMPyP bounded to DNA at several porphyrin-DNA ratio, it was observed a similar decrease in the spectra amplitude without a noticeable shift in their apparent distance of the the first vicinity iron-nitrogen and/or oxygen (1.85Å) related to the pure porphyrin. In this last case an increase in the Debye-Waller factor was also simultaneously detected. The results showed that the porphyrin should interact strongly with DNA through binding, with a significant contribution on angular distortion degree in the bonds around the Fe-porphyrin neighborhood.

Support and acknowledgments: Brazilian agencies FAPESP, CAPES, CNPq, LNLS (National Synchrotron Light Laboratory, Campinas, Brazil,rought project XAS 400/98 and facilities).

**References:**

1. R.F. Pasternack et al., Science 269 (1995) 935.
2. R.F. Pasternack et al., Biophys. J. 75 (1998) 1024.
3. S.C.M. Gandini et al., J. Inorg. Biochem. 73 (1999) 35.

FICHA DE INSCRIÇÃO

## PBIO12. Sulfur Phasing Using Cu-K $\alpha$ Radiation from Rotating Anode

Ambrosio, A. L. B.<sup>1</sup>, Nagem, R. A. P.<sup>2</sup>, Rojas, A. L.<sup>1</sup>, Navarro, M. V. A. S.<sup>1</sup>, Golubev, A. M.<sup>3</sup>, Garratt, R. C.<sup>1</sup> & Polikarpov, I.<sup>1</sup>

<sup>1</sup> CBME/IFSC/USP, São Carlos, Brazil; <sup>2</sup> LNLS, Campinas, Brazil; <sup>3</sup> Petersburg Nuclear Physics Institute, Gatchina, St. Petersburg, Russia

The crystal structure of a class II Lys49-PLA<sub>2</sub>, from the venom of *Agkistrodon contortrix laticinctus* snake, was solved at 1.61 Å through the SAD method using the anomalous signal from sulfur atoms. This protein is a typical enzyme from a large and well-studied family of phospholipases A<sub>2</sub>. The native monomer contains 14 cysteines (7 disulfide bonds) and 2 methionines among 121 amino acids residues. A total of 359 diffraction images ( $\Delta\phi = 1^\circ$ ) were collected from a single native P4<sub>1</sub>2<sub>1</sub>2 crystal ( $\sim 0.8 \times 0.8 \times 0.8$  mm) at 100 K using a RIGAKU ultraX 18 Cu-K $\alpha$  rotating anode and a MAR345 dtb image plate detector. A single data set, 99.8% complete, was obtained after processing and scaling all images treating Friedel related reflections separately. The expected anomalous signal was about 1.54%. The anomalous differences were used for sulfur site search. Apart from the 16 protein sulfur atoms, one unexpected sulfur atom was obtained. After phase calculation using the native data set and the 17 sulfur sites, a density modification protocol was performed. The modified phases were used to generate an electron density map that was used for automatic model building. A hybrid model, 90% complete, was obtained after a few cycles of automatic model building. Inspection of this model and the resulting electron density map revealed that the seventeenth sulfur site was related to an ordered sulfate ion held by polar hydrogen-bonds with protein side-chain atoms. Comparison of four data sets processed with different total  $\varphi$  rotation (90°, 180°, 270° and 360°) showed that correct estimation of anomalous differences and their uncertainties were crucial for solving the structure.

PBIO13. Molecular Characterization and Preliminary Structural Studies of  
*Leishmania major* Purine Salvage Enzyme Adenylosuccinate Lyase - ADSL

Mantovani, M.<sup>1</sup>; Pedrosa, A.L.<sup>2</sup>; Cruz, A.K.<sup>2</sup>; Aguilar, C.F.<sup>3</sup> & Thiemann, O.H.<sup>1</sup>

1- *Laboratory of Protein Crystallography and Structural Biology, IFSC-USP, Av. Trabalhador Säocarlense 400, PO Box: 369, 13566-590, São Carlos/SP, Brazil.*  
Email:monique@if.sc.usp.br

2- *Department of Cellular and Molecular Biology, FMRP-USP, Av. Bandeirantes, 3900, 14040-904, Ribeirão Preto/SP, Brazil.*

3-*Laboratory of Structural Molecular Biology, Department of Chemistry, Biochemistry and Pharmacy, National University of San Luis, Av Ej. de los Andes 950 (5700) San Luis, Argentina.*

Many species of *Leishmania* are responsible for serious visceral or skin diseases that show high incidence in tropical and subtropical regions. Since these parasites are auxotrophs to purine nucleotides, they have developed a specific set of enzymes involved in the purine nucleotide salvage pathway that allows them to get the purines from their host. The enzyme adenylosuccinate lyase (ADSL) plays an important role in this pathway, representing a potential target for the design of inhibitors used in the treatment of leishmaniasis. This work aims to characterize the ADSL gene and the structure of ADSL enzyme from *Leishmania major* Friedlin. Restriction analysis and Pulse Field Gel Electrophoresis (PFGE) followed by Southern hybridizations showed that ADSL is a single copy gene and is located in the chromosome 5 of this parasite. The open reading frame of ADSL identified from the *L. major* genome effort was amplified by the Polymerase Chain Reaction (PCR) and cloned into an expression vector (pCR-TOPO/T7). After transformation into *Escherichia coli* BL21(DE3) pLyS, the expression of the recombinant ADSL was induced with 0.1mM IPTG. SDS-PAGE analysis of the protein content of induced cultures showed the presence of a protein band of the expected size. A purification protocol of the recombinant enzyme was established and initial crystallization trials resulted in several crystals. Preliminary X-ray studies showed that crystals belong to a tetragonal crystal system and diffract to medium resolution. Crystallization strategies are being refined to obtain high quality ADSL crystals as required for high resolution structural studies.

Work supported by: FAPESP, HHMI, WHO/TDR, PRONEX and the University of São Paulo

## OFFN01. Local Structure in Strained Manganite Thin Films

Souza-Neto N. M., Laboratório Nacional de Luz Síncrotron, Brazil,

[narcizo@lnls.br](mailto:narcizo@lnls.br)

Ramos A. Y., Laboratório Nacional de Luz Síncrotron, Brazil, [aramos@lnls.br](mailto:aramos@lnls.br)

Tolentino H. C. N., Laboratório Nacional de Luz Síncrotron, Brazil, [helio@lnls.br](mailto:helio@lnls.br)

Ranno L., Laboratoire Louis Néel, France, [ranno@grenoble.cnrs.fr](mailto:ranno@grenoble.cnrs.fr)

Materials showing the Colossal-Magnetoresistance effect have attracted considerable interest due to potential for technological applications. Mixed manganite thin films have received special attention due to their potential for construction of new generation magneto-electronic devices. The study of these materials can establish an explicit connection between local structure and global properties. However it is not yet perfectly known how the substrate induced strain affects the local structure and the magnetism and transport properties. [1,2].

We report on X-ray absorption study of  $\text{La}_{0.7}\text{Sr}_{0.3}\text{MnO}_3$  films, epitaxially grown by laser ablation on tensile ( $\text{SrTiO}_3$ ) and compressive ( $\text{LaAlO}_3$ ) substrates. Data were collected at D04B-XAS1 and D08A-SGM beamlines of LNLS for Mn K and  $\text{L}_{2,3}$  edges. In-plane and out-of-plane information was obtained by setting the angle between electric field vector of the incident photon beam and film surface to values close to 0 degrees and 90 degrees respectively.

XANES analysis shows modifications on  $\text{MnO}_6$  octahedra, with opposite directions for tensile and compressive films. This result has been confirmed by EXAFS in the case of tensile substrate, where the average MnO distance increase/decrease according to substrate induced strain.

We also report on *ab initio* XAS simulations in structures for different strain and polarization setups. The best structural choice to account for a tensile or compressive contribution is the model of distorted  $\text{MnO}_6$  average octahedra.

Analysis of polarization contributions of EXAFS spectra shows a very small increase on Mn-Mn bond length in the film plane for tensile substrate with respect to a relaxed film. Correlatively with MnO modifications, this indicates that there are no significant modifications of the Mn-O-Mn angle.

All these results indicate that the strain should be principally accommodated in the film plane by cooperative distortion of the  $\text{MnO}_6$  octahedra.

- [1] Miniotas, A., Vailionis, A., Svedberg, E.B. and Karlsson, U.O., *J.Appl. Phys.* 89, 2134-2137 (2001)..
- [2] Qian, Q., Tyson, T.A., Kao, C.-C., Prellier, W., Bai, J., Biswas, A. and Green, R.L. *Phys. Rev. B* 63, 024430 (2001).
- [3] A.Y. Ramos, N.M. Souza-Neto, C. Giacomelli, H.C.N. Tolentino, E. Favre-Nicolin, L. Ranno, *AIP Conf. Proc.*, 652 (2003) 456-461.

Acknowledgments : CAPES, FAPESP (1999/12330-6), CNPq

## OFFN02. Electrochromism in Au-NiO Films

Ferreira, F.F.; Haddad, P.S.; Fantini, M.C.A.; Brito, G.E.S.

Instituto de Física, USP

furlan@if.usp.br; phaddad@if.usp.br; mfantini@if.usp.br; gbrito@if.usp.br

Electrochromic materials exhibit significant, reversible optical absorption at visible wavelengths when controlled electrochemically [<sup>i</sup>].

Among the electrochromic materials, nickel oxide is one of the best for applications in display devices, smart windows, batteries and gas sensors due to its high stability under cycling [<sup>ii</sup>]. Nickel oxide is an anodic coloring material that changes color from light gray to dark brown.

It is known that the incorporation of metallic particles in transition metal oxide films alters the optical absorption in the visible region [<sup>iii</sup>].

Theoretical studies were carried out and proved that Au-NiO films have selective absorption in the visible region [<sup>iv</sup>]. Different from the original NiO, transmitted/reflected colors were obtained by the addition of gold nanoparticles inside the oxide matrix [<sup>v</sup>].

Different methods of deposition are used to deposit composite films. Among them, sputtering, sol-gel, dip coating and spin coating are the most utilized.

The aim of this work is to characterize electrochemically composite gold-nickel oxide films obtained by three different methods: (*i*) sputtering, (*ii*) sputtering + sol-gel and (*iii*) sol-gel and dip coating. (*i*) The Au-NiO films were deposited by reactive *dc* magnetron sputtering from Au and Ni targets in an Ar + O<sub>2</sub> atmosphere in multi-layered deposition steps; (*ii*) by combination of sputter-deposited nickel oxide films and gold nanoparticles, deposited by the sol-gel and dip coating methods (*iii*) and also, the gold-nickel oxide films were prepared by sol-gel and dip coating in a multi-layered process.

The simultaneous measurements of the I vs. V plot and spectral transmission of the films, cycled in a 0.1M KOH solution, were recorded with an optical fiber spectrometer (Dual Fiber Optic Spectrometer, S2000 Series) equipped with a DT-1000 Deuterium Tungsten Source from Ocean Optics. The scanning rate was 10 mV·s<sup>-1</sup> and the spectra were taken every 20 seconds, after ten stabilization anodic/cathodic cycles.

The cyclic voltammetry measurements showed that all the samples did not have a significant electrochemical activity under the initial intercalation/de-intercalation cycles. With increasing number of cycles, there was a constant increase in the number of species intercalated/de-intercalated in the films.

The charge capacity of the NiO<sub>x</sub> film deposited by the sol-gel method is much larger than that presented by the NiO<sub>x</sub> film deposited by sputtering. This difference can be associated to the larger porosity and crystalline structure of the material deposited by the sol-gel method. The sputtered films are polycrystalline, while the ones deposited by sol-gel and dip coating are amorphous.

The particle sizes were estimated by SAXS measurements and confirmed by TEM experiments [<sup>vi</sup>].

Therefore, the color of Au-NiO<sub>x</sub> films can be tailored by the use of pre-determined growth conditions.

### Referências

- [<sup>i</sup>] T. Oi, Ann. Rev. Mater. Sci. 16 (1986) 185.
- [<sup>ii</sup>] C.A. Vincent, F. Bonion, M. Lizzari, B. Scrosati, *Modern Batteries*, Edward Arnold, London, 1987.
- [<sup>iii</sup>] S. Toyama, O. Takei, M. Tsuge, R. Usami, K. Horikoshi, S. Kato, Electrochim. Commun. 4 (2002) 540.
- [<sup>iv</sup>] F.F. Ferreira, M.C.A. Fantini, A. Gorenstein, Solid State Ionics (*in press*).
- [<sup>v</sup>] F.F. Ferreira, P.S. Haddad, M.C.A. Fantini, G.E.S. Brito, Solid State Ionics (*submitted*).
- [<sup>vi</sup>] P.S. Haddad, F.F. Ferreira, G.E.S. Brito, M.C.A. Fantini, J. Sol-Gel Sci. Technol. (*submitted*).

PFFN03. *In-Situ* X-Ray Diffraction of NiO<sub>x</sub> Films Deposited on Be Substrate

Sánchez M.A.E\*, Fantini M.C.A

*Instituto de Física, USP*

espinoza@if.usp.br, mfantini@if.usp.br

NiO<sub>x</sub> is widely studied due to its electronic/ionic intercalation ability [1]. In the present work we deposited NiO<sub>x</sub> films on Be and indium tin oxide (ITO)/glass substrates, using reactive RF sputtering. The films over Be are suitable for back-incidence X-ray diffraction experiments during *in-situ* electrochemical cycling. The films have thickness around 300 nm and were grown at room temperature, 200°C and 300°C. The samples were galvanostatically cycled more than five times to stabilize their electrochemical response, prior to structural analysis. Experiments of Rutherford Back scattering (RBS) spectroscopy showed an [O/Ni] = 1,05 composition ratio in pristine samples and a thickness of 380 nm. All the X-ray diffraction experiments utilized Ni-filtered Cu-K $\alpha$  radiation (1.2 kW) and Bragg-Brentano geometry. *In-situ* X-ray diffraction experiments were done in a hermetic steel cell, using 0.1M KOH electrolyte and Pt as counter-electrode. *Ex-situ* X-ray diffraction measurements of films in colored and bleached states were also performed, after cycled in galvanostatic and potentiostatic conditions.

The diffractogram of the sample deposited at room temperature shows only a weak diffraction peak at the (111) cubic NiO angular position, demonstrating that the material has a poor degree of crystallinity. The Lorentzian fit of the diffraction profile exhibits an enlargement of the (111) peak width of the film at the bleached state, indicating an increase of stress under hydrogen intercalation, regardless any shift in the peak's angular position. After some cycles the film cracked as a consequence of mechanical stress.

The films deposited at 200°C and 300°C are more crystalline and, they do not present any variation of lattice parameter at colored and bleached states when deposited on top of Be. This behavior is attributed to the substrate, which does not allow free contraction/expansion of the NiO<sub>x</sub> film on it. On the other hand, films deposited on ITO + glass substrates show a negative shift of the lattice parameter from bleached to colored states. The cyclic voltammetries revealed that oxidation and reduction process indeed occur in both substrates, and that the film deposited at 200°C has ten times more charge density capacity than the one deposited at 300°C. This charging difference is due to the material's structural and morphological properties.

\*CNPq

[1] P.M.S. Monk, R.J. Mortimer, D.R. Rosseinsky, *Electrochromism: Fundamentals and Applications*, VCH Verlagsgesellschaft, (1995).

## PFFN04. Preparação e Caracterização de uma Vitrócerâmica Obtida a Partir do Sistema Ternário BaO-B<sub>2</sub>O<sub>3</sub>-TiO<sub>2</sub>, Contendo a Fase B-BBO

*Feitosa, C. A. C.<sup>a</sup>, Zanatta, A. R.<sup>b</sup>, Mastelaro, V. R.<sup>b</sup>*

<sup>a</sup> Universidade Federal do Maranhão, carneiro@if.sc.usp.br

<sup>b</sup> Instituto de Física de São Carlos, Universidade de São Paulo

Neste trabalho estudamos a devitrificação superficial do vidro ternário ( $x_1\%$ )TiO<sub>2</sub> - ( $x_2\%$ )BaO - ( $x_3\%$ )B<sub>2</sub>O<sub>3</sub>, para a preparação controlada de vitrócerâmicas contendo a fase cristalina  $\beta$ -BaB<sub>2</sub>O<sub>4</sub> ( $\beta$ -BBO). O objetivo do trabalho é determinar como a concentração do titânio interfere nas fases cristalizadas e na cinética de cristalização isotérmica do processo de devitrificação. Preparamos vidros com três percentagens molares diferentes de TiO<sub>2</sub> ( $x_1\% = 4\%, 8\% \text{ e } 15\%$ ), mantendo fixa a relação entre as percentagens molares de BaO e B<sub>2</sub>O<sub>3</sub> ( $x_2\% / x_3\% = 8/9$ ). Os vidros foram preparados por fusão dos óxidos em cadiño de platina num forno resistivo. Amostras dos vidros, polidas mecanicamente, foram submetidas a um tratamento térmico para a obtenção das vitrócerâmicas. O grau de cristalização das vitrócerâmicas é controlado pela temperatura e o tempo de tratamento. As amostras foram tratadas em 620°C, por tempos de 1h até 20h. As amostras foram caracterizadas pelas técnicas de análise térmica diferencial, difratometria de raios-x, espectroscopia Raman, microscopia eletrônica de varredura e microscopia óptica. Neste estudo observamos que, a função do Titânio é diminuir a taxa de cristalização, as vitrócerâmicas preparadas apresentam a camada cristalizada orientada, a fase cristalina presente nas vitrócerâmicas foi  $\beta$ -BaB<sub>2</sub>O<sub>4</sub> ( $\beta$ -BBO) e apresentam o efeito de geração de segundo harmônico evidenciado.

**PFFN05. Síntese e Caracterização de Filmes da Fase  $\beta$ -BaB<sub>2</sub>O<sub>4</sub> a Partir da Composição 48BaO-48B<sub>2</sub>O<sub>3</sub>-4TiO<sub>2</sub> Depositados Por Evaporação por Feixe de Elétrons.**

*Maia, L.J.Q.\*; De Vicente, F.S.; Zanatta, A.R.; Mastelaro, V.R.; Siu Li, M.*

*Instituto de Física de São Carlos – Universidade de São Paulo*

*\*e-mail: lauro@if.sc.usp.br*

A fase beta borato de bário ( $\beta$ -BaB<sub>2</sub>O<sub>4</sub> ou  $\beta$ -BBO) é um material importante para aplicações em óptica não-linear nas regiões do visível e ultravioleta<sup>1</sup>. Recentemente, a preparação de filmes finos de  $\beta$ -BBO tem recebido grande atenção por suas aplicações em dispositivos ópticos integrados, as aplicações na forma de filmes finos são conversores e moduladores de frequência em guias de onda e chaveadores em avançados sistemas de óptica integrada<sup>2-3</sup>. Este trabalho consiste em sintetizar e caracterizar filmes de  $\beta$ -BBO depositados sobre substratos de safira(0001), quartzo z e MgO(100) utilizando o método físico evaporação por feixe de elétrons. Como fonte de deposição, utilizou-se uma amostra na forma de pastilha tratada à 500°C/5h obtida do pó cerâmico contendo a fase  $\beta$ -BBO sintetizado pelo método dos precursores poliméricos modificado a partir da composição 48BaO.48B<sub>2</sub>O<sub>3</sub>.4TiO<sub>2</sub>. Durante a deposição dos filmes os substratos foram mantidos sob aquecimento à 650°C e após a deposição foram mantidos aquecidos à 650°C por aproximadamente 30 minutos. Na caracterização destas amostras foram utilizadas as técnicas de difratometria de raios-X ( $\theta$ -2 $\theta$ ), espectroscopia Raman e microscopia de força atômica. Os filmes depositados sobre substratos de safira (0001) e quartzo (001) apresentaram-se policristalinos com rugosidades de 1,3nm e 0,9nm, respectivamente. As espessuras estão entre 1,5 $\mu$ m e 1,9 $\mu$ m. O substrato MgO(100) favoreceu o crescimento preferencial do plano (006) com grau de orientação preferencial de 0,88 comparável ao de outros filmes encontrados na literatura. Os filmes geraram o segundo harmônico da luz a 1064nm do laser Nd:YAG pela emissão de luz verde à 532nm. A eficiência de geração de segundo harmônico dos filmes é comparáveis ao do quartzo (010) monocrystalino.

Palavras-chave:  $\beta$ -BaB<sub>2</sub>O<sub>4</sub>, filmes finos, evaporação por feixe de elétrons.

Os autores agradecem a FAPESP pelo suporte financeiro.

- [1] C.T. Chen, B.C. Wu, A.D. Jiang e G.M. You, *Scientia Sinica B* 28 (3) 235-243 (1985).
- [2] P. Becker, *Advanced Materials* 10 (13) 979-992 (1998).
- [3] T. Yogo, K. Kikuta, K. Niwa, M. Ichida, A. Nakamura e S.I. Hirano, *J. of Sol-Gel Sci. and Technol.* 9 (2) 201-209 (1997).

## OPQM01. Supramolecular Associations *via* Intermolecular Secondary Interactions in Dimethyl – Thallium Complexes.

Sauli Santos-Jr<sup>a</sup>, Eduardo E. Castellano<sup>a</sup>, Javier Ellena<sup>a</sup>, Mónica Toma<sup>c</sup>, José S. Casas<sup>b</sup>, María S. García-Tasende<sup>b</sup>, Agustín Sánchez<sup>b</sup> and, José Sordo<sup>b</sup>.

<sup>a</sup>Departamento de Física e Informática, Instituto de Física de São Carlos, Universidade de São Paulo, Caixa Postal 369, CEP – 13560-970 São Carlos, SP, Brazil.

<sup>b</sup>Departamento de Química Inorgánica, Facultad de Farmacia, Universidad de Santiago de Compostela, E-15706 Santiago de Compostela, Spain.

<sup>c</sup>Department of Inorganic Chemistry, "Al. I. Cuza" University, Iasi, Rumania.

The determination of the three-dimensional structures of heavy-metal chelates and of some potentially useful chelating agents is a very important tool in the study of complexes that may act as antidotes against poisoning by ingestion of heavy metals. A detailed knowledge of these complexes is expected to assist in the design of molecular structures and procedures that are more effective in counteracting the life threatening processes inevitably developed by individuals with chronic heavy-metal intoxication. Within this framework a series of dimethylthallium(III) complexes were studied. Here we present complexes of the type [TlMe<sub>2</sub>L], where L=2-mercaptop-3-pyridine carboxylic acid(I), 6-mercaptop-3-pyridine-methoxycarboxylate(II), 2-mercaptop-3-pyridine-methoxycarboxylate(III), 6-mercaptop-3-pyridine-ethoxycarboxylate(IV) and 2-mercaptop-3-pyridine-ethoxycarboxylate(V). The study of the supramolecular arrangement of these complexes shows that, in spite of the differences in space group symmetry and substituents in the ligand, the crystals packing are remarkably similar. The complexes form infinite polymers in one, two and three dimensions, based upon Tl-S covalent bonds and intermolecular secondary interactions. Tl-S covalent bonds are in the range 2,776 Å – 2,813 Å, whereas Tl...S intermolecular and intramolecular weak interactions cover a narrow range, from 3,008 Å – 3,379 Å. The complexes also present strong hydrogen bond intermolecular interactions. Compounds (IV) and (V) form two-dimensional nets while (I) forms a three-dimensional one, the three of them stabilized by hydrogen bonds. Compounds (II) and (III) form one- and three-dimensional nets, respectively, generated only by covalent bonds and intermolecular Tl...S and Tl...O secondary interactions.

Acknowledgment.- We gratefully acknowledge support from "Agencia Española de Cooperación Internacional", Fapesp(Brazil) and CNPq(Brazil).

## OPQM02. Use of the Cambridge Structural Database in Study of Single and Partial Double C-X (X=C,N, O) Bonds in Organic Molecules in Crystalline State

Kiralj R. and Ferreira M. M. C

Instituto de Química, Universidade Estadual de Campinas. E-mails: [rudolf@iqm.unicamp.br](mailto:rudolf@iqm.unicamp.br), [marcia@iqm.unicamp.br](mailto:marcia@iqm.unicamp.br)

The Cambridge Structural Database (CSD) [1] is an organic/organometallic crystal structures database with various possibilities of visualization and analysis of the hits. The current CSD version (November 2002) contains 272066 crystal structures determined by diffraction methods (X-ray, neutron, synchrotron) [2]. This is an encouragement to study multiple C-X bonds, where X is usually C, N or O in typical organic compounds. Another reason to study these bonds is their presence in bioactive molecules as drugs and natural biomolecules, and in environmental pollutants as polycyclic aromatic hydrocarbons (PAHs) and their derivatives. Moreover, C-C bonds were among the first ones exhibiting structure correlation as bond length-bond order relationships [3]. Today, when the number of determined crystal structures with high-level precision is increasing, it is possible to update such relationships, generalize to other bond types and molecular classes, and by careful analysis qualify and even quantify delocalization, substitution and crystal packing effects on bond lengths. Furthermore, in structural, organic and theoretical chemistry, simple equations for calculation of bond lengths from some simple variables, are welcome. The aim of this work is to present new proper findings on bond length-bond order relationships taking into account those phenomena affecting the bond length. Current findings on extremely long C-C bond length around 3 Å [4] put traditional teaching on chemical bonding to be reexamined and more generalized, what is also the aim of this work. This presentation discusses accurate CSD searches appropriate for chemometric analysis, and generation of bond variables as bond orders, topological indices, crystal packing effect parameters. Finally, regression equations for bond length prediction are established, validated and interpreted. The compounds under study are PAHs, nucleobases, aza-PAHs and carbon allotropic modifications and carbon clusters, all obtained from CSD.

- [1] F. H. Allen, *Acta Cryst.*, **B58** (2002) 380.
- [2] The Cambridge Structural Database. <http://www.ccdc.cam.ac.uk/support/>
- [3] L. Pauling, L. O. Brockway, J. Y. Beach, *J. Am. Chem. Soc.*, **57** (1935) 2705.
- [4] J. J. Novoa *et al.*, *Angew. Chem. Int. Ed.*, **40** (2001) 2540.

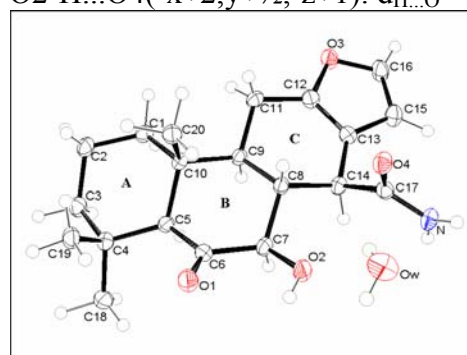
The authors acknowledge FAPESP for the support.

## PPQM03. Crystallographic Structure of the $7\beta$ -hydroxy- $6\alpha$ -oxovouacapan- $17\beta$ -amide

Rodrigues, L. P.<sup>1</sup>; Resende, J.A.L.C.<sup>1</sup>; Guilardi, S.<sup>1</sup>; Ellena, J.<sup>2</sup>; Santos-Jr, S.<sup>2</sup>; Branco, P.A.C.<sup>3</sup>; Piló-Veloso, D.<sup>3</sup>; Rubinger, M.M.M.<sup>4</sup>

<sup>1</sup> IQ/UFU – silvana@ufu.br; <sup>2</sup> IFSC/USP; <sup>3</sup> ICEX-UFMG; <sup>4</sup>DQ-UFV.

O ácido  $6\alpha,7\beta$ -diidroxi-vouacapan- $17\beta$ -óico (ADV) é um furanoditerpeno natural, extraído do óleo do fruto de *Pterodon polygalaeformis* Benth (Sucupira Branca)<sup>[1]</sup>, que apresenta atividade antiinflamatória sedativa distinta dos inibidores da ciclo-oxigenase<sup>[2]</sup>. Visando um futuro estudo de QSAR, vários derivados do ADV foram sintetizados pelo Grupo da Profa. Dra. Dorila Piló-Veloso do ICEX/UFMG. Dando prosseguimento ao estudo estrutural dos vouacapanos derivados do ADV, este trabalho apresenta a estrutura cristalina do composto  $7\beta$ -hidroxi- $6\alpha$ -oxovouacapan- $17\beta$ -amida (POLAM). Dados de intensidade de difração de raios-X foram coletados em um difratômetro Nonius KappaCCD, a 120K usando radiação MoK $\alpha$  (0,71073Å). A estrutura foi resolvida por métodos diretos (SIR-97) e refinada anisotropicamente pelo método dos mínimos quadrados ( $F^2$ ), utilizando matriz completa (SHELXL-97). As posições dos átomos de hidrogênio foram localizados em mapas de Fourier-Diferença e seus parâmetros de vibração térmica foram assumidos como sendo iguais a 1,5 (para átomos de hidrogênio metila e hidroxila) e 1,2 (para os demais átomos de hidrogênio) vezes o valor do parâmetro de deslocamento isotrópico do átomo ao qual estão ligados. O composto ( $C_{20}H_{29}NO_4 \cdot H_2O$ ,  $M_r = 363,44 \text{ g mol}^{-1}$ ) cristaliza no sistema monoclínico, grupo espacial  $P2_1$ ,  $a=6,1540(2)$ ,  $b=9,7450(3)$ ,  $c=15,5558(5)\text{\AA}$ ,  $\beta=96,1390(10)^\circ$ ,  $V=927,54(5)\text{\AA}^3$ ,  $Z=2$ ,  $D_c=1,301 \text{ g cm}^{-3}$ ,  $F(000)=392$ ,  $S=1,234$ ,  $R_1=5,05\%$  para 2906 reflexões com  $I>2\sigma(I)$  e 318 parâmetros refinados. A unidade assimétrica é constituída de uma molécula de POLAM e uma de água. Como observado no composto META ( $6\alpha,7\beta$ -dihidroxi-N-metil-vouacapan- $17\beta$ -amida)<sup>[3]</sup>, a molécula de água estabiliza o empacotamento cristalino, sendo responsável por três das cinco ligações de hidrogênio:  $Ow-H''...O2$ :  $d_{H...O2}=2,285\text{\AA}$ ,  $d_{Ow...O2}=2,969\text{\AA}$  e  $\angle = 136^\circ$ ;  $Ow-H'...O4$  ( $2-x, \frac{1}{2}+y, 1-z$ ):  $d_{H...O4}=2,360\text{\AA}$ ,  $d_{Ow...O4}=3,057\text{\AA}$  e  $\angle = 157^\circ$ ;  $N-H2...Ow$  ( $x+1, y, z$ ):  $d_{H...O}=2,052\text{\AA}$ ,  $d_{N...Ow}=2,884\text{\AA}$  e  $\angle = 164^\circ$ ;  $N-H1...O1$  ( $-x+2, y-\frac{1}{2}, -z+1$ ):  $d_{H...O}=2,168\text{\AA}$ ,  $d_{N...O1}=3,041\text{\AA}$  e  $\angle = 174^\circ$  e  $O2-H...O4(-x+2, y+\frac{1}{2}, -z+1)$ :  $d_{H...O}=2,057\text{\AA}$ ,  $d_{O2...O4}=2,714\text{\AA}$  e  $\angle = 146^\circ$ .



A conformação dos anéis A, B e C são respectivamente: cadeira, bote distorcido e meia cadeira. Em comparação aos vouacapanos saturados<sup>[3,4]</sup> no carbono C6, ocorre a mudança da conformação do anel B de cadeira para bote distorcido, provavelmente devido a existência do grupamento cetônico nesta posição.

Referências Bibliográficas: [1] Mahajan, J. R. & Monteiro, M. B. J. Chem. Soc. Perkin Trans, **1973**, 520-525. [2] Numan, E. A. et al. Braz. J. Med. Exp. Soc. **1982**, 15, 540. [3] Branco, M. C. Estudo Cristaloquímico de Amidas derivadas do ADV por difração de raios-X. Dissertação de Mestrado em Ciências, IQSC-USP, **1997**. [4] Ruggiero, S. G. et al. Acta Cryst. C, C53, 982, **1997**.

Figura 1: Representação ORTEP da unidade assimétrica

FAPEMIG, FAPESP, CNPq e CAPES.

## PPQM04. The X-ray Structure of the N-ciclohexyl-7 $\beta$ -hydroxy-6 $\alpha$ -oxovouacapan-17 $\beta$ -amide

Resende, J.A.L.C. (PG)<sup>1</sup>; Oliveira, G.B. (IC)<sup>1</sup>; Guiliardi, S. (PQ)<sup>1</sup>; Ellena, J. (PQ)<sup>2</sup>; Santos-Jr, S. (PG)<sup>2</sup>; Branco, P.A.C. (PG)<sup>3</sup>; Piló-Veloso, D. (PQ)<sup>3</sup>; Rubinger, M.M.M. (PQ)<sup>4</sup>

<sup>1</sup> IQ/Universidade Federal de Uberlândia—silvana@ufu.br;

<sup>2</sup> IFSC/Universidade de São Paulo; <sup>3</sup> ICEx—Universidade Federal de Minas Gerais; <sup>4</sup> DQ—Universidade Federal de Viçosa.

Os furanoditerpenos extraídos das sementes dos gêneros *Pterodon*<sup>[1]</sup> e *Caesalpinia*<sup>[2]</sup> são caracterizados pela fusão de três anéis ciclohexano com um anel furano. Estes compostos, também chamados de vouacapanos, apresentam atividade biológica: antiinflamatória, analgésica, anti-Para3 (Vírus Parainfluenza tipo 3) e herbicida. Este trabalho tem por objetivo a obtenção da estrutura cristalina do composto N-cicloexil-7 $\beta$ -hidroxi-6 $\alpha$ -oxovouacapan-17 $\beta$ -amida (POLCHA) visando implementar o banco de dados estruturais de vouacapanos. Um monocrystal do composto POLCHA foi utilizado para a coleta de dados de intensidade, a 120K, em um difratômetro Nonius KappaCCD usando radiação MoK $\alpha$  (0,71073 Å). A estrutura foi resolvida por métodos diretos (SIR-97) e refinada anisotropicamente pelo método dos mínimos quadrados (F<sup>2</sup>), utilizando matriz completa (SHELXL-97). As posições dos átomos de hidrogênio foram localizadas nos mapas de Fourier-Diferença. Dados Cristalográficos: C<sub>26</sub>H<sub>39</sub>NO<sub>4</sub>, Mr = 429,59 g mol<sup>-1</sup>, Ortorrômbico, P2<sub>1</sub>2<sub>1</sub>2<sub>1</sub>, a = 8,994(5), b = 20,534(5), c = 25,265(5) Å, V = 4666,01(30) Å<sup>3</sup>, Z = 8, Dc = 1,217 g cm<sup>-3</sup>, F(000) = 1856, S = 1,047, R<sub>1</sub> = 5,47% para 6538 reflexões com I > 2σ(I) e 732 parâmetros. Semelhante ao observado para outras amidas derivadas do ADV, o composto cristaliza com duas moléculas por unidade assimétrica<sup>[3]</sup>. A diferença entre as duas moléculas ocorre, principalmente, sobre os ângulos diedros que envolvem as ligações C9-C11, C11-C12, C8-C14 e C14-C17. O anel A apresenta conformação cadeira nas duas moléculas. Os anéis B e C apresentam conformação diferente, respectivamente, meia cadeira e meio bote na molécula 1 e bote distorcido e cadeira na molécula 2.

O empacotamento cristalino é mantido por ligações de hidrogênio intermoleculares na direção [100]: N'-H'...O4 (d<sub>H...O</sub> = 2,018 Å, d<sub>N...O4</sub> = 2,850 Å e  $\angle$  = 160,96°) e N-H...O4<sup>i</sup> (d<sub>H...O4</sub><sup>i</sup> = 2,092 Å, d<sub>N...O4</sub><sup>i</sup> = 2,893 Å e  $\angle$  = 150,93°; i = 1+x, y, z). Observam-se também ligações de hidrogênio intramoleculares entre os grupamentos hidroxila e cetônico: O2-H2...O1 (d<sub>H2...O2</sub>=1,928 Å, d<sub>O2...O1</sub>=2,615 Å e  $\angle$ =130,88°) e O2'-H2'...O1' (d<sub>H2'...O2'</sub>=1,844 Å, d<sub>N...O4</sub>=2,621 Å e  $\angle$  = 127,25°).

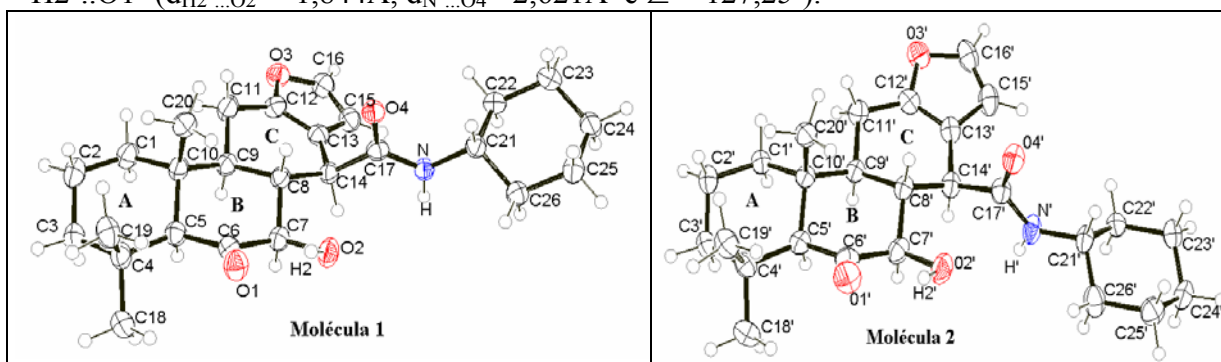


Figura 1: Representação ORTEP das moléculas independentes da unidade assimétrica.

Referências Bibliográficas: [1] Jiang, R. W. et al. *J. Nat. Prod.* **2001**, 64, 1266.

[2] Demuner, A. J. et al. *J. Nat. Prod.* **1996**, 59, 770. [3] Resende, J.A.L.C. et al *23<sup>a</sup> Reunião Anual da SBQ*, **2000**, QO-186.

FAPEMIG, FAPESP, CNPq e CAPES.

## PPQM05. Crystal Structure of Nitrooxyquinones

Pereira, M.A.<sup>1</sup>; De Simone, C.A.<sup>1</sup>; Malta, V.R.S.<sup>1</sup>; Goulart, M.O.F.<sup>1</sup>; Abreu F.C.<sup>2</sup>; Lopes A. C. de O.<sup>1</sup>.

<sup>1</sup> Universidade Federal de Alagoas : map@qui.ufal.br

<sup>2</sup> Universidade Federal de Sergipe

The combination of different pharmacophoric groups in a single molecule to obtain "hybrid drugs" is a strategy frequently used to design new compounds potentially useful in the management of diseases with complex and heterogeneous pathogenesis. The use of hybrids could solve pharmacokinetic problems and replace the use of mixture of drugs<sup>(1)</sup>.

The structure 2-(nitrooxymethyl)quinones is novel compound and have two pharmacophoric groups, the quinone moiety and the organic nitrate. To our knowledge, there is no report of this functional group combination in any molecule.

Organic nitrates are recognised as able to relax vascular smooth muscle and represent the oldest class of NO donors that have been clinically applied<sup>(2,3)</sup>. NO is currently one of the most studied molecules in the biomedical sciences. This interest is driven by the multiplicity of roles that NO plays<sup>(2-4)</sup>. The NO release from organic nitrates requires either enzymatic or nonenzymatic bioactivation where a three-electron reduction thiol-dependent is involved (The biochemical mechanism of NO release from organicnitrates has not been fully defined<sup>(5)</sup>. Nitrosothiol formation and enzymatic conversion have been considered to explain the formation of nitric oxide from nitrates<sup>(3,6)</sup>. Specific thiols, for example, cysteine, interact with nitrates to give nitrites and NO in sequence<sup>(3)</sup>.

**Crystal Data:** C<sub>15</sub>H<sub>9</sub>N<sub>1</sub>O<sub>5</sub>, M= 283.23, D<sub>x</sub> = 1.537g.cm<sup>-3</sup>, a=6.957(4), b=21.740(1), c=8.105(3)Å, β=93.12(3)°, V=1224.0(8)Å<sup>3</sup>, monoclinic P21/c, Z=4, F(000)=584.0, MoK<sub>α</sub> radiation ( λ=0.71073), μ= 0.12 mm<sup>-1</sup>, S= 1.052, R<sub>1</sub>=0.05 for 1073 reflections with I>4σ(I) and 191 refined parameters. The structure was solved by the Direct Method and difference Fourier syntheses and refined anisotropically by full-matrix least-squares on F<sup>2</sup><sup>(7)</sup>.

### References:

1. Nicolaus, B. J. R. Symbiotic Approach to Drug Design. In *Decision Making in Drug Research*; Gross, F., Ed.; Raven Press: New York, 1983; pp 173-186.
2. Pfeiffer, S.; Mayer, B.; Hemmens, B. *Angew. Chem. Int. Ed. Eng.* **1999**, 38, 1714.
3. Gasco, A.; Fruttero, R.; Sorba, G. *Il Farmaco* **1996**, 51, 617.
4. Wang, P. G.; Xian, M.; Tang, X.; Wu, X.; Wen, Z.; Cai, T.; Janczuk, A. *J. Chem. Rev.* **2002**, 102, 1091.
5. Thatcher, G. R. J.; Weldon, H. *Chem. Soc. Rev.* **1998**, 27, 331.
6. Feelisch, M.; Noack, E. A. *Eur. J. Pharmacol.* **1987**, 139, 19.
7. Farrugia, L.J.- WinGX. *J.Appl.Cryst.*(1999), **32**,837-838

**Acknowledgements :** CNPq, CAPES, FINEP, FAPEAL

## PPQM06. Crystal Structure of ent-16a, 17b-methoxy-17-hydroxy-19-kauran Acid – ACF-158b

Pereira, M.A.<sup>1</sup>; Malta, V.R.S.<sup>1</sup>; De Simone, C.A.<sup>1</sup>; Santos, G.L<sup>1</sup>; Nascimento, M.C. B. S.<sup>2</sup>, Morais, A.A.<sup>2</sup>, Filho, R.B.<sup>3</sup>, Vieira, I.J. C.<sup>3</sup>

<sup>1</sup> Universidade Federal de Alagoas : map@qui.ufal.br

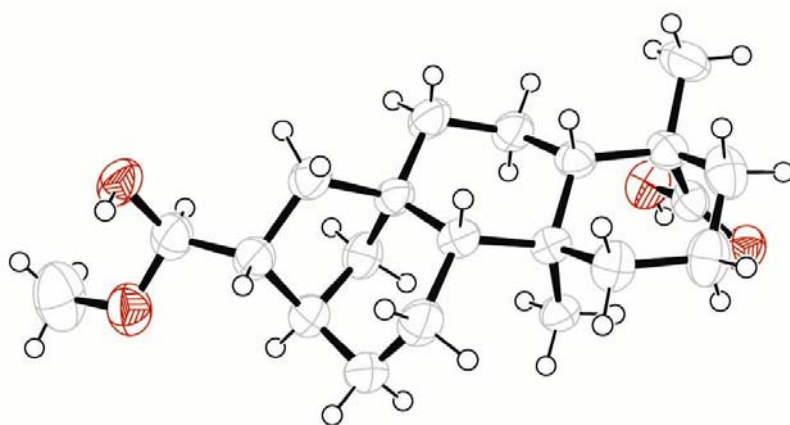
<sup>2</sup> Universidade Federal Rural do Rio de Janeiro: Profqui@aol.com

<sup>3</sup> Universidade Estadual do Norte Fluminense

Do estudo fitoquímico de uma espécie da família **Annonaceae**, *Annona cacans* Warn., dentre outras substâncias naturais isoladas do extrato em acetato de etila dos frutos fresco da planta, obteve-se um novo diterpeno o derivado Kaurânico, **ACF-158b**.

Os compostos **Kaurânicos** pertencem a uma classe de substâncias naturais conhecidas como **diterpenos**, originalmente encontrados em plantas e fungos, podendo também ocorrer em organismos marinhos e insetos. Possuem uma ampla variedade de atividades biológicas tais como: hormonal, atuando no crescimento de plantas, abortiva, anti-hipertensiva, inibitória de crescimento de plantas, repelente de insetos e atividade anti-HIV<sup>1,2</sup>.

Os parâmetros cristalográficos foram os seguintes:  $a = 8,4324(2)$ ,  $b = 10,7639(2)$ ,  $c = 21,1593(6)\text{\AA}$ ;  $V = 1920,53(1) \text{ \AA}^3$ ;  $Z = 4$  moléculas/cela; radiação MoK $\alpha$  ( $\lambda = 0,71073$ );  $T = 298\text{K}$ . Sistema cristalino ortorrômbico, grupo especial  $P2_12_12_1$ . Foram coletadas 4312 reflexões únicas, sendo 3502 consideradas observadas ( $I > 2\sigma(I)$ ). A estrutura foi resolvida utilizando-se os Métodos Diretos e refinada pelo método de mínimos quadrados. O pacote de programas utilizado foi o WINGX<sup>3</sup>. Os índices de discordância finais foram:  $R = 0,0509$ ,  $R_{\text{all}} = 0,0675$  e  $\text{GOF} = 1,06$ .



### Referências:

- Takahashi, J. A. Tese de Doutorado. Estudo Fitoquímico de *Xilopia frutescens* Aubl., e Transformações Microbianas de Kauranos, Afidicolanos e Estemodanos (UFMG – 1994).
- Wu, Yang-Chang; Hung, Yu-Chun; Chang, Fang-Rang; Consentino, Mark; Wang, Hui-Kamg and Lee, Kuo-Hsiung. *J. Nat. Prod.* **1996**, 59, 635-637.
- Farrugia, L.J.- WinGX. *J.Appl.Cryst.(1999)*, **32**,837-838

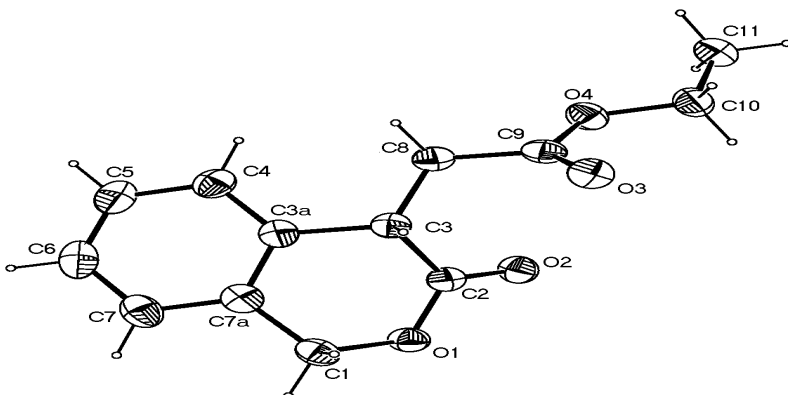
**Agradecimentos :** CNPq, CAPES, FINEP, FAPEAL

## PPQM07. Crystal Structure of (3-Oxo-isochroman-4-yl)-acetic acid ethyl ester

Pereira, M.A.<sup>1</sup>; De Simone, C.A.<sup>1</sup>; Malta, V.R.S.<sup>1</sup>; Goulart, M.O.<sup>1</sup>; Cavalcanti J. C. M<sup>1</sup>.

<sup>1</sup> Universidade Federal de Alagoas : map@qui.ufal.br

A coleta dos dados de intensidade dos raios-X difratados pelo monocrystal em estudo foi realizado através do Difratômetro Automático Kappa CCD (Enraf-Nonius, 1999). A determinação estrutural foi feita através do uso dos Métodos Diretos utilizando-se do programa SHELXS86(Sheldrick,1990) enquanto o refinamento da mesma foi realizado pelo Método dos Mínimos Quadrados por meio do programa SHELXL97 (Sheldrick,1997). O desenho foi obtido através do programa ORTEP-3 (Farrugia, 1997). Os principais parâmetros cristalográficos foram os seguintes:  $a = 7,9780(1)$ ,  $c = 36,7233(4)\text{\AA}$ ;  $V = 2337,4(5) \text{ \AA}^3$ ;  $Z = 8$  moléculas/cela;  $F(000) = 992$ ;  $D_c = 1,331 \text{ Mg/m}^3$ ; radiação MoK $\alpha$  ( $\lambda=0.71073$ ). Sistema cristalino tetragonal, grupo especial P4<sub>1</sub>2<sub>1</sub>2. Foram coletadas 12600 reflexões, sendo 2059 reflexões independentes. Foram refinados 155 parâmetros utilizando-se 1881 reflexões e o índice de discordância final foi de 0.031. Os índices de discordância finais foram:  $R = 0.0314$ ,  $R_{\text{all}} = 0.0371$  e  $\text{GOF} = 1,05$ .



As distâncias e ângulos interatômicos estão dentro dos valores normais e esperados para estes

tipos de ligações.Um plano médio passando pelos átomos C3, C3a, C7a, C1, O1 e C2 revelou que os quatro primeiros átomos estão situados num mesmo plano [ângulo de torção de 1.4( $^{\circ}$ )] enquanto os átomos O1 e C2 estão 0,978 Å abaixo de tal plano conferindo-lhe uma conformação distorcida.

### Referência:

- Enraf-Nonius (1999).CCD-4 Software. Version 5.0. Enraf-Nonius, Delft, The Netherlands.
- Farrugia, L.J. (1997). Ortep-3. An Interactive Molecular Graphics Program for Windows. University of Heidelberg, Germany.
- Sheldrick, G.M. (1990). SHELXS-97. Program for the Solution of Crystal Structures Acta Cryst. **A46**, 467-473.
- Sheldrick, G.M. (1997). SHELXL-97. Program for the Refinement of Crystal Structures. University of Göttingen, Germany.

**Agradecimentos :** CNPq, CAPES, FINEP, FAPEAL

## PPQM08. Crystal Structure of 3 $\beta$ -(5 phenyl-2E,4E - pentadienoyloxy)-olean-12-ene

Pereira, M.A.<sup>1</sup>; Malta, V.R.S.<sup>1</sup>; De Simone, C.A.<sup>1</sup>; Silva, V.R.M<sup>1</sup>; Humberto, M.M.S<sup>1</sup>; Sant'ana, A.E.G<sup>1</sup>.

<sup>1</sup> Universidade Federal de Alagoas : map@qui.ufal.br

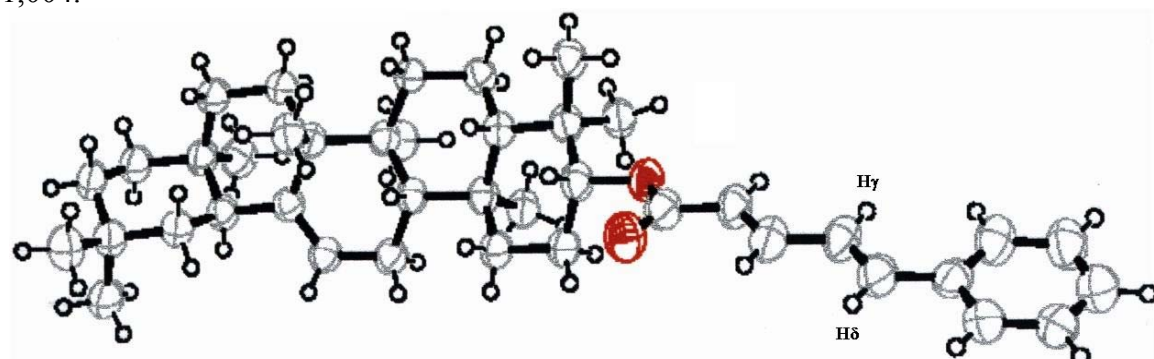
Plantas da família Apocynaceae são amplamente utilizadas na medicina popular como antitumoral, antifúngica, vermífuga, anti-anêmica, no tratamento de febres intermitentes, inapetência, diarréia, úlcera, prisão de ventre e bronquite<sup>1</sup>.

Como parte do programa de análise da família Apocynaceae, cujo estudo é baseado em princípios ativos<sup>2</sup>, foi selecionada para investigação a espécie *Peltastes peltatus* (Vell.) Woodson. O gênero *Peltastes* é raro e até o momento, não foi encontrado relato de avaliação da composição química e biológica de outras espécies deste gênero. O espécimen estudado foi coletado no município de Marechal Deodoro, Alagoas.

O fracionamento cromatográfico do extrato etanólico das folhas de *P. peltatus* resultou no isolamento do triterpenoide pentacíclico, 3 $\beta$ -(5 phenyl-2E,4E-pentadienoyloxy)-olean-12-ene.

A proposta inicial da estrutura desse composto foi baseada em dados espectrais de RMN <sup>1</sup>H e <sup>13</sup>C e técnicas bidimensionais. No entanto, não foi possível definir a estereoquímica dos hidrogênios  $\gamma$  e  $\delta$  (ver figura). Tal definição se deu a partir da análise dos dados cristalográficos de raios-X.

Os parâmetros cristalográficos foram os seguintes:  $a = 25.573(3)$ ,  $b = 10.453(1)$ ,  $c = 14.159(2)\text{\AA}$ ;  $\beta = 113.674(8)^\circ$ ;  $V = 3466.2(8) \text{ \AA}^3$ ;  $Z = 4$  moléculas/cela;  $F(000) = 1280$ ;  $D_c = 1.117 \text{ Mg/m}^3$ ; radiação MoK $\alpha$  ( $\lambda = 0.71073$ ). Sistema cristalino monoclinico, grupo especial C2. Foram coletadas um total de 8041 reflexões, sendo 4910 reflexões observadas com  $I > 2\sigma(I)$ . A estrutura foi resolvida utilizando-se os Métodos Diretos e refinada pelo método de mínimos quadrados. O pacote de programas utilizado foi o WinGX<sup>3</sup>. Os índices de discordância finais foram:  $R = 0.0689$ ,  $R_{\text{all}} = 0.1004$  e GOF = 1,004.



### Referência:

1. Cruz, G.L. 1982. Dicionário das plantas úteis do Brasil. 2 ed. Rio de Janeiro, Civilização Brasileira
2. Yunes RA, Pizzolatti MG, Sant'Ana AEG, Hawkes GE, Calixto JB. 1993. The structure of velutinol A, an anti-inflammatory compound with a novel pregnane skeleton. Phytochemical Analysis 4: 76-81.
3. Farrugia, L.J.- WinGX. J.Appl.Cryst.(1999), 32,837-838

**Agradecimentos :** CNPq, CAPES, FINEP, FAPEAL

# PPQM09. Structural Studies of the 4-Tioxopirimidine C<sub>14</sub>H<sub>14</sub>N<sub>2</sub>O<sub>2</sub>S with potential biological activities

*Lariucci, C.<sup>1</sup>, Lima, K.A.P.<sup>2</sup>, Vencato, I.<sup>3</sup>*

Physics Institute, UFG. <sup>1</sup>lariucci@fis.ufg.br, <sup>2</sup>karllaadriana@zipmail.com.br,

<sup>3</sup>vencato@fis.ufg.br

*Napolitano, H. B.<sup>4</sup>*

Physics Institute of São Carlos, USP. <sup>4</sup>hamilton@if.sc.usp.br.

*Cunha, S.<sup>5</sup>*

Chemistry Institute, UFBA. <sup>5</sup>silviodc@ufba.br.

In this work we obtained the structural parameters of the organic compound C<sub>14</sub>H<sub>14</sub>N<sub>2</sub>O<sub>2</sub>S by X-ray diffraction aiming to elucidate the presence of the requirements for biological activities. The 4-tioxopirimidine was synthesized through the reaction of benzoyl isocyanide with the ethyl β-aminocrotonate. After several trials with different solvents we carried out the aza-anellation using Et<sub>2</sub>O followed by refluxe in THF. The yield was 25% and this compound showed modest antibacterial activity (500 µg/mL) against *Escherichia coli* (gram-negative, ATCC 8739) and *Staphilococcus aureus* (gram-positive, ATCC 6538). The data collection was performed at room temperature using CAD4 diffractmeter at IFSC/USP with CuKα monochromatic radiation. The main crystallographic parameters of the monoclinic structure, belonging to the P2(1)/c space group, are: a = 15.282(3) Å, b = 7.276(1) Å, c = 14.679(3) Å, β = 117.10(3)°, Z = 4 molecules/unit cell, V = 1452.99 Å<sup>3</sup> and F(000) = 520.0. 2737 unique reflections were measured with R(int) = 0.0119. The crystal structure was solved by direct methods and it was refined anisotropically with full matrix least square on F<sup>2</sup> using the SHELX97 program [1]. The final model shows a disagreement of 0.0501. Beside the 4-Tioxopirimidine molecule one solvent water molecule was found in the asymmetric unit. The crystalline packing is driven by the presence of three hydrogen bonds of type N–H...O, O–H...N<sup>(-x+1, -y-1/2, -z+1/2)</sup> and O–H...S<sup>(-x+1, -y, -z+1)</sup> between the compound and the aside solvent molecules. The distances between donor and acceptor are 2.857 Å, 2.997 Å and 3.291 Å and dihedral angles are 175.92°, 178.40° and 175.9°, respectively. These hydrogen bonds are one requirement for C<sub>14</sub>H<sub>14</sub>N<sub>2</sub>O<sub>2</sub>S biological activities.

## Acknowledgments

To Prof. E. E. Castellano (IFSC/USP) for data collection;

To FUNAPE/UFG for financial support;

To FAPESP and CNPq for fellowships to HBN and KAPL, respectively.

## References

- [1] Sheldrick, G. M. (1997). *SHELX97 Program for the Solution and Refinement of Crystal Structures*. University of Göttingen. Germany.

## PPQM10. Crystal Structure of the 3-benzoxazol-2-yl-7-hydroxy-chromen-2-one

Franca, E. F.(IC)<sup>1</sup>; Souza, K. C. (IC)<sup>1</sup>; Machado, A. E. H. (PQ)<sup>1</sup>; Guilardi, S.(PQ)<sup>1</sup>; Santos-Jr., S. (PG)<sup>2</sup>; Ellena, J. (PQ)<sup>2</sup>.

<sup>1</sup> IQ - Universidade Federal de Uberlândia – silvana@ufu.br;

<sup>2</sup> IFSC - Universidade de São Paulo – sauli@if.sc.usp.br.

Derivados de cumarina, em geral, apresentam elevada fluorescência, na região do visível, que depende da posição e natureza dos grupos substituintes. Hidroxicumarinas substituídas possuem propriedades fotoquímicas e fotofísicas que as justificam como corantes para laser, branqueadores ópticos ou marcadores biológicos<sup>[1]</sup>. Nopresente trabalho elucidou-se a estrutura cristalina e molecular do composto 3-benzoxazol-2-il-7-hidroxi-cromen-2-ona (CUMAOH) por difração de raios-X<sup>[2]</sup>. Este derivado de cumarina apresenta boa estabilidade fotoquímica, elevado rendimento quântico de fluorescência em diferentes solventes, grandes deslocamentos de Stokes e baixa eficiência de geração de oxigênio singlete (cerca de 6%)<sup>[1]</sup>. Os dados de intensidade dos feixes de raios-X difratados pelo monocrystal foram coletados em um difratômetro Nonius KappaCCD, à temperatura de 120 K, usando radiação de MoK<sub>α</sub> (0,71073 Å). A estrutura foi resolvida por métodos diretos (SIR-97) e refinada por mínimos quadrados (F<sup>2</sup>), utilizando matriz completa (SHELXL-97). Os átomos de hidrogênio foram localizados através de sucessivas sínteses de Fourier-diferença.

O composto ( $C_{16}H_{9}NO_4 \cdot CH_3OH$ ), Mr = 311,28 g/Mol, cristaliza no sistema triclinico, grupo espacial P  $\bar{1}$ , Z = 2,  $\mu(MoK_{\alpha}) = 0,111 \text{ mm}^{-1}$ , a = 6,561(5) Å, b = 7,349(5) Å, c = 15.358(5) Å,  $\alpha = 79.724(5)^\circ$ ,  $\beta = 78.980(5)^\circ$ ,  $\gamma = 74.194(5)^\circ$ , V = 693,1(7) Å<sup>3</sup>, D<sub>c</sub> = 1,492 Mg/m<sup>3</sup>, S = 1,058, R(int.) = 0,0953, R1 = 5,09% para 1820 reflexões com I > 2σ(I) e 245 parâmetros refinados.

A representação ORTEP da unidade assimétrica (constituída por uma molécula de cumarina e um metanol de cristalização) é dada na Figura 1. O empacotamento é mantido por ligações de hidrogênio entre moléculas de cumarina e metanol: O-H...O2: d<sub>0...O2</sub> = 2,87 Å, d<sub>H...O2</sub> = 2,21 Å,  $\angle = 126,3^\circ$ ; O-H...N: d<sub>0...N</sub> = 2,93 Å, d<sub>H...N</sub> = 2,10 Å,  $\angle = 145,8^\circ$  e O4-HO4...O<sup>(i)</sup>: d<sub>04...O</sub> = 2,63 Å, d<sub>HO4...O</sub> = 1,81 Å,  $\angle = 177,4^\circ$  [(i) = (-x,-y+1, -z+1)].

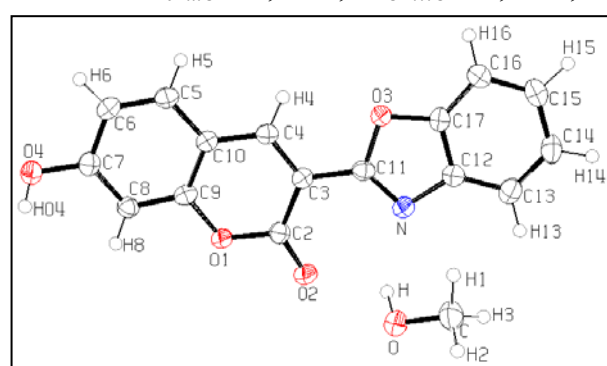


Figura 1 – Representação ORTEP.

O ângulo entre o plano do anel cumarínico e o plano do substituinte benzoxazol é de 8,21(8)°. O aumento do ângulo entre os planos mencionados, com relação ao ângulo observado para a cumarina não substituída na posição 7 [5,24(8)°]<sup>[3]</sup>, deve-se à presença de interações intermoleculares mais fortes. O átomo de oxigênio da hidroxila fica 0,12 Å acima do plano do anel cumarínico.

**Referências Bibliográficas:** [1] MACHADO, A. E. H. et al. *J. Photochem. and Photobiol. A*: 141 (2001), 109-116. [2] LUAN, X. H. et al. *Advances in Colour Science and Technology*, v.5 (2002), 18-23. [3] GUILARDI, S. et al. *Acta Cryst.*, E58 (2002), 985-987.

FAPEMIG, FAPESP e CNPq.

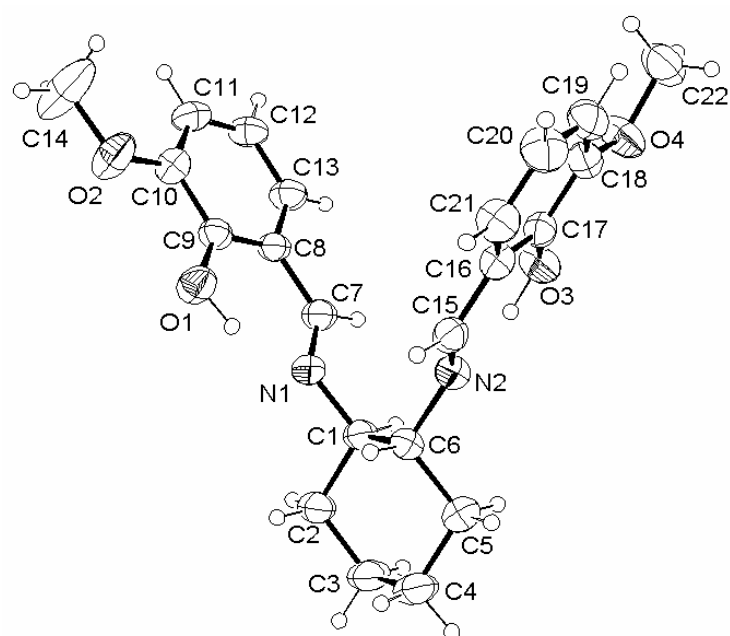
## PPQM11. Estrutura Cristalina e Molecular do C<sub>22</sub>H<sub>26</sub>N<sub>2</sub>O<sub>4</sub>

**Mafud, A. C, IQSC - USP, acmafud@lycos.com, Gambardella, M.T.P., IQSC – USP, teca@iqsc.usp.br**

Os dados de intensidade de difração de raios-X foram coletados em um difratômetro automático CAD4, a 293K, utilizando radiação K $\alpha$ Mo (0,71073 Å) e um monocrystal de dimensões 0,33 x 0,13 x 0,13 mm.

Dados Cristalográficos: sistema triclinico; a=10,0972(9), b=10,974(1), c=11,083(1)Å,  $\alpha$ =115,234(1),  $\beta$ =112,430(8),  $\gamma$ =95,290(9) $^{\circ}$ , V=1030,97 Å<sup>3</sup>; grupo espacial P $\bar{1}$ ; Z = 2 moléculas por cela unitária; Dc = 1,245 Mg/m<sup>3</sup>; 5596 reflexões medidas ( $2,3 \leq \theta \geq 28,7^{\circ}$ ); 5308 independentes (Rint = 0,0176).

A estrutura foi resolvida usando Métodos Diretos e refinada por Mínimos Quadrados. A confiabilidade entre o modelo real e o obtido foi avaliada através dos fatores de discordância R(F) e Rw(F2), os quais foram 0,049 e 0,116 para 2432 reflexões observadas [ $I \geq 2\sigma(I)$ ].



As distâncias e ângulos de ligação apresentam os valores esperados.

O ciclohexano tem a conformação de meio bote.

Os hidrogênios das hidroxilas (O1 e O3) foram localizados em mapas de Fourier diferença e refinados com Uiso igual a 1,5 vezes Ueq do átomo ao qual esta ligado.

As hidroxilas estão envolvidas em ligações de hidrogênio intramoleculares cujas geometrias estão mostradas na Tabela abaixo.

Tabela. Geometria das Ligações de Hidrogênio.

	D-H	H...A	D...A	$\angle(DHA)$
O1-H1O...N1	0.94(2)	1.77(2)	2.642(3)	152(2)
O3-H3O...N2	0.97(2)	1.68(2)	2.584(2)	153(2)

Agradecimentos: Ao Prof. Dr. Edward R. Dockal da UFSCar pelo fornecimento das amostras.

Ao CNPq pelo apoio financeiro.

## PPQM12. Short Hydrogen Bonds in Salts of Pyromellitic Acid [C<sub>6</sub>H<sub>2</sub>(COOH)<sub>4</sub>]

*Diniz, R.<sup>1</sup>, Ellena, J.<sup>2</sup>, Sansiviero, M. T. C.<sup>1</sup> and Fernandes, N. G.<sup>1</sup>*

<sup>1</sup> UFMG, <sup>2</sup> USP – São Carlos. \* nelsongf@dedalus.lcc.ufmg.br

Short hydrogen bonds (SHB) are very interesting in Chemistry, because the interactions between the atoms in SHB are not well known. In O-H-O group, the hydrogen bond is short if O---O distance is among 2.4 and 2.5 Å. The aim of this work is identify SHB in acid salts. In this work eight acid salts (Na, K, Mn, Ni, Cu and Zn) of pyromellitic acid [C<sub>6</sub>H<sub>2</sub>(COOH)<sub>4</sub>] were synthesized and studied by X-ray diffraction. In Na, Mn, Ni, Cu and Zn salts the ligand is the ion C<sub>6</sub>H<sub>2</sub>(COO)<sub>2</sub>(COOH)<sub>2</sub> [H<sub>2</sub>Pm] and in K salt it is the ion C<sub>6</sub>H<sub>2</sub>(COO)(COOH)<sub>3</sub> [H<sub>3</sub>Pm]. These salts crystallize in monoclinic system, except Na salt that crystallize in triclinic system in P-1 space group. K salt crystallize in P2<sub>1</sub>/c space group, Cu salt in Pn and Mn, Ni and Zn in C2/c space group. The crystal data are show in Table 1.

Table 1. Crystal data of Na, K, Mn, Ni, Cu and Zn salts of pyromellitic acid.

Compound	Na <sub>2</sub> H <sub>2</sub> Pm	KH <sub>3</sub> Pm	MnH <sub>2</sub> Pm	NiH <sub>2</sub> Pm	CuH <sub>2</sub> Pm	ZnH <sub>2</sub> Pm
Formula	C <sub>10</sub> H <sub>8</sub> O <sub>10</sub> Na <sub>2</sub>	C <sub>10</sub> H <sub>11</sub> O <sub>11</sub> K	C <sub>10</sub> H <sub>16</sub> O <sub>14</sub> Mn	C <sub>10</sub> H <sub>16</sub> O <sub>14</sub> Ni	C <sub>10</sub> H <sub>16</sub> O <sub>14</sub> Cu	C <sub>10</sub> H <sub>16</sub> O <sub>14</sub> Zn
Space group	<i>P</i> 1̄	<i>P</i> 2 <sub>1</sub> /c	<i>C</i> 2/c	<i>C</i> 2/c	<i>P</i> n	<i>C</i> 2/c
a / Å	5.4957(2)	7.5608(6)	22.2145(6)	21.8694(7)	6,763(1)	21,9485(5)
B / Å	6.8035(2)	19.514(1)	9.8034(3)	9,7406(4)	10,923(1)	9,7595(4)
C / Å	8.7243(2)	9.7306(7)	7.3935(2)	7,2448(2)	9,646(1)	7,2915(2)
α	79.78(3)	90.0	90.0	90,0	90,0	90,0
β	75.84(3)	111.108(6)	105.391(2)	105,391(2)	91,925(3)	105,507(3)
γ	69.50(3)	90.0	90.0	90,0	90,0	90,0
V	294.75(2)	1339.4(2)	1551.16(6)	1487,96(8)	801,58(4)	1505,02(9)
R (F <sup>2</sup> )	0.072	0.081	0.075	0,059	0,037*	0,047
wR (F <sup>2</sup> )	0.118	0.166	0.104	0,102	0,114	0,088
S (F <sup>2</sup> )	1.19	1.44	1.26	1,29	1,38	1,06

\* R(F)

X-Ray data show that only Na, K and Cu atoms are coordinated to ligand. Na and K atoms are coordinated to seven O atoms with complex arrangement. Na atom is coordinate to two water molecules and four ligand molecules. The ligand present monoatomic bridge and quelate coordinations. In K salts, the metal are coordinate to three water molecules and three to ligand molecules with monodentate and bidentate coordinations. In Cu salts, the metal are coordinate to three water molecules and two ligand molecules in monodentate coordination. The other salts are ionic and the metal atom is coordinate to six water molecules in octahedral geometry. In Fe salt synthesis, did not obtained good single crystals to single crystal X-Ray diffraction. Powder X-Ray diffraction of this salts shows that Fe salt is isostructural to Co salt<sup>1</sup>. These salts present intramolecular SHB, except Cu salt. Only in Fe and Co salts, this SHB is crystallographic symmetric. The H atom is in mirror plane. The other salts present asymmetric SHB. The O---O distance observed are 2.396(6), 2.387(2), 2.412(2), 2.381(3)<sup>1</sup>, 2.414(3) and 2.415(3) Å to Na, K, Mn, Co, Ni and Zn respectively.

**Acknowledgments:** Prof. Eduardo Castellano of IFSC-USP for availability of KAPPA-CCD equipment, Prof. Marcos Pimenta of DF-UFMG for Raman spectroscopy data and CDTN for D<sub>2</sub>O.

<sup>1</sup> Ward, D. L., Luehrs, D. C.; Acta Cryst. C39, 1370-1372 (1983).

## PPQM13. Estudo Estrutural do Composto Orgânico C<sub>7</sub>H<sub>11</sub>ClNO<sub>3</sub>

Napolitano, H. C. A. S.<sup>1</sup>; Santos, R. H. A.<sup>2</sup>; Santos, L. da Silva<sup>3</sup>; Freitas, O.<sup>4</sup>

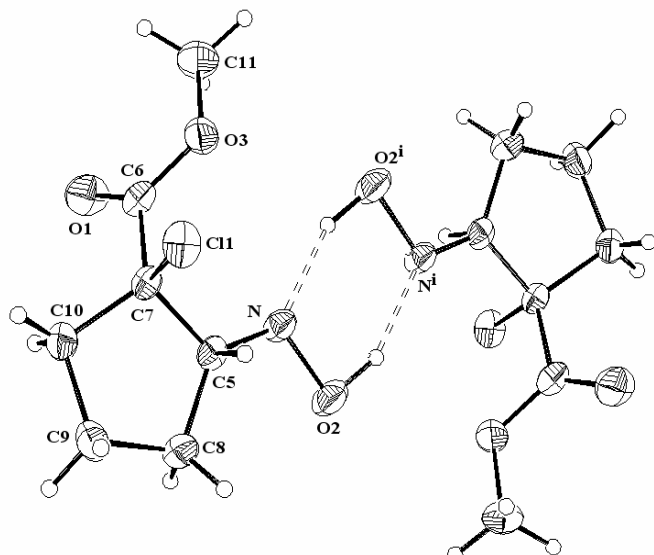
<sup>1,2</sup> Instituto de Química de São Carlos (IQSC), USP. <sup>1</sup>napolitano@iqsc.usp.br;

<sup>2</sup>reginas@iqsc.usp.br.

<sup>3,4</sup> Universidade Federal do Pará, Centro de Ciências Exatas e Naturais, Departamento de Química.

O composto orgânico C<sub>7</sub>H<sub>11</sub>ClNO<sub>3</sub> foi estudado por difração de raios X, visando obter informações detalhadas sobre a sua estrutura. A coleta de dados foi realizada no difratômetro automático CAD4 da Enraf Nonius do IQSC/USP. As medidas de intensidades foram feitas usando a radiação K $\alpha$  do Mo, monocromatizada por cristal de grafite, no intervalo de  $\theta$  entre 3,45° e 26,29°. Durante a coleta foram utilizadas as reflexões (20 $\bar{2}$ ), ( $\bar{2}\bar{2}\bar{5}$ ) e (121) para o controle da intensidade. Os parâmetros cristalográficos são: grupo espacial P $\bar{1}$ ,  $a = 6,122(2)$ ,  $b = 7,546(2)$ ,  $c = 10,771(3)$  Å,  $\alpha = 69,35(3)$ °,  $\beta = 75,12(3)$ °,  $\gamma = 89,01(3)$ °;  $Z = 2$  moléculas/cela,  $V = 448,5(2)$  Å<sup>3</sup>,  $F(000) = 202$ . Foram medidas 1813 reflexões únicas com  $R_{\text{int}} = 0,0546$ . A resolução e refinamento da estrutura foram feitas utilizando o sistema WinGX [1].

O modelo final obtido apresenta fator de discordância final de 0,0674. A Figura ilustra a molécula e sua dimerização através de um centro de inversão da molécula, sustentada pela ligação de hidrogênio N...O<sub>2</sub>-H<sup>i</sup> ( $i = -x, -y, -z+2$ ), com distância N...O<sub>2</sub><sup>i</sup> de 2,808 Å, e ângulo de 153,94°.



Representação da dimerização do composto C<sub>7</sub>H<sub>11</sub>ClNO<sub>3</sub>.

[1] L.J. Farrugia, *J. Appl. Cryst.*, 1999, **32**, 837-838.

CNPq, CAPES, FAPESP

## PPQM14. Crystal Structure of a Chromite

Santos, J.S.<sup>1</sup>, Doriguetto, A.C.<sup>2</sup>, Fernandes, N. G.<sup>1</sup>

<sup>1</sup> Universidade Federal de Minas Gerais, joab@dedalus.lcc.ufmg.br,  
nelsongf@dedalus.lcc.ufmg.br, <sup>2</sup> Universidade de São Paulo - São Carlos,  
dorigue@if.sc.usp.br

A cromita,  $\text{FeCr}_2\text{O}_4$ , é um mineral pertencente à família do mineral espinélio  $\text{MgAl}_2\text{O}_4$ . Os compostos desta família cristalizam-se no sistema cúbico, grupo espacial  $Fd\bar{3}m$ . Entretanto, poucos estudos foram realizados com o objetivo de investigação estrutural de cromitas naturais, que de um modo geral são substituídas.

Neste trabalho é analisada uma amostra de cromita natural, coletada num incrustamento rochoso no município de Piumhi, no sudeste de Minas Gerais. A cromita foi separada e purificada em ciclos de aquecimento com HCl, HF e  $\text{HNO}_3$  concentrados. Após cada ácido, a amostra foi lavada com HCl 1:1. Para caracterização, foram utilizadas as seguintes técnicas: difração de raios X de pó (difratômetro Rigaku Geigerflex, monocromador de grafite e tubo de Cu com varredura entre 3 e  $100^\circ$  em  $2\theta$ ), microssonda eletrônica (aparelho Jeol, modelo JXA 8900RL com um espectrômetro Noran-EDS), fluorescência de raios X (espectrômetro Shimadzu, modelo EDX-800, dotado de um tubo de Rh). Do difratograma de pó gerado, obteve-se o parâmetro de rede  $a = 8,33(4)$  Å e o volume da célula unitária  $V = 579(8)$  Å<sup>3</sup>, característicos do grupo dos espinélios. Por microssonda eletrônica foram detectados os elementos Mg, Al, Cr e Fe além de traços de Ti e V. A análise por fluorescência obteve os resultados semelhantes aos encontrados com a microssonda eletrônica.

Os espinélios podem apresentar-se sob duas formas estruturais: espinélio normal ou invertido. Se os sítios tetraédricos, representados por ( ), são ocupados pelos cátions bivalentes A<sup>II</sup> e os sítios octaédricos, representados por [ ], são ocupados por cátions trivalentes B<sup>III</sup>, a estrutura é chamada de espinélio normal. No espinélio invertido, os cátions trivalentes B<sup>III</sup> estão distribuídos entre os sítios octaédricos e tetraédricos e os cátions bivalentes A<sup>II</sup> estão no sítio octaédrico. A análise estrutural da cromita foi obtida com a radiação Mo K $\alpha$  de um difratômetro Kappa CCD da Enraf Nonius, modelo FR590. Considerando a distribuição de cátions na estrutura do espinélio e os resultados das análises químicas, vários modelos foram testados. Dentre os quais,  $(\text{Fe}_{0,44}\text{Mg}_{0,56})[\text{Cr}_{1,34}\text{Al}_{0,66}]\text{O}_4$  foi o que melhor se ajustou aos dados experimentais de difração de monocrystal. Isto é, os cátions  $\text{Mg}^{2+}$  e  $\text{Fe}^{2+}$  estão distribuídos no sítio tetraédrico enquanto  $\text{Al}^{3+}$  e  $\text{Cr}^{3+}$  estão no sítio octaédrico. Neste caso, os fatores de discrepância obtidos foram  $R(F)=0,0573$ ,  $WR(F2)=0,1611$  e  $S=1,243$ . As distâncias interatômicas são Mg(Fe)-O de 1,978(5) Å e Cr(Al)-O de 1,979(2) Å. Estes resultados são semelhantes aos obtidos por DORIGUETTO, (2000) para  $\text{Fe}_3\text{O}_4$ .

**Agradecimentos:** Prof. Eduardo Castellano do IFSC-USP por ceder o equipamento KAPPA-CCD que tornou possível a realização deste trabalho.

### Referências Bibliográficas

DORIGUETTO, A.C. Tese de Doutorado, Departamento de Química, UFMG, Belo Horizonte, MG, Brasil 176 p. 2000.

## PPQM15. Charge Density of Zn[H<sub>2</sub>O]<sub>6</sub>·[C<sub>10</sub>H<sub>4</sub>O<sub>8</sub>]

Diniz, R.<sup>1</sup>, Rodrigues, B. L.<sup>1</sup>, Ellena, J.<sup>2</sup>, Gustafsson, T.<sup>3</sup> and Fernandes, N. G.<sup>1\*</sup>  
<sup>1</sup> Universidade Federal de Minas Gerais; <sup>2</sup> Universidade de São Paulo – São Carlos; <sup>3</sup> University of Uppsala. \* nelsongf@dedalus.lcc.ufmg.br

The aim of this work is investigated the charge density distribution in the crystal of hexaaquazinc(II) dihydrogen piromellitate – ZnH<sub>2</sub>Pm {[Zn(H<sub>2</sub>O)<sub>6</sub>][C<sub>6</sub>H<sub>2</sub>(COO)<sub>2</sub>(COOH)<sub>2</sub>]}, mainly of hydrogen bonds. The crystal structure of this compound is show in Figure 1.

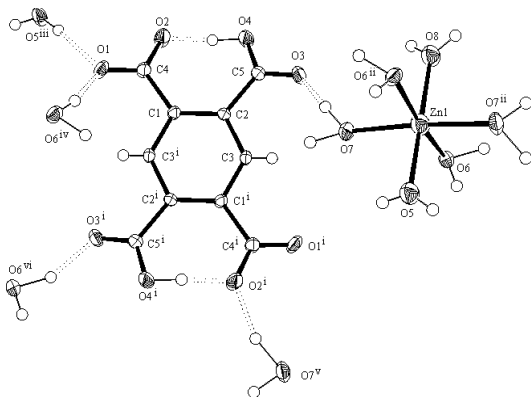


**Figure 1.** Crystal structure of ZnH<sub>2</sub>Pm. Thermal ellipsoid was drawn with 50% probability. Symmetry codes: I ( $-\frac{1}{2}-x, \frac{1}{2}-y, -z$ ); ii ( $-x, y, \frac{1}{2}-z$ ); iii ( $-\frac{1}{2}+x, \frac{1}{2}+y, z-1$ ); iv ( $x-\frac{1}{2}, \frac{1}{2}-y, z-\frac{1}{2}$ ); v ( $-\frac{1}{2}-x, y+\frac{1}{2}, -\frac{1}{2}-z$ ) and vi ( $-\frac{1}{2}+x, y-\frac{1}{2}, z-1$ ).

In long hydrogen bond (LHB) A-H---B, the A-H interaction is covalent, while there is an electrostatic interaction between H and B. However, short hydrogen bond (SHB), the interactions between A-H and A---B are not so clear. If A and B are O atoms, the HB is considered short if the O---O distance is around 2.4 - 2.5 Å.

Neutron and X-Ray diffraction of ZnH<sub>2</sub>Pm were obtained. In charge density refinement, neutron data of positions and thermal parameters of H atoms were used. This compound is ionic and presents na asymmetric intramolecular SHB with O---O distance of 2.412(3) Å. Neutron data show that the O-H distances are 1.114(3) and 1.309(3) Å and O-H-O angle is 169,1(2)°. In H<sub>2</sub>Pm ion, the symmetry *m* was used in C atoms, except in C3 that was used *mm2*. In O1 and O3 atoms was used *mm2* symmetry and *3m* in O2 and O4 (Figure 1). All H atoms were considered with cylindrical symmetry.

Static maps around SHB show that the two O-H interactions of O-H-O group are different. There are more deformation density in shorter O-H bond. However, the interaction in SHB is different that observed in typical HB (long and medium HB).

Electron density distribution around Zn atom is aspheric and Zn charge (+1.18) is smaller than its formal charge, +2. The symmetry 2 was used in Zn atom, *mm2* in O5 and O6 atoms and *m* to O7 and O8. The multipole refinements clearly show the distribution of zinc *d* electrons is aspherical. There are excess of electron density in the ligand directions (O5 and O6) and between them (O7 and O8).

**Acknowledgments:** Prof. Eduardo Castellano of IFSC-USP for availability of KAPPA-CCD equipament.

## OPQM16. Novel Crystal Structure of a Sodium and Potassium Nitrate Obtained from the Leg of a Orthoptero of the Tridactylidae Family

*Ellena J.A. - Instituto de Física de São Carlos / USP – javiere@if.sc.usp.br*  
*Castellano E. E. - Instituto de Física de São Carlos / USP – pino@if.sc.usp.br*  
*Ferreira A. - Instituto de Biociências (IB) - Rio Claro/UNESP – depbio@rc.unesp.br*

We report here the X-Ray crystal structure of a Sodium and Potassium Nitrate salt,  $\text{Na}_{0.63}\text{K}_{0.37}\text{NO}_3 \cdot \text{H}_2\text{O}$ , obtained from a rather peculiar and unexpected source. Evolution changes in insects can be characterized by studying morphological variations in their legs, and sometimes by other alterations like the presence of glands inside them as has been widely reported. In this context, a recent study on a specimen of the species Ellipes (Orthoptera- Trydactiloidea-Trydactilidae), collected in the margin of the Araguaia River, in the Bananal Island, showed the presence of a cluster, in the insect of middle legs tibia, of what seemed to be small crystals. The insects are only 1.5 to 3.0 mm in length and the crystals were observed and photographed with an optical microscope. Although it is not the principal aim of this report, it is interesting to point out that the crystals are only present in the middle legs, never in the anterior or posterior legs, and that the size and quantity of the crystals increase with insect age until they occupy most of the interior of the leg. Because of the very small size of the insect legs and the tiny amount of material, handling of the crystals turned out to be a rather difficult task. A further complication was the tendency of the samples to stick to the microscope glass slide. The crystals were very small prisms and the largest found, with dimensions  $0.010 \times 0.005 \times 0.001$  mm, was used for diffraction measurements. The shortest length could not be determined with precision and 0.001 mm is just an upper estimation of its value. To prevent the crystal from sticking to the microscope glass slide, it was soaked in glycerin and then mounted in a 0.2 mm cryogenic loop protein support. Data collection on an Enraf Nonius CCD diffractometer proceeded at 100K during about 20hs. The compound crystallizes in the trigonal space group R32 and was described in a hexagonal cell with  $a = 4.811(1)$  and  $c = 15.956(5)$  Å. The structure was refined by full matrix least squares to a final  $R_1$  value of 0.075, from 114 independent reflections with  $I > 2\sigma(I)$ .

## PPQM17. Molecular and Crystal Structure of the Complex $[\text{Cu}_2\mu-(\text{O}_2\text{CC}_4\text{H}_3\text{O})_4(\text{H}_2\text{O})_2].2\text{H}_2\text{O}$

*Maia, D. F. S. – UFMG (lycan@fisica.ufmg);  
Teles, W. M. – UFJF (teles@quimica.ufjf.br)  
Machado, F. C. – UFJF (cavallier@quimica.ufjf.br)  
Speziali, N. L. – UFMG (nspezial@fisica.ufmg.br);*

Copper(II) carboxylates are bimetallic complexes where the carboxylate groups make bridge connections between two metallic sites, conforming a cage-type structure. Compounds of this kind are extensively studied due to the inherent interest in its structural aspects and because of their potential catalytic and anti-inflammatory properties.

Single crystals of the  $[\text{Cu}_2\mu-(\text{O}_2\text{CC}_4\text{H}_3\text{O})_4(\text{H}_2\text{O})_2].2\text{H}_2\text{O}$  complex were studied by X-ray diffraction. The copper atoms and some oxygens were found via Patterson function analysis, using SHELXD program. The remaining atoms were found by Fourier difference.

The crystal structure, refined in the  $\text{P}2_1$  space group with  $Z=4$ , shows that every copper atom has a water molecule connected to the axial position. The chemical analysis predicts another 4 water molecules in the structure, making hydrogen bonds, but they could not be acceptably located. The Fourier difference proposes 8 strong peaks that can be grouped into two distinct sets of 4. Attempts to associate the peaks of the first stronger group with oxygens lead to inconsistencies indicating an overestimated scattering power. This fact, together with the presence of the other 4 peaks, can be interpreted as disorder of the water molecules.

Each  $[\text{Cu}_2(\text{O}_2\text{CC}_4\text{H}_3\text{O})_4(\text{H}_2\text{O})_2]$  unit in the structure can be divided into a central cage and four rings, representatives of the  $\text{C}_4\text{H}_3\text{O}$  furoic group. The rings are connected to the central cage via  $\sigma$ -bonds allowing them to rotate, at room temperature. Such a freedom is evidenced as an excessively great atomic displacement factor and some deviations in the average bond distances.

The structure refinement, performed with SHELXL program, converged to a residual index  $R_1 = 0.0660$  using 4387 reflections with  $|\text{F}(\mathbf{h})|^2 > 2\sigma(\mathbf{h})$ ; some restraints on bond distances and angles were conveniently imposed on the furoic rings. The structural results will be presented.

**Acknowledgment:** Special thanks to professor Eduardo E. Castellano, USP/IFSC, for the data collection. This work is partially supported by CNPq and FAPEMIG.

## PPQM18. Determinação da Estrutura Cristalina e Molecular do Polímero $[Cd(Cl)_2(HPz)]_n$ e Estudo das Interações Entre seus Monômeros

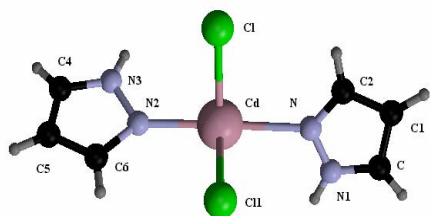
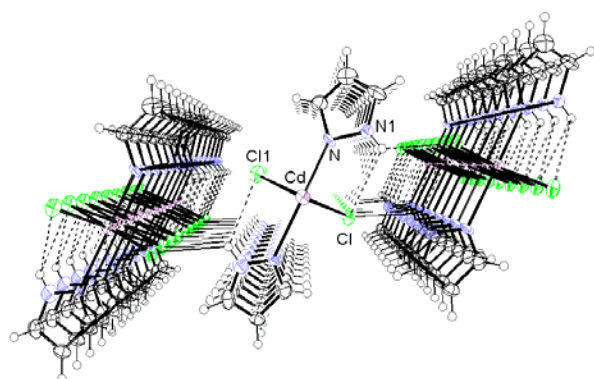
Ferreira, J.G.- Inst. de Química de São Carlos- Usp. E-mail: janagofe@iqsc.usp.br  
 Santos, R.H.A - Inst. de Química de São Carlos Usp E-mail: reginas@iqsc.usp.br  
 Netto, A.V.G. Inst. de Química-Araraquara-Unesp Email:adelgodo@posgrad.iq.unesp.br  
 Silva, A. M. - Inst. de Química - Araraquara-Unesp E-mail: aemauro@iq.unesp.br

Nas últimas três décadas têm-se intensificado o estudo de complexos de metais de transição com o ligante pirazol (HPz). Este ligante e seus derivados podem se coordenar através do nitrogênio piridínico (sítio de coordenação) e também através do nitrogênio pirólico (doador de hidrogênio), atuando com ligantes terminais ou em ponte. Em decorrência disto, muitos destes compostos tem sido extensamente utilizados na química de organometálicos, na bioinorgânica e na química de coordenação.

Para síntese deste cristal utilizou-se cloreto de cádmio(II) e pirazol, na razão molar de 1:2, em metanol. Os cristais se formaram a partir da evaporação desta solução. Os seus dados foram coletados no difratômetro CAD4 da Enraf Nonius. Na resolução da estrutura foi utilizado o método de Patterson.

Esta estrutura cristalizou-se no sistema monoclinico, grupo espacial Cc. Foram coletadas 1220 reflexões, [1176 reflexões com  $I > 2.0 \sigma(I)$ ], e os índices de discordância finais foram:  $R_{\text{obs}}$  0.022 e  $R_{\text{all}}$  0.021

No cristal o cádmio está em posição especial, coordenado a duas moléculas de pirazol ( $d_{\text{Cd-N}} = 2,198(1)$  e  $2.357(1)\text{\AA}$ ) e duas de cloro ( $d_{\text{Cd-Cl}} = 2,698(3)$  e  $2.677(3)\text{\AA}$ ).



O polímero de cadeia infinita se desenvolve na direção  $[0,1,0]$ , ao longo do eixo b cristalográfico. A distância entre os centros metálicos é de  $3,863\text{\AA}$ . Verificou-se a presença de ligações intramoleculares e intermoleculares do tipo não convencionais entre os íons cloretos e os átomos de nitrogênio pirólicos (Tabela 1).

Tabela 1: Tabela das ligações de hidrogênio existentes no polímero

	$N - H \dots Cl$	$N - H$	$H - Cl$	$N - Cl$	$\text{Ângulo}$
Ligações	N3 - HB ... Cl1	0.8596	2.7470	3.366(9)	130.16
Intramoleculares	N1 -- HA ... Cl	0.8604	2.8102	3.328(9)	120.32
Ligações	N3 -- HB ... Cl	0.8596	2.8021	3.386(9)	126.62
Inermolecularres	N1 -- HA ... Cl1	0.8604	2.6997	3.349(8)	133.31

Agradecimentos: Capes, Cnpq e Fapesp

Referência: Farrugia, L. J. Appl. Cryst., 1999, 32, 837-838

PPQM19. A crystallographic Study of (2-acetylpyridine- $\kappa$ N 4-phenylthyosemicarbazone- $\kappa^2$ N<sup>1,S</sup>) methyl-trans-dichlorotin(IV)

Gambardella M.T.P., IQSC/USP, teca@iqsc.usp.br; Francisco R.H.P. IQSC/USP, reginap@iqsc.usp.br; Sousa G. F., UnB, gfreitas@unb.br

The title complex,  $[\text{Sn}(\text{C}_{14}\text{H}_{13}\text{N}_4\text{S})(\text{CH}_3)\text{Cl}_2]$ , was synthesized as part of a research program devoted to the investigation of the coordination modes of thiosemicarbazones with organotin(IV) compounds. The chelating behavior of N,N,S-donor thiosemicarbazones revealed three coordination modes. They can act as a neutral N(azomethine),S-bidentate ligand, as an anionic (-1) ligand bonded through N,N,S and as an anionic (-1) ligand bonded through N(azomethine),S.

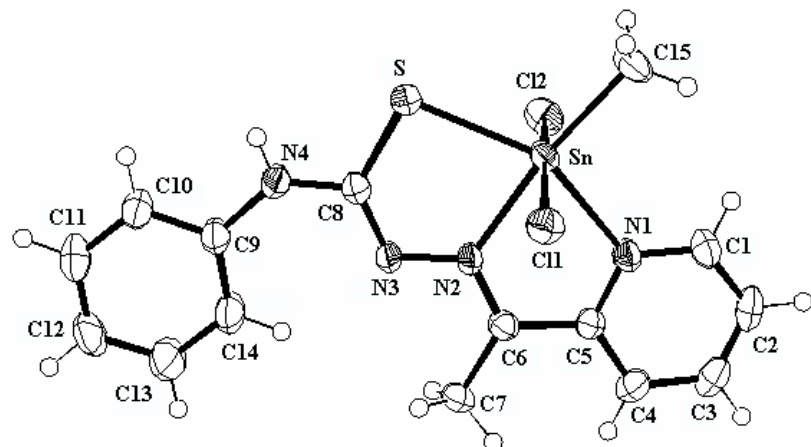
The crystal structure determination was conducted by single crystal X-ray diffraction. The data collection was done on a Enraf-Nonius CAD-4 automatic diffractometer, with graphite monochromated MoK $\alpha$  radiation ( $\lambda = 0.71073 \text{ \AA}$ ).

Crystal Data: centric triclinic space group,  $a = 9.3186(6)$ ,  $b = 9.7939(4)$ ,  $c = 10.3489(10) \text{ \AA}$ ,  $\alpha = 105.958(5)$ ,  $\beta = 95.056(7)$ ,  $\gamma = 102.334(5)^\circ$ ,  $V = 876.23(11) \text{ \AA}^3$ ;  $D_c = 1.796 \text{ Mg.m}^{-3}$ ,  $\mu = 1.885 \text{ mm}^{-1}$ , 5212 reflections measured, 4951 independent ( $R_{\text{int}} = 0.019$ ).

The structure was solved using the heavy-atom method and refined by full-matrix least-squares calculations, after absorption correction by  $\Psi$  scan method. The final R indices are  $R_1 = 0.033$ ,  $wR_2 = 0.071$  for 3853 observed reflections [ $F > 2\sigma(F^2)$ ].

The  $[\text{Sn}(\text{C}_{14}\text{H}_{13}\text{N}_4\text{S})(\text{CH}_3)\text{Cl}_2]$  adopts a packing mode with discrete and neutral molecules, where the Sn(IV) has a distorted octahedral coordination geometry, with the methyl and the thiosemicarbazone derivative at the equatorial plane and the chlorides at the axial trans positions.

The  $\text{C}_{14}\text{H}_{13}\text{N}_4\text{S}$  ligand is N,N,S-coordinated.



CNPq, FINEP, FAPESP, CAPES

PPQM20. Crystallography of Natural Perovskite from the Uberaba Formation  
Sandstones, Minas Gerais, Brazil  
Gravina, É. G.\*; Brod, J. A.\*; Doriguetto, A. C.\*\*; Diniz-Pinto, H.S.\*

— \* Universidade de Brasília, \*\* Universidade de São Paulo/ IFSC  
[egogra@unb.br](mailto:egogra@unb.br)

**Introduction:** In nature, perovskite structure occurs in a variety of minerals, the most common being: perovskite ( $\text{CaTiO}_3$ ), loparite ( $\text{Na}_{0.5}\text{Ce}_{0.5}\text{TiO}_3$ ), lueshite ( $\text{NaNbO}_3$ ), latrappite ( $\text{CaNb}_{0.5}\text{Fe}_{0.5}\text{O}_3$ ), tausonite ( $\text{SrTiO}_3$ ),  $\text{Ce}_2\text{Ti}_2\text{O}_7$ , and  $\text{Ca}_2\text{Nb}_2\text{O}_7$ . In the Earth's crust, perovskite is mostly a primary mineral in alkaline igneous rocks, either in essential or accessory amounts, and a reliable indicator of silica undersaturation. Although it is not a common mineral in sedimentary rocks, detritic perovskite grains are very abundant in sandstones of the Uberaba Formation, in western Minas Gerais State, together with large amounts of other clastic components derived from basic, ultrabasic, and intermediate igneous rocks of alkaline and subalkaline affinity<sup>1</sup>. In a sandstone outcrop near the city of Conceição das Alagoas, perovskite may reach up to modal 28%, occurring as subhedral to anhedral grains, varying in colour from light brown to yellowish brown, greenish yellow, and orange. Skeletal crystals, resulting from alteration to anatase, sphene or calcium carbonate are common. Despite the variation in optical properties, these perovskites revealed little compositional variation during mineral chemistry studies<sup>2</sup>, concentrating near the  $\text{CaTiO}_3$  end-member, with limited solid solution towards more rare-earth and iron rich (e.g.  $\text{CeFeO}_3$ ) terms. **Analytical Methods:** Adequate perovskite crystals were selected for single crystal X-ray diffraction analysis, carried out at the X-ray Laboratory of the USP Institute of Physics and Chemistry at São Carlos, Department of Physics and Materials Sciences. Structural formula calculations used average electron microprobe analyses obtained at the Institute of Geosciences of the University of Brasília, normalised to  $\text{CaTiO}_3$ . Structure refinement was carried out using the HKL DENZO-SCALEPACK<sup>3</sup>, HKL SCALEPACK, SHELXS-97<sup>4</sup>, and SHELXL-97<sup>5</sup> programs. **Discussion:** The X-ray data analysis shows that the studied perovskite is orthorhombic ( $a = 5.3740(4)$  Å;  $b = 5.4480(4)$  Å; and  $c = 7.6320(5)$  Å) and crystallizes in the space group Pbnm, where the  $a$ ,  $b$ , and  $c$  crystallographic axis coincide with binary symmetry axis and are perpendicular to symmetry planes. The  $\text{Ti}^{4+}$  cations occupy 1/4 of the HCP octahedral interstices, and the  $\text{TiO}_6$  octahedrons are inclined relatively to the  $c$  axis and are connected to each other by their apices. The  $\text{Ca}^{2+}$  cations occupy 1/4 of the positions relative to the hexagonal close packing, while  $\text{O}^{2-}$  anions, occupy the remaining 3/4 of these positions. The  $R_1$  e  $wR_2$  values obtained are 4.96% and 12.04%, respectively. **Conclusions:** On the basis of its crystal structure and mineral chemistry, the perovskite in sandstones from the Conceição das Alagoas region may be classified as perovskite sensu stricto ( $\text{CaTiO}_3$ ). Although the  $R_1$  e  $wR_2$  values are relatively high for a simple structure, they are within the acceptable error margins.

**References:** 1) Hasui, Y. 1968. In: 22º Congresso Brasileiro de Geologia, anais. Belo Horizonte, MG. 167-179; 2) Gravina, É. G. 2003. Dissertação de Mestrado, Instituto de Geociências, Universidade de Brasília, Brasília. 220p.; 3) Otwinowski, Z. & Minor, W. 1997. In: Methods in Enzymology, 276, edited by Carter Jr., C.W. & Sweet, R.M., New York, Academic Press, 307-326.; 4) Sheldrick, G.M. 1997a. Univ. of Göttingen: Göttingen, Germany; 5) Sheldrick, G.M. 1997b. Univ. of Göttingen: Göttingen, Germany.

**Acknowledgements:** The authors are grateful to CNPq (Brazilian Research and Development Council) for a MSc grant to E.G. Gravina, and research grants to J.A. Brod, and H.S. Diniz-Pinto. A.C.Doriguetto thanks FAPESP for a postdoctoral fellowship. We are also grateful to the University of Brasília and IFSC-USP, for granting access to laboratory facilities.

# OSAS01. Viability Study For the Installation of a SANS Beam-Line at IPEN/CNEN-SP

*José Mestnik Filho, Instituto de Pesquisas Energéticas e Nucleares  
j mestnik@net.ipen.br*

*José Teixeira, Laboratoire Léon Brillouin, Centre d'Études de Saclay  
teix@lrb.saclay.cea.fr*

## ABSTRACT

It is presented a study of the performance parameters of a hypothetical small angle neutron scattering (SANS) spectrometer running at the IEA-R1 reactor. It is shown that the range of useful momentum transfer  $Q$  for a traditional SANS spectrometer would be  $Q_{\min} = 0.01$  to  $Q_{\max} = 0.6 \text{ \AA}^{-1}$  with a resolution  $\Delta Q/Q$  of 70% at  $Q_{\min}$ . The same useful  $Q$  range could be achieved with resolution  $\Delta Q/Q \leq 20\%$  with a multi-channel collimator in which case the full area of the neutron source is exploited, and as a consequence, a larger sample area and larger monochromator device are necessary. New SANS concepts under development with possibilities to improve the resolution and to decrease the lower limit of momentum transfer will be presented.

## PSAS02. Structure of Charged Phospholipid Vesicles by SAXS

Fernandez\*, R.M., Riske†, K.A., Lamy-Freund\*, M.T. and Amaral\*, L.Q.

\*Instituto de Física da Universidade de São Paulo, Brasil

†Max Planck Institut für Kolloid und Grenzflächenforschung, Golm, Germany

rmorato@fge.if.usp.br, kar@MPIKG-GOLM.MPG.DE

mtfreund@if.usp.br, amaral@if.usp.br

The anionic phospholipid dimyristoyl phosphatidylglycerol (DMPG) in a defined range of low ionic strength presents a transparent and viscous intermediate phase (IP between  $T_m^{on}$   $\sim 20^\circ\text{C}$  and  $T_m^{off} \sim 30^\circ\text{C}$ ) between turbid dispersions of vesicles with rigid and fluid membranes. The structure of the vesicles over the transitions has been already investigated with X-ray [1-3]. A broad peak around  $q = 0.12 \text{ \AA}^{-1}$  exists in all phases, well fitted in terms of a single bilayer, with changeable parameters of thickness and electron density contrast [1,2]. Extending the  $q$  range to both smaller and larger values with a SAXS-WAXS camera evidenced [3] a structure at  $\sim 400 \text{ \AA}$ , exclusively in IP, and existence of ordered chains (peak at  $4.2 \text{ \AA}$ ), only in the gel phase bellow  $T_m^{on}$ . New results obtained in the SAXS beam line of LNLS in 2002 are here presented, focusing the effects of additives as well as the effect of change in the chain length, aiming to disentangle the effects at molecular and bulk levels:

-Study of the effect of the ionic strength on the transitions in DMPG, varying the amount of added salt. Preliminary results [2] obtained with 10 mM and 50 mM dispersions showed that IP disappears at, respectively, 100 and 500 mM salt addition. Results now presented with ionic strength in the interval 2-500 mM and temperature variation show the tendency of formation of multilamellar structures, as the intermediate phase disappears, and DMPG starts to behave as non-charged phospholipids. But a clear formation of a Bragg peak is tricky and of difficult reproducibility.

- Study of the effect of addition of a peptide hormone ( $\alpha$ -MSH) to DMPG, which was shown [4] to have a strong effect on the lipid membrane. A clear change in the bilayer contrast profile is now reported and there is a temperature effect, even when IP is not present.

- Study of another charged phospholipid, dipalmitoyl phosphatidylglycerol (DPPG), which also presents the intermediate phase, although in a smaller temperature interval. DPPG has 16 carbons in the chains, while DMPG has 14. Results evidence existence of 4 different phases in the measured temperature interval ( $25^\circ\text{C}$  -  $50^\circ\text{C}$ ), and a difference in bilayer thickness with entrance in the fluid phase more marked than with DMPG.

Analysis of data follows two methodologies: fitting with strip models [1,2] and indirect Fourier transform with Glatter's PCG software [3].

[1] K.A.Riske, L.Q.Amaral and M.T.Lamy-Freund. *Biochim. Biophys. Acta.* 1511 (2001) 297.

[2] K.A.Riske, Ph.D. Thesis (IFUSP, 2001)

[3] L.Q.Amaral, K.A.Riske and M.T.Lamy-Freund (in preparation)

[4] R.M.Fernandez, M.T. Lamy-Freund. *Biophys. Chem.* 87 (2000) 87.

Research supported by FAPESP, PRONEX / CNPq / MCT and LNLS.

### PSAS03. Gelation and Drying of Weakly Bonded Silica-PPO Nanocomposites

CHAKER J.A.,<sup>a</sup> DAHMOUCHE K.,<sup>a</sup> SANTILLI C.V.,<sup>a</sup> PULCINELLI S.H.<sup>a</sup> and CRAIEVICH A.<sup>b</sup>

<sup>a</sup>Institute of Chemistry, UNESP, P.O. Box 355 14800-970, Araraquara, SP, Brazil

<sup>b</sup>Institute of Physics, USP, P.O. Box 66318 05315-970, São Paulo, SP, Brazil.

E-mail: jachaker@posgrad.iq.unesp.br

Silica-poly(oxypropylene) (PPO) nanocomposites containing PPO with weak physical bonds between the organic (PPO) and inorganic (silica) phases were obtained by the sol-gel procedure. Three precursor sols containing silica and PPO with molecular weights of 1000, 2000 and 4000g/mol were prepared. The structure changes during the whole sol-gel process, i. e. sol formation, sol-gel transition and gel aging and drying were investigated *in situ* by small angle X-ray scattering (SAXS). The experimental SAXS curves corresponding to sols and wet gels containing PPO of molecular weight 1000g/mol indicate that the aggregates formed during the studied process are fractal objects. Close to the sol-gel transition and during gel aging the fractal dimension is  $D=2.5$ . A clearly different structure evolution occurs in samples prepared with PPO with molecular weights 2000 and 4000 g/mol. Our SAXS results indicate the presence of two coexisting and well-defined structure levels, one of them corresponding to small silica clusters and the other to large silica aggregates. These two levels remains along the whole transformation. The SAXS curves of all dry samples are similar to those of the corresponding wet gels suggesting that no significant changes at nanoscopic scale occur during the drying process.

Keywords: hybrids; sol-gel; SAXS;

## PSAS04. SAXS and NMR Study of Siloxane-PMMA Hybrids Prepared by Sol-gel Process

Sarmento, V. H. V., Institute of Chemistry, UNESP, Brazil,  
[victsarm@posgrad.iq.unesp.br](mailto:victsarm@posgrad.iq.unesp.br)

Dahmouche, K., Institute of Chemistry, UNESP, Brazil, [karidahm@iq.unesp.br](mailto:karidahm@iq.unesp.br)

Santilli, C. V., Institute of Chemistry, UNESP, Brazil, [santilli@iq.unesp.br](mailto:santilli@iq.unesp.br)

Pulcinelli, S. H., Institute of Chemistry, UNESP, Brazil, [sandrap@iq.unesp.br](mailto:sandrap@iq.unesp.br)

Craievich, A. F., Institute of Physics, USP, Brazil, [craievich@if.usp.br](mailto:craievich@if.usp.br)

Transparent siloxane-polymethylmethacrylate (PMMA) hybrids were synthesized by the sol-gel process through hydrolysis of methacryloxyproyltrimethoxysilane (TMSM), tetramethoxysilane (TMOS) and polymerization of methylmethacrylate (MMA) using benzoyl peroxide (BPO) as catalyst. These composites have a good chemical stability due to the presence of covalent bonds between the inorganic (siloxane) and organic (PMMA) phases. The effects of siloxane content, pH of the initial sol and BPO content on the structure of the dried gels were analyzed by small-angle X-ray scattering (SAXS). SAXS results revealed the presence of an interference (or correlation) peak at medium q-range for all compositions, suggesting that siloxane groups located at the ends of PMMA chains form isolated clusters that are spatially correlated. The average intercluster distance - estimated from the q-value corresponding to the maximum in SAXS spectra - decreases for samples prepared with increasing amount of TMSM-TMOS. This effect was assigned to the expected increase in the number density of siloxane groups for progressively higher siloxane content. The increase of BPO content promotes a more efficient polymerization of MMA monomers but has no noticeable effect on the average intercluster distance. High pH favors polycondensation reactions between silicon species of both TMOS and TMSM silicon alcoxides, leading to a structure in which all siloxane clusters are bonded to PMMA chains. This effect was confirmed by <sup>29</sup>NMR measurements.

- Brinker, C.J. & Scherer, G. W. (1990). Sol-Gel Science: The Physics and Chemistry of Sol-Gel Processing, pp. 203, San Diego: Academic Press.  
Dahmouche, K., Santilli, C.V., Pulcinelli, S.H. & Craievich, A.F. (1999). J. Phys Chem B 103, 4937-4942.  
Cornu, J.F., PhD Thesis, Institut National des Sciences Appliquees, Villeurbanne (France) 1993.

We acknowledge M.A.L. Margionte for help in samples synthesis, and S.H.. Benedito for NMR measurements. Support from LNLS, FAPESP, CAPES and PRONEX is also acknowledged.

# OSAS05. Isothermal Aggregation of Bi Atoms Embedded in a Soda-Borate Glass: Coarsening of Liquid Nanodroplets and Atomic Diffusion

Craievich A. F.<sup>1</sup> and Kellermann G.<sup>2</sup>

<sup>1</sup> Instituto de Física, USP, C.P 66318, CEP 05315-970, São Paulo SP, Brazil  
e-mail: craievich@if.usp.br

<sup>2</sup> Laboratório Nacional de Luz Síncrotron, Campinas SP, Brazil  
e-mail: keller@lnls.br

This is a study of the kinetic of formation and growth of liquid Bi clusters embedded in a soda-borate glass. Initially homogeneous and Bi doped glass samples are studied by *in situ* small-angle x-ray scattering (SAXS) during isothermal annealing at temperatures close to the soda-borate glass transition (~800-850 K). The annealing temperatures being well above the melting temperature of bulk Bi crystals ( $T_m = 544.4$  K), the spherical clusters are in liquid state from the first stages until the end of their growth. From the results of SAXS experiments, the radius distribution function, the time dependence of the average radius, the radius dispersion and the number density of the liquid nanodroplets are determined. These experimental results are compared to those predicted by the classical theories of growth of spherical clusters embedded in a supersaturated matrix. Complementary measurements of transmission electronic microscopy (TEM) were performed in order to verify the shape of the Bi nanoclusters. The TEM images shows that Bi nanocrystals embedded in the soda-borate glass matrix have a nearly spherical shape and indicates a single-mode radius distribution function. Our experimental SAXS and TEM results regarding the formation and growth of Bi liquid droplets embedded in the studied Bi doped soda-borate glass evidence a clustering process involving three distinct stages: i) an initial short incubation stage, ii) a second fast growth stage during which the size of Bi clusters increases by atomic diffusion and aggregation of isolated Bi atoms, and iii) a final rather slow stage during which most of the isolated Bi atoms are already aggregated but the nanodroplets still grow by coarsening. The stage of nucleation and growth is characterized by an induction period of formation of precursor Bi nuclei and by their growth promoted by atomic diffusion of isolated Bi atoms through the glass matrix. At more advanced stages of annealing, the time variations of the average radius, the density number of the Bi nanodroplets and the volume fraction of the new phase are well described by the equations predicted by the Lifshitz-Slyozov[1] and Wagner[2] (LSW) model for coarsening. The ratio between the nanodroplets radius dispersion and their average value is a nearly time constant during coarsening as established by LSW theory. On the other hand, it was demonstrated that the radius distribution is better described by a log-normal function than by the function proposed by LSW model. The diffusion coefficients of Bi atoms through the studied soda-borate glass during coarsening were calculated from a set of experimental curves of x-ray scattering power (SAXS intensity in absolute scale). This evaluation was performed for different annealing temperatures so as, from an Arrhenius plot, the activation energy of the diffusion process of Bi through the soda-borate glass matrix was also determined.

This work was supported by LNLS, PRONEX, CNPq and FAPESP.

## References

1. I. M. Lifshitz and V. V. Slyosov, J. Phys. Chem. Solids 19, 35 (1961).
2. C. Wagner, Z. Elektrochem. 4, 581 (1961).

PSAS06. SAXS Study of The Mechanisms of Aggregation in Sulphate  
Zirconia sols<sup>+</sup>

*Craievich, A.\*, Riello, P.\*\* Minesso, \*\* A. and Benedetti, A.\*\**

*\*Instituto de Física, Universidade de São Paulo, Brasil, craievich@if.usp.br*

*\*\* Dipartamento Chimica Fisica, Università di Venezia, Italia*

A systematic study, using synchrotron small-angle X-ray scattering (SAXS), of the mechanisms of aggregation of sulphate zirconia colloidal sols under different preparation conditions was performed. The kinetics of the whole aggregation process was followed *in situ* using the SAS beam line of National Synchrotron Light Laboratory (LNLS). The effects of varying acid, water and sulphate contents were analysed. These effects were investigated using open and sealed sample cells. It was observed that two clearly different mechanisms govern the aggregation at the beginning and at advanced stages of the process, respectively. In the early stages, small needle-shaped clusters are formed. They have a time independent cross-section and progressively increasing length. At advanced stages, the initially needle-shaped clusters start to build up a 3D structure, their aggregation being controlled by the classical mechanism of diffusion limited cluster-cluster aggregation (DLCCA). The experimental results indicate a clear effect of sulphate concentration on the structure of the 3D aggregates. Because of the differences in composition and preparation conditions, the final sols exhibit different structural features. However, the results of this investigation suggest that a single and remarkably simple growth model explains equally well the aggregation processes for all of the studied colloidal solutions.

+ Journal of Physical Chemistry B. Accepted (2003).

Support provided by LNLS, PRONEX and FAPESP is acknowledged.

# PMPO01. O Efeito da Adição de Boro na Anisotropia da Expansão Térmica das Fases $\text{Nb}_5\text{Si}_3$ , $\text{Ta}_5\text{Si}_3$ e $\text{Mo}_5\text{Si}_3$

Rodrigues G., Nunes C. A., Suzuki P. A., Coelho G. C.

*Faculdade de Engenharia Química de Lorena – FAENQUIL*

*geovani@phase.faenquil.br*

Trabalhos recentes mostram que compósitos contendo fases metálicas em equilíbrio com um metal ou liga refratária apresentam potencial para aplicações estruturais em altas temperaturas. Dentro desta classe de materiais, encontram-se as ligas dos sistemas Mr-Si-B (Mr = Mo, Nb, Ta, Ti). Em termos de avaliação do potencial de um material multifásico para aplicações em altas temperaturas, é importante conhecer a anisotropia da expansão térmica de cada fase que constitui este material bem como avaliar como os coeficientes de expansão térmica das fases que o constituem variam em função da temperatura, especialmente no caso de aplicações envolvendo ciclagem térmica. Materiais que apresentam fases com um alto grau de anisotropia de expansão térmica ou possuem fases com significativas diferenças nos valores dos coeficientes de expansão térmica estão sujeitos a geração de importantes tensões internas, seguido do aparecimento de trincas e eventual falha do componente em serviço.

Este trabalho teve como objetivo avaliar o efeito da adição de boro nos coeficientes de expansão térmica das fases binárias  $\text{Nb}_5\text{Si}_3$ ,  $\text{Ta}_5\text{Si}_3$ ,  $\text{Mo}_5\text{Si}_3$  e também a determinação dos coeficientes de expansão térmica da fase conhecida como  $T_2$  presente nos sistemas ternários Nb-Si-B, Ta-Si-B e Mo-Si-B com composições  $\text{Nb}_5\text{Si}_{3-x}\text{B}_x$ ,  $\text{Ta}_5\text{Si}_{3-x}\text{B}_x$  ( $0 \leq x \leq 2$ ) e  $\text{Mo}_5\text{SiB}_2$  respectivamente. As ligas foram preparadas a partir de elementos de alta pureza Ta (min.: 99,95%), Nb (min.: 99,8%), Mo (min.: 99,8%), Si (min.: 99,998%) e B (min.: 99,5%). Estas ligas foram fundidas em um forno a arco com eletrodo não consumível de tungstênio, sob atmosfera de argônio e utilizando um cadiño de cobre refrigerado a água. Para garantir a homogeneidade foram realizadas quatro fusões em cada liga. No sentido de produzir microestruturas de equilíbrio as ligas foram tratadas termicamente em um forno a vácuo com elemento resistivo de tungstênio em tempos e temperatura distintos para cada sistema. A caracterização das ligas no estado como-fundido e aquelas tratadas termicamente foi realizada através de análises via difração de raios X e microscopia eletrônica de varredura (MEV). As medidas de difração de raios X em altas temperaturas foram feitas entre a temperatura ambiente e 1473 K.

Os resultados indicaram que a adição de boro nas ligas binárias com composição  $\text{Nb}_5\text{Si}_3$ ,  $\text{Ta}_5\text{Si}_3$  e  $\text{Mo}_5\text{Si}_3$  provoca um decréscimo na anisotropia da expansão térmica destas ligas e este decréscimo é mais significativo nas ligas do sistema Mo-Si. Com relação ao efeito da variação da concentração de boro na fase  $T_2$ , os resultados mostraram que as ligas dos sistemas Nb-Si-B e Ta-Si-B apresentaram comportamentos similares. Foi observada uma diminuição nos valores dos coeficientes de expansão térmica com o aumento da concentração de boro nas ligas.

Apoio financeiro: CNPq (Proc. 141884/2001-0)

## PMPO02. High Resolution X-ray Diffraction Studies in Sm(Co,Cu)<sub>5</sub>.

**Serrano, R. L**

*IFGW, UNICAMP/Laboratorio Nacional de Luz Síncrotron, rlora@ifi.unicamp.br*

**Madrigal, A. P.**

*Faculty of Physics. University of Havana. Cuba, arbelio@ff.oc.uh.cu*

**Rams, E. E.**

*Faculty of Physics. University of Havana. Cuba, estevez@ff.oc.uh.cu*

Sm(Co,Cu)<sub>5</sub> compounds exhibit a considerable magnetic hardness. The explanation for such property has been suggested to result from the complicated structural defects in the crystal. The addition of Cu to the ferromagnetic compound SmCo<sub>5</sub> results in a magnet with a high coercive field value. The obtained magnetic properties depend strongly on the heat treatment conditions. Structurally, previous studies have suggested that complete solubility should be expected between SmCo<sub>5</sub> and SmCu<sub>5</sub> and that Cu enhances the stability of the CaCu<sub>5</sub>-type structure widening its homogeneity range; microscopy observations performed on heat treated Sm(Co<sub>0.5</sub>Cu<sub>0.5</sub>)<sub>5</sub> alloys of the highest coercivity value showed a microstructure with regions of composition near Sm(Co,Cu)<sub>5</sub>, slightly richer in Sm and also showed heavy planar faulting occurring in the basal plane. In order to get a better understanding of the relation between the magnetic properties and, the compositionally induced, structural defects, high resolution x-ray diffraction experiments were performed in Sm(Co<sub>1-x</sub>,Cu<sub>x</sub>)<sub>5</sub> alloys with different Co/Cu content and in Sm(Co<sub>1-x</sub>,Cu<sub>x</sub>)<sub>5</sub> alloys with 2, 5, 7 weight percent of Sm excess. X-ray diffraction patterns showed the presence of the hexagonal CaCu<sub>5</sub>-type structure belonging to a Sm(Co,Cu)<sub>5</sub> phase in all the studied compositions. A splitting effect depending on the Cu content is observed and believed to be due to compositional disorder. The splitting point to a inhomogeneous distribution of Co and Cu through out the samples. An increase of the crystal cell parameters with increasing Cu content supports the idea of the solubility of excess Sm in the CaCu<sub>5</sub>-type structure. Local reordering resulting from the compositional variations could affect the magnetic behavior of the samples with low Cu content. Sm excess with larger heat treatment favors the compositional homogenization of the samples.

# PMPO03. X Ray Powder Diffraction Analysis of Phase Changes in Sintered Hydroxyapatite by the Rietveld Method

*Fancio E., Lima, N. B.*  
IPEN - Instituto de Pesquisas Energéticas e Nucleares  
efancio@terra.com.br, nblima@net.ipen.br

Synthetic hydroxyapatite (HAP)(Ca<sub>10</sub>(PO<sub>4</sub>)<sub>6</sub>(OH)<sub>2</sub>) has been recognized for its biocompatibility and application for biointegration promotion in bone implants and plasma sprayed coatings. Plasma sprayed coatings are formed by rapid quenching of molten HAP particles which impact a metallic substrate at high temperatures. These extreme heating and cooling conditions produce amorphous and metastable phases, affecting the implant stability. The procedures commonly applied in obtaining synthetic HAP also include temperature variations, particularly during crystallization, sintering and cooling.

The study of the mechanisms involved in phase changes by thermal decomposition is related to the control of the decomposition process, which determines the properties of the HAP final product. The X ray diffraction (XRD) patterns were obtained during the heating and after cooling for HAP in powder form. The diffraction pattern during heating was obtained in air at 1300°C. The Rietveld method was applied to the data collected for the two samples analyzed. The program used in this work was dbws9807a. The heating and cooling rate was 10°C/min.

During the heating process, the following reaction and respective phase percentages were observed:  $2 \text{ Ca}_{10}(\text{PO}_4)_6(\text{OH})_2 (86,88 \pm 0,39) \Rightarrow 2 \beta\text{-Ca}_3(\text{PO}_4)_2 (1,91 \pm 0,00) + \beta\text{-Ca}_2\text{P}_2\text{O}_7 (3,04 \pm 2,07) + 3 \text{ Ca}_4\text{P}_2\text{O}_9 (8,16 \pm 0,00) + \text{H}_2\text{O}$ . After cooling, the resulting phases and percentages were:  $\text{Ca}_{10}(\text{PO}_4)_6(\text{OH})_2 (89,59 \pm 0,36) \Rightarrow 2 \alpha\text{-Ca}_3(\text{PO}_4)_2 (5,52 \pm ,42) + \text{Ca}_4\text{P}_2\text{O}_9 (4,89 \pm 0,96) + \text{H}_2\text{O}$

Therefore, the phase change mechanisms for HAP, and the resulting products and phase concentration were distinct for the two processes. The results obtained in least-squares refinement by the Rietveld method showed good pattern fitting with the calculated profile.

Acknowledgements: The authors are grateful to the financial support from FAPESP (Fundação de Amparo à Pesquisa do Estado de São Paulo).

## References

- RIETVELD, H.M.; A Profile Refinement Method for Nuclear and Magnetic Structures. *J.Appl.Cryst.* **2**, p.65-71, 1969.
- YOUNG, R. A.; SAKTHIVEL, A.; MOSS, T. S. E PAIVA-SANTOS, C. O. "DBWS-9411, an upgrade of the DBWS\*.\* programs for Rietveld refinement with PC and mainframe computers". *Journal of Appl Cryst.*, V.28, p.366-367, 1995.
- TUFEKCI, E.; BRANTLEY, W.A.; MITCHELL, J.C.; FOREMAN, D.W.; GEORGETTE, F.S1. Crystallographic characteristics of plasma-sprayed calcium phosphate coatings on Ti-6Al-4V. *Int.J.of Oral & Maxillofacial Implants*. V.14, p.661-672, 1999.
- CHUN-JEN L.; FENG-HUEI L.; KO-SHAO C.; JUI-SHENG S. Thermal decomposition and reconstitution of hydroxyapatite in air atmosfere. *Biomaterials*. V.20, p.1807-1813 1999.
- KELLER,L. X-ray powder diffraction patterns of calcium phosphates analyzed by the Rietveld method . *J.of Biomedical Mat.Res.* V.29, p1403-1413,1995.

## PMPO04. Propriedades Estruturais de Eletrocatalisadores de Pt e Ligas Bimetálicas Pt-Co Suportado em Carbono de Alta Área Superficial.

*Salgado, J.R.C.<sup>1\*</sup>, Lopes, L.P.<sup>2</sup>, Mascarenhas, Y.P.<sup>2</sup> e Gonzalez, E.R.<sup>1</sup>*

<sup>1</sup>*IQSC (CP 780),<sup>2</sup>IFSC (CP 369) / USP, CEP 13560-970, São Carlos, SP*

*\*salgado@iqsc.usp.br*

Eletrocatalisadores a base de Pt e ligas bimetálicas como Pt-Co dispersos em carbono de alta área superficial (Pt/C e Pt-Co/C) estão sendo os materiais mais estudados para a reação de redução de oxigênio (RRO) em célula a combustível alimentada por H<sub>2</sub>/O<sub>2</sub>. O interesse nos estudos é encontrar materiais mais ativos do que Pt/C que promovam a RRO, uma vez que a cinética é lenta e é responsável pelas perdas no desempenho das células a combustível. A preferência pelos materiais bimetálicos para a RRO em relação à Pt/C é atribuído a diversos fatores, dentre eles, uma maior atividade catalítica dos materiais bimetálicos devida a uma mudança na estrutura cristalográfica de orientação cristalina preferencial, ordenada ou desordenada<sup>1-2</sup>. Por isso, o objetivo do presente trabalho é preparar e avaliar as propriedades estruturais de eletrocatalisadores bimetálicos Pt-Co suportado em carbono.

Eletrocatalisadores Pt-Co foram preparados pelo método de SHUKLA *et al.*<sup>2</sup> e para comparação foi utilizado o catalisador comercial Pt/C E-TEK. A avaliação destes materiais consiste na caracterização física mediante difração de raios X (DRX) e energia dispersiva de raios X (EDX). As análises de DRX foram feitas num Difratômetro Rigaku, radiação Cu (K $\alpha$ 1,5406 Å) com 100 kV e 50 mA e passo de contagem de 0,02° com 5s no intervalo 30<2θ<100. Para determinar o tamanho médio das partículas utilizou-se o pico referente ao plano (220) da estrutura cúbica de face centrada (F M –3 M) da Pt em torno de 2θ = 67° e empregou-se a equação de Scherrer<sup>3</sup>. Os difratogramas de raios X foram refinados empregando-se o método de Rietveld e o programa utilizado para o refinamento foi o GSAS<sup>4</sup>.

A composição atômica, determinada por EDX, para o material bimetálico foi 75:25. Os resultados de difração de raios X para os eletrocatalisadores de Pt<sub>75</sub>Co<sub>25</sub>/C mostraram picos intensos e característicos de estrutura cúbica, grupo espacial P M –3 M com  $a = 3,8498\text{ \AA}$  (menor que o valor para a Pt/C:  $a = 3,9320\text{ \AA}$ ). A estrutura corresponde a uma fase ordenada com Co em 0, 0, 0 e Pt em  $\frac{1}{2}, \frac{1}{2}, 0$ . O diâmetro médio das partículas calculado pela fórmula de Scherrer é 0,39 nm para Pt/C e 0,38 nm para Pt<sub>75</sub>Co<sub>25</sub>/C.

Os estudos das propriedades estruturais sugerem uma mudança na estrutura cristalgráfica para os eletrocatalisadores Pt<sub>75</sub>Co<sub>25</sub>/C em relação à Pt/C.

Agradecimentos: CNPq pelas bolsas concedidas.

### Referência Bibliográfica

<sup>1</sup>Toda, T.; Igarashi, H.; Uchida, H.; Watanabe, M. *J. Electrochem. Soc.* 146 (1999) 3750.

<sup>2</sup>Shukla, A. K.; Neergat, M.; Parthasara, Bera; Jayaram, V.; Hegde, M. S. *J. Electroanal Chem.* 504 (2001) 111.

<sup>3</sup>CULLITY, B. D. *In Elements of X-Ray Diffraction*. Addison-Wesley Publishing Co., 1980.

<sup>4</sup>Larson, A. C.; Von Dreele, R. B. *GSAS – General Structure Analysis System*, Los Alamos National Laboratory, 1996.

# PMPO05. Rietveld method structural study of the Galium doped zinc oxide

Antonio, S.G.<sup>1</sup>, Paiva-Santos, C.O.<sup>2</sup>, Gonçalves, A.S.<sup>3</sup>, Davolos, M.R.<sup>4</sup>

1. UNESP – selma@abcacc.iq.unesp.br
2. UNESP – copsanto@iq.unesp.br
3. UNESP – agnagonc@grad.iq.unesp.br
4. UNESP – davolos@iq.unesp.br

Óxido de Zinco ( $ZnO$ ), tem uma estrutura hexagonal wurtzite e é um semicondutor tipo n. Atualmente, a fabricação de óxido de zinco tem trazido grande interesse pela propriedade de se obter filme transparente e condutor, também com propriedades elétrica e óptica.[1] Uma outra vantagem é sua baixa toxicidade e abundância de precursores. Análises com difração de raios X e o método de Rietveld forneceram os resultados da tabela 1[2]. Considerando que (i) o raio iônico do  $Ga^{3+}$  varia entre 0,47 e 0,62 Å, dependendo do número de coordenação, (ii) na estrutura de  $ZnO$  existem “túneis”, com distâncias em torno de 3,8 Å (Fig. 1), (iii) o aumento da cela unitária até 2% de dopante, e (iv) que uma segunda fase,  $ZnGa_2O_4$ , se forma em todas as amostras dopadas e sua quantidade aumenta com a adição de dopante, pode-se concluir que o  $Ga^{3+}$  está entrando intersticialmente na estrutura do  $ZnO$ , e modificando a estrutura em torno de sua posição para formar a segunda fase.

Tabela I. Resultados obtidos nos refinamentos pelo método de Rietveld. Entre parênteses estão os desvios padrão relativos ao ultimo algarismo significativo.

	a	c	%	R <sub>Bragg</sub>	wRp	$\chi^2$	V
puro	3.25026(2)	5.20604(5)	100	1.96	9.70	1.742	47.629(1)
1%	3.25123(2)	5.20419(5)	99.2	2.11	10.56	3.614	47.641(1)
2%	3.25123(2)	5.20417(5)	99.3	2.16	10.76	3.754	47.641(1)
3%	3.25102(2)	5.20440(5)	97.2	2.20	9.04	4.566	47.637(1)
4%	3.25074(2)	5.20403(5)	96.7	2.48	8.96	2.094	47.625(1)
5%	3.25103(2)	5.20440(5)	93.7	2.55	9.98	2.795	47.637(1)

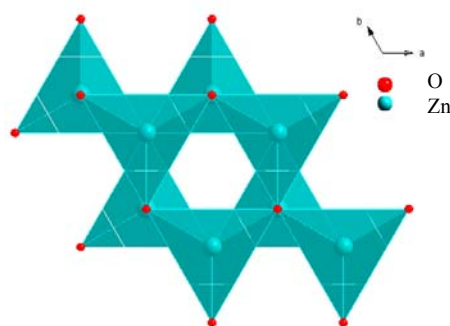


Figura 1. Vista na direção do eixo-c da estrutura do  $ZnO$ .

## Referências

1. Nunes,P,Fortunato,E.,Martins,R. Thin Solid films 2001,383,277.
2. Larson, A. C., Von Dreele, R. B. GSAS – General Structure Analysis System. Los Alamos National Laboratory. EUA. p.233, 2000

## PMPO06. Negative Thermal Expansion Coefficient in the Triclinic Kaolinite

Batista<sup>a</sup>, W.O., Baran<sup>b</sup>, Z., Keller<sup>b</sup>, W.A. [a] Centro Federal de Educação Tecnológica da Bahia [b] Universidade Federal da Bahia

wilson@cefetnet.com.br

Keywords: structural disorder, thermal expansion tensor.

The structural disorder in the layer structured kaolinite  $\text{Al}_2\text{SiO}_5(\text{OH})_4$  has been subject of many studies made at Room temperature but few of them were made at higher temperatures. The thermal expansion of the layer-type structure can be sensitive tool for studying this disorder. The thermal expansion is often expressed empirically as a linear combination of the expansion and rotation of its rigid components formed by polyhedral units. These layers can be regarded as consisting of a tetrahedral sheet of  $\text{SiO}_4$  tetrahedra and an octahedral sheet of  $\text{Al}(\text{O},\text{OH})$  octahedrally coordinated by O and OH. Tetrahedral units linked to the octahedral units, can adjust their orientation by the mechanism of tetrahedra rotation. The aim of this work was to relate details of the layer structures of well-and moderately crystallized kaolinites to the principal expansion coefficients, defined at elevated temperatures [1]. It can also provide some information about structural defects in kaolinite. Unit cell constants as temperature function, obtained by polynomial fit, and its derivatives were used to calculate the coefficients  $\alpha_{ij}$  of the second rank tensor of thermal expansion. The coefficients were calculated in the differential form according to [2] at the interval  $dT$  around each temperature  $T$ . Next, the principal expansion coefficients  $\alpha_i$  were derived and plotted as function of temperature. The latter were given in the Cartesian coordinate system  $e_j$ , where  $e_3 \times c = 0$  and  $e_2 \times b = 0$ . The macroscopic thermal expansion was shown by means of the thermal expansion ellipsoid [3]. All the calculations were carried out by the program written using the Mathcad 2001 software. Output of the program gives the directions of the principal axes of the thermal expansion ellipsoid in the orthogonal and crystallographic axial systems, as well as the thermal expansion coefficients. It can reveal some aspects of temperature dependence of the triclinic crystals, such as kaolinite, which are not immediately obvious from the graphs representing only the unit cell dimensions. An unexpected result obtained was that at least one of the principal thermal expansion coefficients was negative throughout the whole temperature range. This result can be a *posteriori* explained by the recent Rigid Unit Modes (RUMs) model [4]. In this model, the  $\text{SiO}_4$  tetrahedra are rigid units in comparison with intertetrahedral forces. Rotation of these units can reduce the volume making the thermal expansion negative.

- [1] Batista, W.O..Study of the thermal transformations in the Brazilian kaolinites", Thesis, (1999), Universidade Federal da Bahia, Brazil
- [2] Weber Th. et al, "Thermal expansion of  $\text{CuMoO}_4$  below room temperature", Z.Kristallogr. (1998),213, 210-216.
- [3] Sands, D.E., "Vectors and Tensors in Crystallography", (1982), Addison-Wesley, London
- [4] Llammmonds K.D. et al. 'Rigid-unit phonon modes and structural phase transition in framework silicates", Am. Miner., (1996), 81, 1057-1079.

## PMPO07. Effect of Stress on 3YTZ-Al<sub>2</sub>O<sub>3</sub> Composites

*Mir M.<sup>(a)</sup>, M'Peko J.-C. <sup>(b)</sup>, De Souza M.F. <sup>(c)</sup> and Mascarenhas Y.P. <sup>(d)</sup>*

*(a,b,c,d) Institute of Physics at São Carlos, University of São Paulo, C. Postal: 369, 13560-970, São Carlos – SP, Brazil.*

*(a) mmir@if.sc.usp.br*

*(b) peko@if.sc.usp.br*

*(c) mfs@if.sc.usp.br*

*(d) yvonne@if.sc.usp.br*

### Abstract

The microstructural characteristics of zirconia-alumina composites were studied in this work over a wide range of compositions. The two-phase system was prepared following the standard ceramic method, and starting from commercial yttria-stabilized zirconia (3YTZ, Tosoh, Japan) and alumina (AKP-50 Sumitomo, Japan) powders, the former being calcined prior to forming the composites. Volume fractions of 10, 20, 40, 60, 80 and 100 % of 3YTZ were considered. The final microstructure features of such composites were analyzed by scanning electron microscopy (SEM). Internal stress effects are postulated to derive from the alumina sintering on the calcined zirconia during final heat treatment. For monitoring the behavior of such effects upon variation of zirconia volume fraction, diffraction data of all the prepared ceramic samples were measured by Bragg-Bentano X-ray diffractometry (XRD). The Rietveld analysis method was subsequently applied. The evaluation of the resulting strain effects was based on (*i*) the refinement of the peak profile shape using the Thompson-Cox Hastings Pseudo-Voigt function and (*ii*) the variations of the final zirconia cell parameters. The present work strongly suggests the importance of considering the difference in thermal shrinkage of mixed phases when attempting to produce stress-free composite materials.

### Acknowledgments

M. Mir thanks the Centro Latino Americano de Física for a grant. M'Peko acknowledges the support from the Brazilian research funding FAPESP through grant n°. 2000/04460-6. Y.P. Mascarenhas thanks CNPq for a research fellowship.

## PMPO08. Preparation and Characterization of $\text{Y}_1\text{Ba}_2\text{Cu}_{3-x}\text{Ru}_x\text{O}_{7-\delta}$ Polycrystalline Samples.

*Siqueira, E. C.<sup>1</sup>, Macedo, A. G<sup>2</sup>, Brinatti A. M.<sup>3</sup>, Pereira, L. A. A.<sup>4</sup>, Jurelo, A. R.<sup>5</sup>*  
Universidade Estadual de Ponta Grossa  
Departamento de Física

<sup>1</sup>[ezsiq@yahoo.com.br](mailto:ezsiq@yahoo.com.br),

<sup>2</sup>[gerniski@bol.com.br](mailto:gerniski@bol.com.br),

<sup>3</sup>[brinatti@uepg.br](mailto:brinatti@uepg.br),

<sup>4</sup>[laap@uepg.br](mailto:laap@uepg.br),

<sup>5</sup>[arjurelo@uepg.br](mailto:arjurelo@uepg.br)

Neste trabalho será apresentado um estudo do efeito do íon de rutênio no sistema  $\text{YBa}_2\text{Cu}_{3-x}\text{Ru}_x\text{O}_{7-\delta}$ . Nossa objetivo é o de estudar como o íon de rutênio, ao ser substituído no sítio do cobre, altera a supercondutividade no sistema YBCO. Para este estudo, foram preparadas amostras com concentrações de rutênio com  $x$  variando entre 0 e 100 %, utilizando a técnica padrão de reação de estado sólido. Para a caracterização das amostras foram realizadas medidas de transporte eletrônico, de difração de raios-X e microscopia eletrônica. Através das medidas de transporte eletrônico, pôde-se observar claramente o efeito do íon de Ru sobre a transição resistiva. Com a difração de raios-X e microscopia eletrônica, foi possível acompanhar a evolução estrutural da célula unitária em função da dopagem por rutênio.

Palavras chaves : supercondutividade; difração de raios-X; resistividade; microscopia eletrônica

## PMPO09. Rietveld Study of Ferroelectric Ceramics with Tungsten-Bronze Structure

Lopes, L. P.<sup>(1)</sup>; Doriguetto, A. C.<sup>(2)</sup>; Mascarenhas, Y. P.<sup>(3)</sup>; Coimbrão, N. F.<sup>(4)</sup>; Garcia D.<sup>(5)</sup>; Eiras, JA<sup>(6)</sup>

<sup>(1,2,3)</sup> USP/IFSC; <sup>(4,5,6)</sup> UFSCar/DF; e-mails: <sup>(1)</sup>luizifsc@bol.com.br;

<sup>(2)</sup> dorigue@if.sc.usp.br; <sup>(3)</sup> yvonne@if.sc.usp.br; <sup>(5)</sup> ducinei@df.ufscar.br;

<sup>(6)</sup> eiras@df.ufscar.br

Since the discovery of dielectric relaxion behaviour in one of the lead niobate phases<sup>[1]</sup> extensive research efforts have been dedicated to study tungsten-bronze-type relaxor ferroelectrics such as the  $(M_1 M_2)Nb_2O_6$  oxides ( $M_1$  and  $M_2$  are metals). The structure and ferroelectric properties of these materials depends on the metallic species, its quantity, and its distribution among the different crystalline sites. In the present work we have studied the PBLN series  $(Pb_{1-(x+y)}Ba_xLa_y)Nb_2O_6$  by powder X-ray diffraction (XRD) using the Rietveld formalism. Three different compositions were synthesized varying the  $La^{3+}$  amount:  $(Pb_{0.56}Ba_{0.44}La_{0.00})Nb_2O_6$  (PBLN1);  $(Pb_{0.55}Ba_{0.44}La_{0.007})Nb_2O_6$  (PBLN2); and  $Pb_{0.54}Ba_{0.44}La_{0.014}Nb_2O_6$  (PBLN3). The XRD patterns were collected on Rigaku Denki powder automatic diffractometer, CuK $\alpha$  radiation, range of  $3 < 2\theta < 87^\circ$ , step size of  $0.02^\circ/\text{min}$ , time of  $5''$ . The three samples show nearly equal tetragonal unit cell lengths. In fact, the DRX patterns do not show any difference, except for the peaks around  $46^\circ 2\theta$ , which split from PBLN1 to PNLN3. Differently from Brusset et al. results<sup>[2]</sup>, which pointed out to an orthorhombic phase (Cm2m) for the  $Pb_{0.7}Ba_{0.3}Nb_2O_6$ , our samples are isostructural to SBN structure (P4bm)<sup>[3]</sup>, presenting O-Nb-O chains along the c axis similar to perovskite structure. The niobium atoms are octahedrally coordinated and occupy two different sites: Nb1 and Nb2 (lighter and darker octahedral, respectively in Fig. 1). The  $NbO_6$  units packing in the plane (001) forms tetragonal (site A1) and pentagonal (site A2) holes, which are randomly occupied by  $Pb^{2+}$ ,  $Ba^{2+}$ , and  $La^{3+}$  ions. However, for all samples the A1 and A2 sites are not completely occupied. The  $Pb^{2+}$  ions are present in A1 and A2, whereas  $Ba^{2+}$  atoms occupy only A2.

It is important to emphasise that  $La^{3+}$  incorporation promotes the migration of  $Pb^{2+}$  from A1 to A2. Therefore, since it was not observed any phase transition and no change in the cell parameters among the studied samples, the differences observed in its ferroelectrics properties could be attributed to  $Pb^{2+}$  exchange between A1 and A2. The  $La^{3+}$  ions are expected to substitute the  $Pb^{2+}$  in A1. However, the  $La^{3+}$  distribution could not be determined due to its small amount in the studied samples. Another important structural result observed here is the absence of disorder in the two axial oxygen atoms as observed for SBN structures<sup>[3]</sup>.

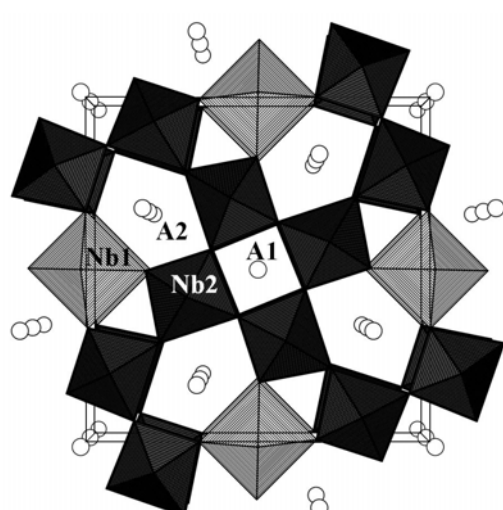


Fig 1. Crystal Structure in the plane (001)

Acknowledgements: FAPESP (00/09722-9 and 01/06993-4) and PADCT/CNPq

[<sup>1</sup>] Goodman, G. (1953) *J. Amer. Ceram. Soc.* 36, 368.

[<sup>2</sup>] Brusset, H. et al. (1972) *Bull. Société chim. France* (vol = year) 926.

[<sup>3</sup>] Chernaya, T. S. et al. (1997) *Kristallografiya* 3, 421.

## OMPO10. Crystal Structure Refinement of a Th-rich Weeksite Group Mineral

*Carvalho, F. M. S. (flavioms@usp.br), Atencio, D. (datencio@usp.br) and  
Andrade, M. B. (mabadean@terra.com.br)  
Departamento de Mineralogia e Geotectônica, Instituto de Geociências,  
Universidade de São Paulo*

Weeksite is a tectosilicate characterized by a Si:U ratio of 5:2. The most recent determination of its crystalline structure was made from a single crystal from Yavapai County, Arizona, USA, with formula  $K_{1.26}Ba_{0.25}Ca_{0.12}[(UO_2)_2(Si_5O_{13})].H_2O$ .

Weeksite display compositional variations, as for example the Ba-rich weeksite ( $K/Ba = 0.76/0.35$ ) that occurs along fractures in the pegmatitic tourmaline granite of Perus, São Paulo, Brazil.

This work presents the results of a preliminary of a crystal structure refinement study (using the GSAS software) of a weeksite specimen from the Mina do Macaco, São Geraldo do Baixio, Minas Gerais, Brazil. Chemical and X-ray powder diffraction data show it is a Th-rich member of the weeksite group, not yet described in the literature.

Preliminary results, with  $Rwp$  index 0.1655, revealed the following unit cell parameters:  $a_o$  14.1676(9),  $b_o$  14.1935(9),  $c_o$  35.754(2) Å. These results slightly differs from those for the Yavapai crystal [ $a_o$  14.209(2),  $b_o$  14.248(2),  $c_o$  35.869(4) Å].

The possible structural sites occupied by Th will be investigated on the basis of WDS chemical data and Fourier difference maps.

## PMPO11. Quantitative Phase Analysis of Sr<sub>2</sub>CeO<sub>4</sub> using Rietveld Refinement

Góes, M.S.<sup>\*1</sup>; Ferrari, J.L.<sup>2</sup>; Pires, A.M.<sup>2</sup>; Paiva-Santos, C.O.<sup>1</sup>; Davolos, M. R.<sup>2</sup>

<sup>\*1</sup>Laboratório Computacional de Análises Cristalográficas e Cristalinas – LabCACC.  
Dept. de Físico-Química. Instituto de Química - UNESP. R. Francisco Degni, s/n. Bairro  
Quitandinha. 14800-900. Araraquara, SP. <sup>\*</sup>marcio@labcacc.iq.unesp.br

<sup>2</sup>Grupo de Materiais Luminescentes - GML. Depto. de Química Inorgânica. Instituto de  
Química - UNESP. Araraquara, SP.

A busca de dispositivos de tela plana, ou FEDs (*Field Emission Display*) tem sido de grande interesse devido a sua alta resolução de imagem e potencial aplicação comparável ou superior aos tubos de raios catódicos. O material luminescente Sr<sub>2</sub>CeO<sub>4</sub>, que é um dos candidatos à aplicação em FEDs, foi obtido tendo como precursores oxalatos de estrôncio e de cério precipitados a partir da mistura de soluções de sais de nitrato contendo 33% at de Ce<sup>3+</sup> e 67% at de Sr<sup>2+</sup> em temperatura e pH controlados. A decomposição foi realizada em fornos convencionais com tratamento térmico a 1100°C em ar durante 12 h. O produto de decomposição foi caracterizado por difratometria de raios X e sua estrutura cristalina refinada pelo método de Rietveld. Pelas análises pode-se verificar a presença de três fases Sr<sub>2</sub>CeO<sub>4</sub>, SrCeO<sub>3</sub> e SrCO<sub>3</sub> sendo suas porcentagens em massa de 53,196(1), 38,611(1) e 8,193(2), respectivamente. Os índices de qualidade do refinamento foram Rwp = 0,1460, Rp = 0,0992, S (=  $\sqrt{\chi^2}$ ) = 1,47 e o R<sub>Bragg</sub> para a fase de Sr<sub>2</sub>CeO<sub>4</sub> igual a 0,0476, indicando que os refinamentos foram realizados adequadamente para permitir uma análise confiável das estruturas cristalinas. A quantidade da fase Sr<sub>2</sub>CeO<sub>4</sub> determinada superou valor encontrado na literatura de produtos obtidos através de síntese de estado sólido a 1000°C em ar durante 12 h. O método utilizando oxalato de estrôncio e de cério como precursor restringe a formação de outras impurezas.

Palavras-Chaves: Método de Rietveld, cerato luminescente, análise quantitativa de fases.

Agradecimentos: CNPq-PIBIC e FAPESP

## PMPO12. Estrutura e microestrutura de Co<sub>7-x</sub>Ni<sub>x</sub>Sb<sub>2</sub>O<sub>12</sub>, (0 ≤ x ≤ 4).

*Paiva-Santos, C. O [copsanto@iq.unesp.br]. e Antonio, S. G., Instituto de Química-UNESP, LabCACC (SP); Brito, M. S. L. e Lucena, J. B., Universidade Federal da Paraíba (PB); Gama, L., Universidade Federal de Campina Grande (PB); Longo E., UFSCar, LIEC.*

O Co<sub>7-x</sub>Ni<sub>x</sub>Sb<sub>2</sub>O<sub>12</sub> é um espinélio do tipo misto. Materiais com composição 0≤x≤4 foram preparados por rota química e caracterizados por difração de raios X e o método de Rietveld para analise da estrutura cristalina e análise anisotrópica da microestrutura. Observou-se que a adição do níquel causa a diminuição do volume da cela unitária e o aumento da microdeformação de rede. Não se observa uma anisotropia significativa na microdeformação. Apenas para x = 3 o cristalito apresentou dimensão suficiente para ser determinada com DRX e não foi observada anisotropia. A diminuição do volume era esperada, pois o raio iônico do Ni<sup>2+</sup> é menor que o do Co<sup>2+</sup>. Para x = 4 observou-se a formação de 3 fases cristalinas, ou seja, 86% em massa de Co<sub>3</sub>Ni<sub>4</sub>Sb<sub>2</sub>O<sub>12</sub>, 6% de Ni<sub>7</sub>Sb<sub>2</sub>O<sub>12</sub> e 8% de NiO. Concluiu-se que o Ni é incorporado na estrutura cristalina do espinélio até uma quantidade menor que x = 4.

## PMPO13. Hydrated and Anhydrous Forms of the Room Temperature Phase of $K_4(Mo_{0.5}W_{0.5})O_4$

Moreira, A.M. – UFMG ([alexmelo@fisica.ufmg](mailto:alexmelo@fisica.ufmg));

Archanjo, B. S. – UFMG ([braulio@fisica.ufmg](mailto:braulio@fisica.ufmg))

Guarnieri, A. A. – UFV ([guarnier@ufv.br](mailto:guarnier@ufv.br))

Pinheiro C. B. – Université de Lausanne ([carlos.basilio@ic.unil.ch](mailto:carlos.basilio@ic.unil.ch))

Speziali, N. L. – UFMG ([nspezial@fisica.ufmg.br](mailto:nspezial@fisica.ufmg.br))

X-ray powder diffraction and calorimetric experiments have been used to study the crystal structures and thermotropic phase transitions of  $K_2Mo_xW_{(1-x)}O_4$  ( $0 \leq x \leq 1$ ) compounds. Two phase transitions were found with transition temperatures  $T_I \sim 730$  K and  $T_{II}$  between 640 and 593 K depending on  $x$ . All compositions have shown a similar behavior to those previously described in the literature for the  $x = 0$  and 1. At room temperature, the crystal has a  $C2/m$  symmetry, while between  $T_I$  and  $T_{II}$  a modulated orthorhombic structure is observed; at the higher temperatures the structure symmetry is  $P6_3/mmc$ .

For the  $x = 0.5$  compound, two distinct structures were found at room temperature depending on the thermal history. The diffraction pattern obtained before any thermal treatment was refined using Rietveld method in the  $C2/m$  ( $Z = 4$ ) space group. Once the samples are heated till temperatures above 700 K and then studied at room temperature in a dry atmosphere, a new phase is observed. The corresponding diffraction pattern can be fitted using orthorhombic symmetry in a two fold unit cell ( $Z = 8$ ).

DSC measurements have been performed and some peaks evidenced water loss.

It is interesting to remark that once normal atmosphere is re-established in a few minutes the crystal goes again to the monoclinic  $C2/m$  phase.

Attempts to obtain an orthorhombic structure are in progress with Rietveld method.

**Acknowledgment:** Special thanks to Dr. G. Goulart for the help with DSC experiments. This work is partially supported by CNPq and FAPEMIG.

PMPO14. “Structural Analysis of SnO<sub>2</sub> Doped Semiconductors by the Rietveld Method”

Carrió J. A. G.\* , Piccoli S.\*\*, Borgia R. A. \*\*, S Gutierrez. S.\*\*\*, Arana J. A. V.\*\*\*,  
Paiva Santos C. O. \*\*\*.

\* Centro Universitario Salesiano de São Paulo (UNISAL-American)

Universidade Presbiteriana Mackenzie

\*\* UNISAL –American

\*\*\* IQ – Araraquara / UNESP

Semiconductor solid sensors of pollution gases allow the possibility of “in-situ” analysis. This is the reason because of these materials are intensively studied. At the IQ-Araraquara were synthesized nano-structured semiconductor oxides with the objective of maximizing their sensibility and selectivity. In this work we present a structural analysis of some of these materials. Polycrystalline samples of SnO<sub>2</sub> doped with different amounts of ZnO and WO<sub>3</sub> were prepared, and X-rays powder diffraction data were collected, with a laboratory conventional diffractometer. The structures of the materials were studied using the Rietveld method. The GSAS profile function Nr. 4 was used to fit the profiles. This function allows an anisotropical analysis of the crystallite size, based on the algorithms of P. Stephens. The cell parameters and Sn-O interatomic distances grow with increasing the amount of dopants. Discordancess parameters are in the order of Rwp=15,5%, Rp=11,2% and R-Bragg=5.3%.

References:

- Larson, A.C. and Von Dreele, R.B. (1993) GSAS, *Generalized Structure Analysis System*, Document LAUR 86-748 (Los Alamos National Laboratory, Los Alamos).
- C. O. Paiva Santos, IQ-UNESP, 2000
- D. Balzar, Commission on Powder Diffraction, International Union of Crystallography, Newsletter No. 24, Dec. 2000
- P.W. Stephens, J. Appl. Cryst. **32** (1999) 281-289.

Acknowledgments: BICSAL - UNISAL –American, Escola de Engenharia and FCBEE, Universidade Presbiteriana Mackenzie

(1) Juan A. G. Carrió, (19)34056911 e-mail: juan.carrio@am.unisal.br,  
jgcarrio@mackenzie.com.br

## PMPO15. Synthesis and Structural Characterization of the $Y_{1-x}Cd_xMnO_3$ System.

*Agüero O. E. and Torriani I. L.*

*Instituto de Física Gleb Wataghin-UNICAMP, SP, Brasil  
Leyva A.G., Konig P., Polla G. and Vega D.  
Centro Atómico Constituyentes (CNEA). Buenos Aires, Argentina.*

The discovery of colossal magnetoresistance in perovskite-type manganese oxides has stimulated research on this type of oxides. Many mixed oxides of general formula  $R_xA_{1-x}MnO_3$  ( $R$ : trivalent rare earth,  $A$ : alkaline-earth), belong to the group of orthorhombic distorted perovskites. The mixture of divalent and trivalent cations and the simultaneous occurrence of  $x Mn^{+3}$  and  $(1-x) Mn^{+4}$  ions, all with different radius, introduce an important mismatch in the original orthorhombic crystal structure. The phase diagram of these families is non-symmetric and hole or electron doping cause dissimilar effects. Usually a complex phase diagram results. In our study on the  $Y_{1-x}Ca_xMnO_3$  system<sup>1</sup> where the pure Ytrium compound has a hexagonal structure, it was shown that for high Ytrium concentrations, different phases were segregated and no orthorhombic structure for nominal  $x$  concentration was obtained with the solid-state reaction synthesis method. To explain this result Cadmium was chosen as a possible dopant element to study a similar system, because it would introduce a small radius mismatch in the structure.

In this work we have examined the effect of cadmium doping for all range of  $x$  concentration in the  $YMnO_3$  hexagonal compound. The conditions to obtain the orthorhombic perovskite structure were investigated and the different phases obtained characterized.

The samples were synthesized from two different methods: solid-state reaction and Liquid-Mix. X-ray Powder Diffraction (XRD) from 4K to 300 K, Scanning Electron Microscopy (EDS and WDS), Thermogravimetric Analysis (TG) and Differential Thermal Analysis (DTA) were used to characterize the samples. From diffraction data the crystalline phases were analyzed and the structural parameters determined using the Rietveld method. Some points of the structural phase diagram were determined.

Solid state reaction samples for  $T$  between 1000 and 1400° C, show a very high depletion of Cd; for  $T > 1200^{\circ} C$  the Cd loss is complete. For  $T < 1200^{\circ} C$  the samples are not single phase. The perovskite like phase appears at 1100° C for  $x \sim 0.5$ , with a small quantity of segregated phases.

A single orthorhombic phase  $(Y-Cd)MnO_3$  is obtained in the range  $0.15 \leq x \leq 0.25$  at 700° C from Liquid-Mix method in oxygen atmosphere . Outside of this range the samples also contain other crystalline phases and amorphous components. At 800° C the pure Ytrium perovskite ( $x = 0$ )  $YMnO_3$  is obtained. XRD measurements at low temperature (20 -300K) for all samples show a slight change in the cell parameters as a function of temperature without any structural change.

- [1] D. Vega, G. Polla, A.G. Leyva, P. Konig, H. Lanza, A. Esteban, H. Aliaga, M.T. Causa, M. Tovar, B. Alascio, J. Sol. Stat. Chem. 156, 458 (2001).

## PMPO16. The New IPEN-CNEN/SP Neutron Powder Diffractometer

*Parente, C.B.R.<sup>1</sup>, Mazzocchi, V.L.<sup>1</sup>, Mascarenhas, Y.P.<sup>2</sup>*

*cparente@curiango.ipen.br; vlmazzo@curiango.ipen.br; yvonne@if.sc.usp.br*

*<sup>1</sup>Instituto de Pesquisas Energéticas e Nucleares – IPEN-CNEN/SP*

*<sup>2</sup>Instituto de Física de São Carlos – USP - campus de São Carlos*

A new IPEN-CNEN/SP neutron powder diffractometer, already presented to the community in a previous SBCr meeting, is under construction at the 2 MW thermal IEA-R1m research reactor. It is an upgrading of the old IPEN-CNEN/SP multipurpose neutron diffractometer. The old diffractometer was a single-detector instrument with a boron trifluoride ( $\text{BF}_3$ ) detector and a flat copper mosaic single crystal monochromator. The main modifications introduced in the old instrument are: installation of a position sensitive detector (PSD) and a bent perfect single crystal monochromator. The PSD is formed by eleven linear detector elements, clamped together at each end to form a rigid plane. A linear detector element is a proportional counter manufactured by Reuter-Stokes Inc. The 25 mm outside diameter stainless steel cylindrical tube of a element have a wall thickness of 0.5 mm and an active detector length of 610 mm. The anode wire is nickel chrome with a diameter of 0.015 mm. The specific resistance of the wire is *ca.* 3500  $\Omega$ . The gas fill of the counters is 8 atm of  $^3\text{He}$ , for neutron detection, and 4 atm of Ar, for stopping the reaction products (with 0.5%  $\text{CO}_2$  for quenching). The PSD is installed in a detector shielding which is supported by two arms fixed in a large rotary table. This table provides the instrument with the  $2\theta$  angular movement. A smaller rotary table, placed underneath and concentric with the larger one, provides the  $\omega(\theta)$  movement. Both tables are driven by a computer controlled geared mechanism. The computer also makes the data acquisition. The assemblage formed by rotary tables and mechanism is the same that had been used in the old diffractometer. A rotating oscillating collimator, placed at the entrance to the detector shielding, eliminates parasitic scattering from furnace or cryorefrigerator heat shields in the vicinity of the sample, while only reducing the scattered intensity by *ca.* 10%. The collimator also makes the PSD less sensitive to ambient background leaking in through the shielding entrance. Placed at a distance of 1600 mm from sample, the PSD spans an angular range of  $20^\circ$  of a diffraction pattern, resulting in a quite good resolution for the instrument. In order to increase the neutron beam flux at the sample position, a focusing Si monochromator will be installed in the instrument. With a take-off angle of  $84^\circ$ , the monochromator can be positioned to produce 4 different wavelengths, namely 1.111, 1.399, 1.667 and 2.191 Å. A beam shutter will protect operator during sample manipulation or installation of any device in the monochromatic beam. Other parts constructed for the new instrument are: a in-pile collimator, a monochromatic beam collimator and a neutron shield, large enough to accommodate the monochromator, the beam shutter and the monochromatic beam collimator. In comparison to the former instrument, the new diffractometer will have better resolution and will be *ca.* 600 times faster in data acquisition.

The authors acknowledge the financial supports given by Fundação de Amparo à Pesquisa do Estado de São Paulo (FAPESP), under project no. 95/05173-0, and Ministério da Ciência e Tecnologia, under project RXENZCS.

# OECR01. Protein Folder: molecular models for building 3D cartoons of protein structures

*Garratt, R.C., Abel, L.D.S., & Carvalho, J.C.Q.*

*Instituto de Física de São Carlos, Universidade de São Paulo (richard@if.sc.usp.br)*

Often the initial difficulties which students experience in assimilating the basic concepts behind protein structure are associated with a lack of familiarity in visualizing objects in three-dimensional space allied to the inherent complexity of the molecules themselves. Much use is currently made of specialized computer graphics software and hardware with adequate depth cueing, stereo vision etc. in order to overcome some of the perceived difficulties. Furthermore it is useful for some purposes to reduce the complexity of the molecule by employing a cartoon or ribbon diagram in order to describe the polypeptide fold rather than an explicit all-atom representation.

A more traditional solution to the problem, which is still widely employed for teaching purposes, is the use of 3D physical models. Those which are commonly available are usually all-atom in nature. This is clearly of great value, particularly for representing basic structural components such as elements of secondary structure, but the models rapidly become cumbersome for whole proteins and need to be permanently mounted in a given orientation.

We have developed a kit composed of injection-molded plastic components which represent parts of elements of protein secondary structure. They can be united via male/female connections to produce cylinders of any length (used to represent  $\alpha$ -helices) and flattened ribbons terminating in arrowheads (used to represent  $\beta$ -sheet strands). These components can be united via PVC coated copper wire, representing turns and coils. The latter may be bent such as to follow the course of the polypeptide chain or simply used to unite two elements of secondary structure in order to highlight the molecular topology. The models so produced combine the advantages of a simplified cartoon-like representation with that of a physical 3D model. In addition, the  $\beta$ -sheet components come with lateral holes for the explicit inclusion of 'pseudo hydrogen-bonds' yielding a model of greater mechanical stability.

The components come with no explicit scale so that the user may either chose his own or adopt no specific scale at all for purely topological models. Furthermore the components come in several different colours which the user may use to highlight specific structural features and functionally important regions or in order to differentiate  $\alpha$ -helices from  $3_{10}$  helices for example.

Despite their limited number and simplicity, the design of the pieces and their readily deformable material allow for the easy demonstration of the chirality of component secondary structures and their distortions, including chain and sheet twist,  $\beta$ -saddles and barrels, shear numbers, supercoiling,  $\beta$ -bulges, helix breaks etc. Experience shows that as a teaching aid, the models are most effectively used interactively, during classes in which students build their own structures based on minimal structural information and employing the basic rules of protein folding.

Financial support: FAPESP (CEPID)

Informações adicionais:

Apresentador: Richard C. Garratt, IFSC, São Carlos, richard@if.sc.usp.br

## OECR02. Development and Study of Oxide Crystals with Programmed Lattice Parameters Gradients

Reyes Ardila, D. ([dreyes@usach.cl](mailto:dreyes@usach.cl)), Barbosa, L. B ([luciara@if.sc.usp.br](mailto:luciara@if.sc.usp.br)), Kakuno, E. M. ([edson@fisica.ufpr.br](mailto:edson@fisica.ufpr.br)), Camparin, H. ([globalbrasil@onda.com.br](mailto:globalbrasil@onda.com.br)), Cusatis, C. ([cusatis@fisica.ufpr.br](mailto:cusatis@fisica.ufpr.br)), Andreeeta, J. P. ([andreeeta@if.sc.usp.br](mailto:andreeeta@if.sc.usp.br))

Crystals with an intrinsic continuous change in its lattice spacing  $d$  along a determined z-direction, with lattice parameter gradient of at least 0.1%/cm, are named delta- or gradient-crystals (GCs) and are predicted to open a new field in optics of short wave electromagnetic radiation. Two- and three-dimensional GCs can be used like optical lenses to construct X-ray and gamma-ray microscopes and telescopes, while one-dimensional GC can be used as a collecting and amplifying monochromator. Tight control over the GC composition in all their dimensions is fundamental to have improved performance in their applications as focusing spectrometer with an adjustable width wavelength band pass, and as diffracting element with adjustable average wavelength or energy of the diffracted peak. We describe the preparation of GCs of SrMoO<sub>4</sub>-CaMoO<sub>4</sub> by using a technique based on laser processing. Subsequent thermal treatment and polishing of the as-grown compounds yields GCs with highly desirable physical properties for most potential applications. These crystals are structurally highly perfect, reflecting the variable-metric principle in which the spacing between the crystalline planes of the same family changes with position in the crystal. We show that the lattice spacing in the grown crystal can be accurately controlled, and that the adapted technique should be applicable to a wide variety of metal oxides and even organic materials.

CaMoO<sub>4</sub> (CMO) and SrMoO<sub>4</sub> (SMO) are completely miscible compounds that crystallize in the scheelite structure with tetragonal lattice, space group I4<sub>1</sub>/a, and room temperature lattice parameters  $a_{\text{CMO}} = 5.227 \text{ \AA}$ ,  $c_{\text{CMO}} = 11.435 \text{ \AA}$ ,  $a_{\text{SMO}} = 5.415 \text{ \AA}$ ,  $c_{\text{SMO}} = 12.056 \text{ \AA}$ . Evidences of these phases and its solid solution formation were confirmed by the powder X-ray diffraction (XRD) pattern of crushed CGCs grown under the same experimental conditions. Composition data of Ca, Sr and Mo show corresponding cationic concentration gradients of ~25, ~25 and ~0 at.-%/cm in 25 mm of CGC. This condition represents gradients of relative changes of interplanar distances  $\Delta d/d_{\text{av}}/z$  in the range 1.4%/cm ( $a$  planes) and 2.1%/cm ( $c$  planes), where  $\Delta d$ ,  $d_{\text{av}}$ , and  $z$  are measured between two points as interplanar distances difference, the average of them and length of grown CGC, respectively. A tridimensional plot of X-ray rocking curves (RCs) of the (1 1 2) reflection as a function of the shift in the corresponding Bragg angle of SMO and the length of grown GC in a short time thermally treated and unpolished sample (total GC length 12.4 mm) reproduces expected composition linearly varying with distance. The full width half maximum (FWHM) values of these RCs change from ~44 to ~99 arcsec and present some substructures in some cases that are attributed to changes in the stressed state of the crystal structure. Long time thermally treated and chemically etched GCs certainly relieve the stress problem. By recording Laue and Bragg modes topographic X-ray Laue diffraction pictures of Mo  $K_{\alpha}$ , Mo  $K_{\beta}$  and Mo white X-rays in a sample of 25 mm length we confirm high crystal quality and mosaicity, and verify an expected  $\Delta d/d_{\text{av}}/z$  equals to 1.65%/cm for the family of reflections (1 1 2), (2 2 4) and (3 3 6). The values of  $\Delta d/d_{\text{av}}/z$  and FWHM of RCs in these GCs are comparable or better than those reported for other materials with similar structural features but processed in a very different way.

## OINS01. Evidence of Point-Defect Annihilation During Structural Relaxation of Amorphous III-V Semiconductors

*Azevedo, G. de M; Laboratório Nacional de Luz Síncrotron, Campinas, SP, Brazil  
(azevedo@lnls.br)*

*Ridgway, M. C.<sup>2</sup>; Glover, C. J, The Australian National University, Canberra, Australia*

*Yu, K. M. Lawrence Berkeley National Lab., Berkeley, USA*

*Foran, G. J., Australian Nuclear Science and Technology Organization*

Despite decades of extensive experimental studies, the structure of amorphous semiconductors and, consequently, their electronic properties, remain largely unresolved. Most experimental probes yield information on an “average atom” averaged out over a large length scale. EXAFS is an ideally suited technique to study the structure of amorphous materials since it yields atom-specific short range order information, such as coordination numbers, bond lengths and static and thermal disorder.

The determination of the presence of chemical disorder (like-atom bonds) has been the aim of most previous EXAFS studies of amorphous III-V’s because the presence of these bonds is a signature that permits the identification of the appropriate topological description of their structure. The identification of chemical disorder has been hampered by sample preparation-specific artifacts, such as deviations from stoichiometry, voids, inhomogeneities and lack structural relaxation due to high non-equilibrium conditions prevalent during the growth of the semiconductor layers. Indeed, thermally-induced structural relaxation in amorphous Si and Ge (i. e. heat release concomitant to structural modifications prior to crystallization) has been abundantly documented in the literature. However, in amorphous III-V’s, it has never been directly characterized at the atomic level.

In this contribution, we present results on the structural characterization with EXAFS of fully relaxed, artifact-free amorphous InP, GaAs and InAs grown by MOCVD and rendered amorphous by ion implantation. Our results indicate that thermal relaxation in III-V’s is mediated by annihilation of heteropolar bonds and by a reduction in the width of the bond angle distribution, in accordance to the relaxation mechanism observed in amorphous Ge and Si. Moreover, the relaxed amorphous structure has a concentration of 10% of like-atom bonds, indicating that a Polk-Like Continuous Random Network is better suited to describe the topology of amorphous III-V’s, in agreement with recent first-principles calculations by Lewis et al. (Phys. Rev. B 57 (1998) 1594).

## OINS02. Advances in High Throughput Crystallography for the Home Lab: Bright Sources, Fast Detectors, Robotics, and Cr Radiation Phasing

*Ferrara, J.D.*

Rigaku/MSC, Inc. 9009 New Trails Drive, The Woodlands, TX 77381

The landscape of the home laboratory has changed dramatically in the last year. The introduction of a big wheel, microfocus rotating anode generator, the FR-E SuperBright and an optic optimized for this new generator, the MicroMax CMF, has pushed the limit on the maximum resolution poorly diffracting samples can yield in the home laboratory. In addition to the FR-E SuperBright, two other microfocus generators have been introduced in the last three years, the MicroMax-002, a sealed tube microfocus x-ray generator, and the MicroMAX-007, a rotating anode microfocus generator. Both of these systems are designed to improve throughput by reducing downtime.

A fast detector with high signal-to-noise, high dynamic range, high sensitivity and large aperture is necessary to truly take advantage of this downstream hardware. To reach this goal we have designed and built the R-AXIS HTC, a three image plate detector with a 10 second dead time between images of 20 seconds or longer exposure time approaching the speed of a CCD detector. A complementary CCD detector, the Saturn 92, has been developed to provide even faster throughput for ligand binding studies.

The shift to the high throughput crystallography paradigm requires that structure determination become an automated procedure. At this time most data collection is begun with user mounting the sample on the instruments, centering the sample and initiating data collection. Rigaku/MSC has collaborated with a pharmaceutical company to develop ACTOR, a system for Automatic Crystal Transport, Orientation and Recovery, to allow the user to collect nearly continuously on a minimum of 60 samples with no intervention except to load and unload magazines of all samples at the beginning and end of the data collection run. We have designed complete flexibility in the system to allow integration with virtually any goniometer, maximum reuse of existing crystal handling devices for ease of use and new tools to facilitate crystal handling using current accepted methods.

Finally, we have introduced a diffraction system optimized for Cr radiation. This system provides a substantial enhancement of the anomalous signal from the sulfur present in nearly all proteins. This signal enhancement has been shown to be sufficient to allow the solution of the structure from the single wavelength anomalous data with low redundancy. This is a shift in methodology from that use of Cu radiation which requires high redundancy. The ability to solve protein structure without using selenomethionine or other heavy atom methods has the potential to greatly improve the rate at which structures are solved, especially in the context of the vast number of structures required to determine the proteome of an organism. Chromium radiation may also be used to augment the signal from heavy derivatives.

The implications of these advancements to the macromolecular crystallographer will be discussed.

## PINS03. Structural Modifications at the NiO<sub>6</sub> Octahedra in NdNiO<sub>3</sub> Across the Metal-Insulator Transition Measured by EXAFS

Piamonteze, C.<sup>1,2</sup>, Tolentino, H. C. N.<sup>1</sup>, Ramos, A. Y.<sup>1,3</sup>, Massa, N. E.<sup>4</sup>, Alonso, J. A.<sup>5</sup>, Martinez-Lope, M. J.<sup>5</sup>, Casais, M. T.<sup>5</sup>

<sup>1</sup> Laboratório Nacional de Luz Síncrotron, Campinas, Brasil, [cinthia@lnls.br](mailto:cinthia@lnls.br)

<sup>2</sup> IFGW-UNICAMP, Campinas, Brasil

<sup>3</sup> LMCP-CNRS, Université de Paris 6, Paris, France

<sup>4</sup> Universidad Nacional de La Plata - CEQUINOR, La Plata, Argentina

<sup>5</sup> Instituto de Ciencias de Materiales de Madrid, CSIC, Madrid, Spain

Transition metal oxides with the perovskite structure exhibit a variety of interesting properties like high-T<sub>C</sub> superconductivity and colossal magnetoresistance. In particular, Ni perovskites ( $R\text{NiO}_3$ , where  $R$  is a rare earth) present metal-insulator (MI) transition as temperature decreases. Since the rare earth ion does not fill all the empty space left between the NiO<sub>6</sub> octahedra, these systems present a distorted perovskite structure where the NiO<sub>6</sub> octahedra tilt and rotate to accommodate the structure. The MI transition temperature,  $T_{\text{MI}}$ , increases as the rare earth size decreases, indicating a correlation between the electronic behavior and the structural distortion. From neutron diffraction measurements the crystallographic structure was found to be orthorhombic for  $R=\text{Pr, Nd, Sm and Eu}$ . In such structure there is one Ni site with all Ni-O separations approximately equal. Across the transition the major modification seen by neutron diffraction concerns the angles Ni-O-Ni, between the octahedra. Almost no modification is seen at the Ni-O separation. For smaller R ions (Ho ... Lu and Y) it was found a monoclinic distortion with two different Ni sites and above the transition, at the metallic phase, the orthorhombic structure is established. We have studied the structural properties of Ni perovskites using EXAFS (Extended X-Ray Absorption Fine Structure)<sup>i</sup> at Ni K edge for NdNiO<sub>3</sub> ( $T_{\text{MI}}=200\text{K}$ ). Our results show the existence of different Ni-O distances at both electronic phases that may be associated to a distorted Ni site or to two different Ni sites. Decreasing the sample temperature an increase at the Debye-Waller factor is observed (the Debye-Waller factor measured by EXAFS includes both structural and thermal disorder) across  $T_{\text{MI}}$  evidencing a local structural modification at Ni coordination shell. The results obtained by EXAFS complement the precedent diffraction results showing that even though the average structure seen by diffraction is very symmetric, the EXAFS results show a distortion at the NiO<sub>6</sub> octahedra that is probably non-cooperatively arranged through the structure.

### References

<sup>i</sup>C. Piamonteze et al., Physica B **320**, 71 (2002)

# PEMU01. Caracterização Estrutural de Cerâmicas Ferroelétricas ( $Pb_xLa_{1-x}TiO_3$ ) e Através da Técnica de Espectroscopia de Absorção de Raios-X (XAS) e da técnica de Espectroscopia de Fotoelétrons Excitados por Raios-X (XPS)

Neves, P. P. IFSC / USP – *person@if.sc.usp.br*

Mastelaro, V. R. IFSC / USP – *valmor@if.sc.usp.br*

Eiras J. A. UFSCar. Departamento de Física da UFSCar, São Carlos, SP

Michalowicz, A. Université de Paris XII Val de Marne França.

As cerâmicas ferroelétricas de composição  $Pb_{1-x}La_xTiO_3$  (PLT) apresentam o fenômeno de Transição de Fase Difusa (TFD) quando átomos de chumbo são substituídos por átomos de Lantânia. Alguns estudos realizados em materiais de composição  $PbTiO_3$  e  $PbTi_xZr_{1-x}O_3$  mostraram que existe uma correlação entre a estrutura à curta distância e as transições de fase nestes materiais. Este trabalho tem por objetivo propor a caracterização estrutural das cerâmicas PLT através de técnicas não convencionais de raios-X que fornecem principalmente informações estruturais à curta distância como, por exemplo: as técnicas de XAS e XPS.

Neste trabalho apresentamos os resultados das medidas de XAS na borda K do átomo de titânio, de XPS nas amostras de composição  $PbTiO_3$  e  $Pb_{0,70}La_{0,30}TiO_3$  e de medidas de composição utilizando a técnica de WDS.

A análise dos espectros XANES e EXAFS da borda k do átomo de titânio mostraram que existe uma mudança significativa na ordem local à medida que a concentração de lantânia aumenta, principalmente nas amostras que apresentam o fenômeno de TFD. Através da análise dos espectros EXAFS foi observado que ocorre uma diminuição da desordem a medida que a concentração de lantânia aumenta. Enquanto que na amostra  $PbTiO_3$  a primeira esfera de coordenação é composta por três diferentes distâncias Ti-O, na amostra contendo 30% de lantânia foi possível simular com apenas um tipo de ligação Ti-O. Apesar disso, os espectros XANES na borda do titânio mostram que mesmo para a amostra com 30% de lantânia a estrutura local não é do tipo cúbica.

Medidas de XPS realizadas nas amostra  $PbTiO_3$  e  $Pb_{0,70}La_{0,30}TiO_3$  não mostraram mudanças significativas para os espectros de Ti e Pb. Para os átomos de Lantânia e Oxigênio os espectros de XPS apresentam algumas diferenças.

Uma análise de composição feita nas amostras do sistema PLT utilizando a técnica de WDS mostrou que a composição das amostras contendo 5 e 30% de lantânia estão bem próximas da composição nominal e daquelas obtidas pela técnica de difração de Raios-X utilizando o método de Rietweld.

Um projeto submetido ao LNLS com objetivo de complementar os estudos estruturais propondo medidas de XAS em função da temperatura já foi aprovado e as medidas serão realizadas no primeiro semestre de 2003. Também para o primeiro semestre de 2003 está programado a realização de medidas de XPS para as outras composições do PLT e do sistema PBZT. Daremos também início a cálculos teóricos de espectros XANES através do programa FEFF8.2.